Physical Organic Chemistry on the Nicotinic Acetylcholine Receptor

Thesis by

Wenge Zhong

In Partial Fulfillment of the Requirements

for the Degree of

Doctor of Philosophy

California Institute of Technology

Pasadena, California

1998

(Submitted May 11, 1998)

© 1998

Wenge Zhong

All Rights Reserved

To *Zhong & Xinlian*

Acknowledgments

I have been very fortunate to constantly receive assistance and intellectual input during my graduate career from the highly talented faculty and students here, who make Caltech a truly wonderful institution. I realize that my appreciation for the help from many people is far beyond any verbal expression.

I am extremely grateful to my advisor, Professor Dennis A. Dougherty, for his guidance, encouragement, and patience. His vision for science and his contagious optimism were very much appreciated. I am thankful for his willingness to let me freely explore new projects and his assistance in choosing my career path. I have certainly enjoyed the many luxurious days off when my daughter was sick, and I deeply appreciated his understanding of such family matters and his help in many other ways. I have said 'seven' times to many of my friends, I could not have hoped for a better mentor. I have unfathomable respect for him both as a scientist and as a person.

I greatly acknowledge my mentor in biology, Professor Henry A. Lester, for his advice, wisdom, and tolerance. I appreciated very much the opportunity to learn the principles of electrophysiology directly from him. I can not thank him enough for his encouragement when times were tough. While constantly being amazed by his breadth and depth of knowledge in many research fields, I also enjoyed his great sense of humor. I will always have fond memories of the Lester family-group parties.

I thank the other members of my committee, Professors Andy G. Myers, Jacqueline K. Barton, and Barbara Imperiali, for their support and guidance during these

years. Professor Myers kindly provided many solutions to my synthesis problems. I thank Professor Norman Davidson for teaching me valuable lessons on the importance of control experiments and treating me as a scientist.

Thanks must go out to many outstanding colleagues. Dr. Mark W. Nowak taught me almost everything that I know about molecular biology and electrophysiology. He has been a tremendous pleasure to work with. I am truly thankful to Dr. Cesar Labarca for many insightful discussions on research and other issues. Patrick C. Kearney paved the path for us to follow and his courage was deeply admired. Thanks go to Dr. Anthony P. West, Jr., for his ideas and friendship. I consider myself very fortunate to be a colleague of Drs. Scott K. Silverman and Pamela A. England. I learned a lot about how to do high quality science from them.

Special thanks go to Justin P. Gallivan, Haiyun Zhang, Jun Li, Lintong Li, and Dr. Yinong Zhang for fruitful collaborations. Justin has been a great driving force for the studies described in Chapter 2 of this thesis. Haiyun and Jun have performed single channel analysis in a study discussed in Chapter 4. Lintong, a very diligent scientist, and Yinong collaborated with me on the tethered agonist project. I also thank the other members of the unnatural group, Gabriel S. Brandt, Marcus C. Sarofim, Drs. Hong Dang and Yanhe Tong, and Niki Zacharias, for a stimulating yet friendly environment.

My warmest gratitude goes to Sarah M. Ngola, Jennifer C. Ma, Sandro Mecozzi, Laura S. Mizoue, Alison McCurdy, Jonathan Forman, and Bruce Hietbrink for sharing enthusiasm in molecular recognition. I thank Sarah for her help while we are both writing up our theses and preparing for the talks. I am especially grateful to Jennifer for giving

me many free rides to San Diego about four years ago. I thank Sandro for his friendship. Jesse Lin deserves special thanks for discussing with me all my synthetic problems. I have had many delightful conversations with Seth A. Miller, Jeff A. Clites, Craig Anderson, Michael Murray, Joshua A. Maurer, and S. Joshua Jacobs, who are among the most wonderful and the brightest people I have met at Caltech. Many members in the Lester group also deserve thanks. Help from Drs. Yongxin Li, Paulo Kofuji, Ming Li, Yan Li, Jancy McPhee, and Melihat Nowak, Hairong Li, Purnima Deshpande, Jason Sydes, Donghong Ju was greatly appreciated.

I have benefited and will always cherish my friendship with Professor Sunney I. Chan, Dr. Jack Jian Lin, Guangyang Wang, Xuanqi Wang, Drs. Lianping Pan, Shuguang Wu, Guohua Chen and Huimin Zhao, with whom I share many values of life.

I thank Professor Dennis A. Dougherty for proofreading this thesis, and Gabriel S. Brandt, a versatile and meticulous young man, and Justin P. Gallivan for proofreading Chapters 1 and 4. All remaining errors are my responsibility.

I reserve my final thanks for my family. I thank my parents, brother, and sister for always believing in me. I thank my daughter for teaching me the sheer joy of life. Finally, my heart goes out to my dear wife, whose has made everything in my life unimaginably magnificent. Without her, I could not think about the future.

Abstract

An exciting new field, physical organic chemistry on the brain, is emerging as a major frontier at the interface between chemistry and neurobiology. In a collaborative effort, the Dougherty group in chemistry and the Lester group in biology here at Caltech are trying to develop chemical-scale understanding and insight into the structure and function of neuroproteins that are implicated in brain functions. The present work, physical organic chemistry on the nicotinic acetylcholine receptor (nAChR), uses the principles and the methods of physical organic chemistry to address some of the fundamental structural and mechanistic questions about this prototype ligand-gated ion channel.

In Chapter 2, we present convincing mutagenesis data to support a crucial role for cation-π interactions in ACh binding to the nAChR, confirming the proposal by Dougherty and Stauffer eight years ago. In this study, a wide spectrum of methods were used, ranging from *ab initio* quantum mechanical calculation and organic synthesis to molecular biology and electrophysiology. We found that at one and only one site - αTrp 149 - EC_{50} correlates strongly with the cation-π binding ability of the aromatic sidechain. We take this as clear evidence that the αTrp 149 sidechain is in van der Waals contact with the quaternary ammonium group of ACh, engaging in a strong cation-π interaction. This finding represents the most precise structural information to date on this complex, multisubunit protein.

In Chapter 3, we report investigations of constitutively active nAChR molecules. By incorporating Tyr-O3Q, an amino acid with a quaternary ammonium group, at α 149 using the nonsense suppression method in *Xenopus* oocytes, we observed large standing currents in the absence of external agonists. Studies with various channel blockers and nAChR antagonists as well as single channel analysis indicate that these active channels are indeed the nAChRs. This finding not only provides strong evidence to support the model developed in studies reported in Chapter 2, but also opens the possibility for much broader exploration of the tethered agonist approach in studying ion channels.

In Chapter 4, we describe our quest for chemical insight into the structural basis which underlies the conformational changes from agonist binding to channel opening. We found supporting evidence for an earlier hypothesis that δAsp 180 and/or γAsp 174 play an important role in such conformational changes. By using a double-mutant cycle method, we unveiled remote couplings (over a distance of some 50 Å) in receptor activation between these acidic residues thought to be near the agonist binding site and the hydrophobic leucines at the 9' position in the M2 pore region. The βLeu9' couples most strongly to these acidic residues. In addition, we document studies aimed to probe a putative hydrogen bond at subunit interfaces.

In Chapter 5, methods in electrophysiology, molecular biology, and synthesis of various amino acids are summarized. In Chapter 6, we discuss studies to explore the cation-π interaction in superamolecular systems. The design and synthesis of a potential alkali metal ion host are described.

Table of Contents

Acknowledgments....iv

Abstract....vii

List of Figures....xii

List of Schemes....xv

List of Tables....xvi

Chapter 1. Physical Organic Chemistry on the Brain....1

1.1 Introduction....2

1.2 Physical Organic Chemistry on the Brain....4

1.3 The Nicotinic Acetylcholine Receptor (nAChR)....7

1.4 The Agonist Binding Site in the nAChR....11

1.5 The Cation-π Interaction....13

1.6 References....20

Chapter 2. Physical Organic Chemistry on the Nicotinic Acetylcholine Receptor: αTrp 149 is the Cation-π Site for ACh Binding....25

2.1 Introduction....26

2.2 αTrp 149 Interacts Uniquely with ACh....28

2.3 None of αTrp86, αTrp184, and γTrp55/δTrp57 Interacts Strongly with ACh....31

2.4 αTrp 149 Is the Cation-π Binding Site in the nAChR....35

2.5 The Role of αTrp 149 in Binding TMA, Nicotine, and *d*-Tubocurarine....44

2.6 Conclusions and Discussion....49

2.7 References....53

Chapter 3. Introducing A Tethered Agonist into the nAChR.....55

3.1 Introduction.....56

3.2 Introducing Tyr-O3Q at α 149.....57

3.3 ACh Induces Additional Inward Currents.....60

3.4 α-Bungarotoxin and *d*-Tubocurarine Block Standing Currents.....61

3.5 Single Channel Studies of the Constitutively Active Receptor.....63

3.6 Conclusion and Future Directions.....64

3.7 References.....67

Chapter 4. Coupling Between Distant Regions in the nAChR: Acidic Residues Near the Agonist Binding Site and Hydrophobic Ones in the Channel Pore.....68

4.1 Introduction.....69

4.2 Coupled Effects Between Leu9' in the M2 and γD174/δD180.....74

4.3 βL9' Couples Most Strongly with γD174 and/or δD180.....77

4.4 Single-Channel Analysis of αL9'SγD174N and αL9'SγD174NδD180N.....79

4.5 Strong Interaction between αY93 and γD174 or δD180 is Unlikely.....92

4.6 Discussion.....96

4.7 References.....98

Chapter 5. Methods in Electrophysiology and Preparation of Mutants and Amino Acids.....100

5.1 Two Electrode Voltage Clamp and EC_{50} Measurements.....101

5.2 Single-Channel Recording and Analysis.....102

5.3 Mutagenesis, mRNA Synthesis, tRNA Synthesis and Oocyte Microinjections 106

5.4 General Procedure for Synthesis of Aminoacyl dCA (dCA-AA)-Synthesis of dCA-Phe.....108

5.5 Preparation of Amino Acids.....109

5.6. Experimental Section.....122

5.7 References.....150

Chapter 6. Exploring the Cation-π Interaction in Molecular Recognition: Design and Synthesis of A Potential Alkali Metal Ion Host.....152

6.1 Introduction.....153

6.2 Synthesis of Host IV.....157

6.3 Synthesis of a 3/4 Molecule Towards a Tetraamide Host.....161

6.4 Purification of the Tetraphosphate Host P4P.....163

6.5 Experimental Section.....165

6.6 References.....174

List of Figures

Figure 1.1. The Molecules of Neurobiology.....6

Figure 1.2. Scematics of the nAChR.....10

Figure 1.3. Cation-π interactions in Artificial Systems.....13

Figure 1.4. The Cation-π interaction.....14

Figure 1.5. Two Views of ACh Esterase Complexed with Decamethonium.....17

Figure 2.1. The Electrostatic Potential Surfaces for Sidechains of Trp, 5-Me-Trp, 5-Br-Trp, and 5-CN-Trp.....33

Figure 2.2. EC_{50} Values for Mutants at α86, α184, and γ55δ57.....34

Figure 2.3. Structures of Trp Derivatives.....37

Figure 2.4. Electrostatic Potential Surfaces for Trp the Various Fluorinated Trps.....39

Figure 2.5. Representative Current Traces and Dose-Response Relations.....40

Figure 2.6. Plot of log[EC_{50}/EC_{50}(wild type)] vs. Quantitative Cation-π Binding Ability.....42

Figure 2.7. Plot of log[EC_{50}/EC_{50}(wild type)] vs. Quantitative Cation-π Binding Ability at α149 for All the Residues Shown in Figure 2.3.....42

Figure 2.8. Model of ACh binding to αTrp149 and the Structure of Tyr-O3Q.....43

Figure 2.9. Plot of log[EC_{50}/EC_{50}(wt)] for TMA vs. log[EC_{50}/EC_{50}(wt)] for ACh for Mutant Receptors.....46

Figure 2.10. EC_{50} (μM) Values for (-)-Nicotine.....46

Figure 2.11. IC_{50} (nM) Values for *d*-Tubocurarine.....48

Figure 2.12. An Agonist Binding Site Model by Analogy to Acetylcholine Esterase....51

Figure 3.1. The Chemical Structure of Tyr-O3Q.....58

Figure 3.2. Behavior of Constitutively Active nAChR Containing Tyr-O3Q atα149...59

Figure 3.3. α-Bungarotoxin Blocks Standing Currents.....62

Figure 3.4. Single Channel Recording of the Constitutively Active nAChR.....63

Figure 3.5. The Structures of Potential Tethered Agonists.....65

Figure 4.1. The M2 Pore Region of nAChR.....70

Figure 4.2. A Putative Hydrogen Bond.....72

Figure 4.3. The Diastereomeric Pairs of Amino Acids.....73

Figure 4.4. Dose-Response Relations.....76

Figure 4.5. Comparisons of EC_{50} Values Before and After the Introduction of Asp-to-Asn Mutations.....79

Figure 4.6. Single Channel Openings and Open-time Histograms.....81

Figure 4.7. Single Channel Dose-Response Relations.....82

Figure 4.8. Kinetic Models for Wild Type and Mutants.....83

Figure 4.9. The Open and Closed-Time Histograms for Event Series.....87

Figure 4.10. Re-analysis of Data in Figure 4.9.....88

Figure 4.11. The Rate Constants for Individual Kinetic Transitions.....90

Figure 4.12. Comparison of EC_{50} Values at α93 With and Without Asp-to-Asn Mutations.....94

Figure 5.1. The General Strategy for dCA-Amnio Acid Synthesis.....108

Figure 5.2. Chemical Structures of Readily Available Amino Acids.....111

Figure 5.3. Residues Containing Sidechain Ammonium Group.....115

Figure 6.1. Host P and Representative Guests.....153

Figure 6.2. Designed Hosts for Alkali metal Binding.....156

Figure 6.3. Retrosynthetic Analysis of Host IV.....157

Figure 6.4. The Structure of Control Molecule for MS Studies.....160

Figure 6.5. The Tetraamide Host.....162

Figure 6.6. Synthesis of **3/4** Molecule.....163

Figure 6.7. The Tetraphosphate Host P4P.....164

List of Schemes

Scheme 5.5.1. Synthesis of 4-Me-Phe **3**.....113

Scheme 5.5.2. Synthesis of Alkylating Compound **6**.....113

Scheme 5.5.3. Synthesis of Homo-Tyrosine **9**.....114

Scheme 5.5.4. Synthesis of Tyr-O3Q **19**.....116

Scheme 5.5.5. Synthesis of Lys-Carbamylcholine **24**.....116

Scheme 5.5.6. Synthesis of 5-CN-Trp **29**.....117

Scheme 5.5.7. Synthesis of 5,7-F_2-Indole **32**.....118

Scheme 5.5.8. Synthesis of 5,6,7-F_3-Indole **35**.....119

Scheme 5.5.9. Synthesis of 4,5,6,7-F_4-Indole **38**.....119

Scheme 5.5.10. Synthesis of 4-Acetyl-Phe **42**.....120

Scheme 5.5.11. Synthesis of O-Acetonyl-Tyr **46**.....120

Scheme 5.5.12. Synthesis of L-*allo*-O-Me-Thr **51**.....121

Scheme 5.5.13. Synthesis of dCA-Thr.....121

Scheme 6.1. Synthesis of Host IV.....159

List of Tables

Table 2.1. EC_{50} Values for Mutants at α86, α184, and γ55δ57.....30

Table 2.2. EC_{50} Values for Mutants at α149.....36

Table 2.3. EC_{50} Values for Different Agonists.....45

Table 2.4. IC_{50} Values for *d*-Tubocurarine.....48

Table 4.1. EC_{50} Values for Mutants with L9'S and/or D-to-N Mutations.....75

Table 4.2. Comparison of Single Channel Data for WT and Mutants.....85

Table 4.3. Equilibrium Constants for Wild Type and Mutants.....89

Chapter 1

Physical Organic Chemistry on the Brain

1.1 Introduction

Developing chemical-scale understanding and insight into the structure and function of membrane proteins of excitable cells defines one of the major frontiers of modern neuroscience (1, 2). In recent years, the powerful combination of modern electrophysiological techniques and site-directed mutagenesis has brought fascinating advancements to the field. Most recently, the development of a new method to incorporate unnatural amino acids into membrane proteins in living cells makes it possible to do more rigorous physical organic chemistry on these molecules - the molecules of our brain functions (1, 2). This thesis work represents a modest contribution to this exciting new field.

Before we discuss physical organic chemistry on the brain in any detail, it is quite helpful first to briefly review the history of physical organic chemistry. The emergence of physical organic chemistry as a separate discipline of chemistry can be traced to as early as 1874 when van't Hoff and Le Bel first introduced the concept of tetrahedral geometry of around saturated carbon centers (3, 4). It became a very active field when reactive intermediates such as carbocations, carbanions, carbon radicals, and carbenes were subsequently investigated (5-15). In 1920's and 1930's, the mechanisms of nucleophilic substitution reactions were clearly understood (16, 17, 18), and Huckel theory of molecular orbitals as well as linear free energy relationships were well established (19). In 1940, Louis Hammett published one of the most influential books in chemistry of all time, *Physical Organic Chemistry*, which not only named the field, but also attested to its maturity. Ever since then, more advanced physical techniques such as

flash photolysis, matrix isolation and modern laser technology have been used extensively for the studies of reactive intermediates and even transition states (20, 21, 22). In the 1950's and 60's, the field has seen a few of its greatest triumphs, exemplified by the principles of orbital symmetry by Woodward, Hoffmann and Fukui (23, 24), the development of host-guest chemistry (often referred as superamolecular chemistry nowadays) by Pedersen, Cram, and Lehn (25-28), and conformational analysis by Barton (29).

While constantly receiving intellectual influences from a wide array of subjects, physical organic chemistry has always had profound impact on, not merely accompanied, other fields such as organic synthesis, organometallic chemistry, biochemistry, medicinal chemistry, and materials science. In fact, many of the exciting developments in chemistry today are emerging from interfaces between chemistry and physics, biology, or materials science. It is clear that physical organic chemistry will continue to play a critical role in such new directions (1, 2, 26).

We emphasize here that one of the active fields in which physical organic chemistry has been very much involved is mechanistic enzymology, a field pioneered by Westheimer and others in early 50's (30). The paramount importance of understanding mechanisms of enzymatic reactions relies on its relation to pharmacology, fundamental biology and chemistry. The pursuit of a practical cure for a disease profits from an understanding of the action of the enzymes involved at a chemical level. This aspect of physical organic chemistry, detailed structure-function relationship studies, is

revolutionizing drug design, just as the earlier understanding of reaction mechanisms revolutionized organic synthesis (31).

Recently, an exciting new research area is burgeoning at the interface between physical organic chemistry and neurobiology. In a collaborative effort, the Dougherty group in chemistry and the Lester group in biology here at Caltech are trying to do physical organic chemistry on the molecules of the brain. This field, dubbed physical organic chemistry on the brain by Dougherty, uses the principles, the tools, and the methods of physical organic chemistry to address fundamental structural and mechanistic questions about the molecules of thought, memory, and sensory perception (1, 2). In the following, I will briefly describe these molecules and the approaches that are taken to answer some of the fundamental questions.

1.2 Physical Organic Chemistry on the Brain

To do physical organic chemistry on the brain is to develop chemical-scale understanding of the structure-function relationships of the molecules of our brain functions (1, 2). Brain functions are based on cell-cell communications between neurons in the nervous system, which are mediated by alternating chemical/electrical signals (32, 33, 34). The site of action, the space in between the two interacting neurons, is called the synapse. In a human brain, there are about 10^{12} neurons, each of which composes roughly 10^3-10^4 synapses. It is truly a daunting task to try to understand the intricate structures and basic mechanisms of such a complex system. Fortunately, to chemists and molecular biologists, the issue can be reduced to the study of the molecules at synapses

that bring about synaptic transmissions. These are the small neurotransmitter molecules and their corresponding neuroreceptors which are integral membrane proteins. Classical application of physical organic chemistry to neurobiology - pharmacology - has focused on the structure-function studies on neurotransmitters such as acetylcholine, dopamine, and serotonin. Now the challenge is to understand at a chemical-scale the neuroproteins that are involved in basic brain functions (1, 2).

These integral membrane proteins include ion channels, ligand-gated and G protein-coupled neuroreceptors, neurotransmitter transporters, and related structures (shown in Figure 1.1) (32, 33, 34). One prominent structural feature of these neuroproteins is that they often contain multiple transmembrane segments. Addtionally, many of them are multisubunit structures. As such, the sophisticated methods of X-ray crystallography and NMR techniques are not readily applicable to these molecules. In the Dougherty/Lester collaboration, we employ a combination of modern electrophysiological techniques and the *in vivo* nonsense suppression method for unnatural amino acid incorporation to perform precise and systematic structure-function relationship studies on these molecules.

While electrophysiology provides the necessary tools for functional studies, the critical element in our approach is the *in vivo* nonsense suppression method. This method was originally developed by the Schultz group at Berkeley for *in vitro* unnatural amino acid incorporation in soluble proteins (35, 36). We adapted and extended the method to *in vivo* studies of membrane proteins in the heterologous expression system of the *Xenopus* oocyte (37). The details of the method have been discussed elsewhere (38).

It is sufficient to state here that this is now a standard procedure in this lab. Residues containing a biotin moiety (39), a photolabile caging group (40), and a number of other functional groups have been incorporated (41). Ester bonds and photocleavable amide bonds have also been incorporated into the protein backbone (42, 43). The present work has focused on structure-function relationship studies on a specific neuroreceptor, the nicotinic acetylcholine receptor (nAChR).

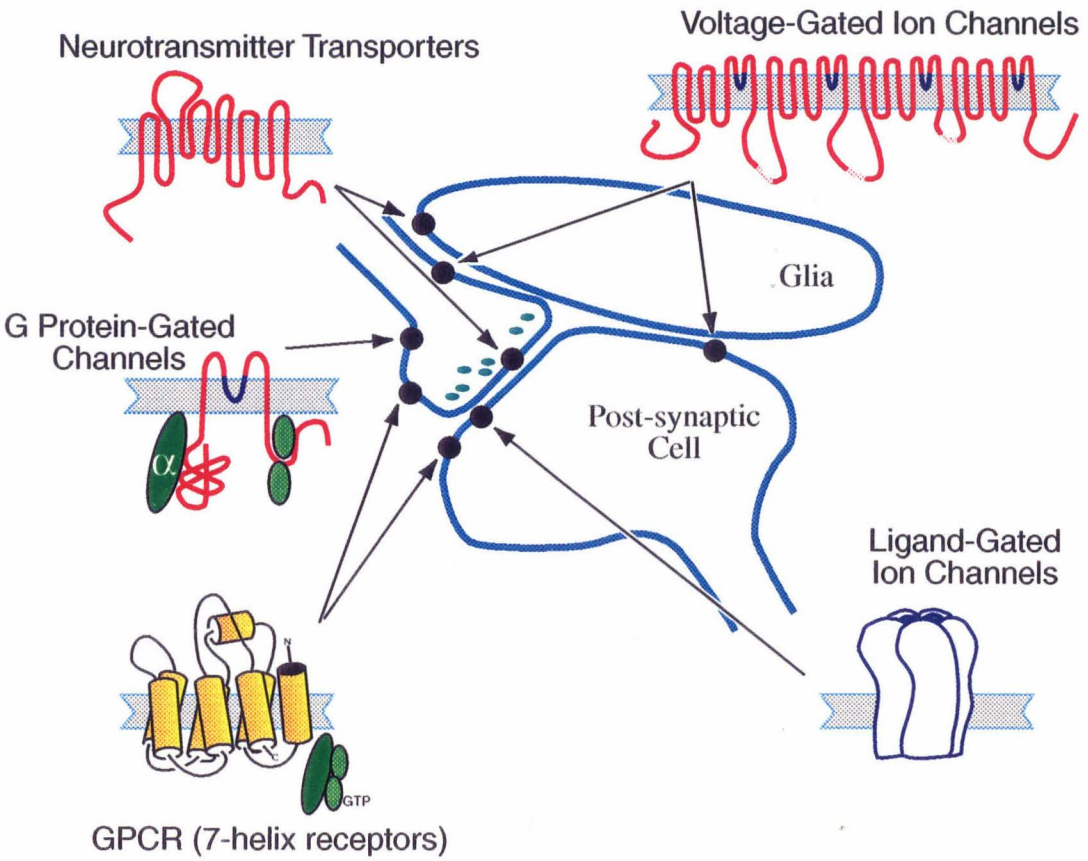

Figure 1.1. The molecules of neurobiology.

1.3 The Nicotinic Acetylcholine Receptor (nAChR)

The nicotinic acetylcholine receptor is the prototype ligand-gated ion channel, belonging to a superfamily which also includes receptors for serotonin, glycine, γ-aminobutyric acid (GABA), and an invertebrate glutamate-gated chloride channel (44, 45, 46). The receptors are designated "nicotinic" because nicotine is a full agonist which mimics the actions of acetylcholine (ACh), and to distinguish them from very different muscarinic ACh receptors (which are G protein-coupled receptors) (34). There are two main types of nAChRs - the muscle and the neuronal nAChRs. The former is primarily located at neuromuscular junctions. At the motor endplate, the arrival of an action potential at the motor nerve ending causes the release into the presynaptic cleft a brief pulse of ACh, whose local concentration reaches 0.1 to 1 mM for less than 1 msec (47). ACh diffuses across the synaptic space and binds to the nAChR present at the postsynaptic membrane and triggers the opening of a non-selective cation-channel within the receptor. When depolarization in the postsynaptic cell reaches a threshold, muscle contraction occurs. In the synapse, the ACh concentration rapidly decreases to background levels (10^{-9} M) as a consequence of diffusion and degradation by ACh esterase (47, 48). Neuronal nAChRs are expressed in the central nervous system (CNS) (49, 50). They are implicated in such basic brain functions as learning and memory as well as possibly pain perception (51, 52, 53). The neuronal nAChR also plays an important role in nicotine addiction (54). My thesis study is focused on the muscle nAChR; however, the questions addressed are, to a large extent, common to both types of receptors.

The muscle type nAChR is the longest known, best studied neuroreceptor (45, 55). Due to the remarkably high density of synapses in electrocyte membranes in the electric organ of the ray *Torpedo*, many ground-breaking biochemical and biophysical studies have been performed. The receptor is a large protein (MW ca. 290 kD), which comprises four homologous subunits with a stoichiometry of $\alpha_2\beta\gamma\delta$ (in adult, the γ subunit is replaced by the ε subunit). The five subunits are arranged in a pentagonal array, at the center of which lies the ion conduction pathway. The order of subunits around the pore is still an unsettled issue, although the most advocated model (Figure 1.2A) is a counter-clockwise arrangement in the sequence of α-γ-α-δ-β when viewed from the extracellular side (56, 57, 58).

The three-dimensional structure of the nAChR has been determined to 9 Å resolution by electron microscopy in the laboratory of Unwin (59). The size and orientation of the intact receptor with respect to the lipid membrane can be clearly seen, but atomic-scale details are still lacking. The quaternary structure is shown in Figure 1.2A. The receptor is about 120 Å long, and 85 Å across at the widest point, which is in the extracellular domain. The extracellular portion extends about 76 Å above the membrane, while the intracellular portion about 16 Å below. The central pore is about 7 Å in diameter, consistent with early predictions based on its selectivity against large cations (60). In the interpretation of the nAChR structure, Unwin estimated the agonist binding site, located in the cavity formed by three rods in the α subunit, to be ca. 30 Å above the lipid membrane. Also, he proposed a hydrophobic plug model for channel gating, which places the highly conserved leucine residues at 9' position in each M2 region at the "gate" of the channel (61). As such, the agonist binding site is separated

from the channel gate by as far as 50 Å, making the nAChR a truly remarkable structure (Figure 1.2B).

A major break-through in the field of ligand-gated ion channels is the complete sequencing of nAChR subunits α, β, and δ by Noda *et al.* (62, 63, 64) and the γ/ε by Claudio *et al.* (65). Based on hydropathy analysis and biochemical studies, nAChR subunits are found to share similar transmembrane topologies. As shown in Figure 1.2C, each subunit consists a large extracellular N-terminal region followed by four transmembrane segments (denoted M1 to M4, respectively). There is a consensus glycosylation site in the N-terminal domain (66), and the loop between M3 and M4 contains consensus phosphorylation sites which are implicated in receptor desensitization (67-70). In the extracellular domain of each subunit, there are two cysteine residues separated by 13 amino acids. In ACh receptors, these cysteine residues are disulfide linked to form a 15 residue loop, often referred as the "signature disulfide loop" (71). Since it is likely that other homologous receptors also contain such loops, these receptors can be called cys-loop receptors (72). Extensive studies have indicated that the M2 region of each subunit constitutes most of the ion channel and that several residues in M2 point directly into the channel lumen (73, 74). Part of M1 has also been suggested to contribute to the formation of the channel (44, 75). More information regarding the channel structure is presented in Chapter 4.

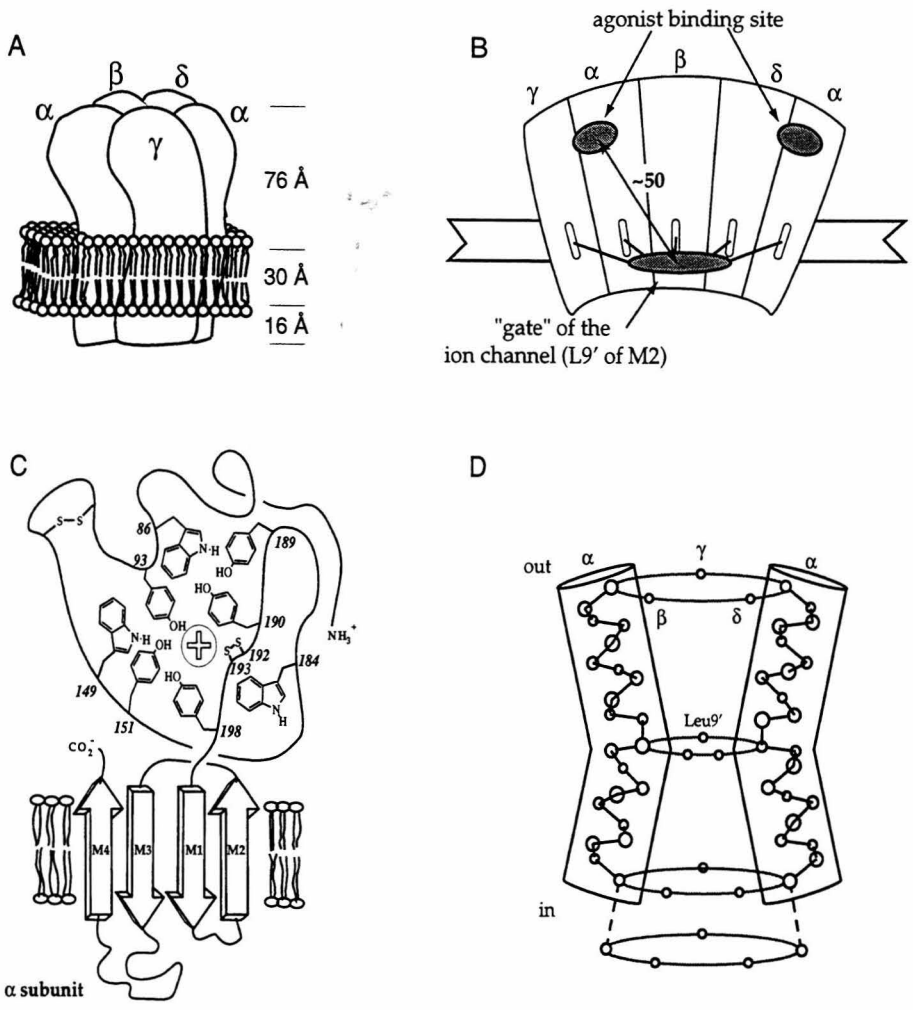

Figure 1.2. Schematics of the nAChR. A. Global layout and dimensions according to the 9 Å structure of Unwin. B. "Cutaway" view showing the proposed relative positions of the agonist binding sites and the gate of the channel. C. Layout of each subunit, using α as an example. There are 4 transmembrane regions (M1, M2, M3, and M4, respectively). M2 is thought to line a major portion of the channel. Note the presence of a large number of aromatic residues in the N-terminal domain of α, which contributes predominantly to the formation of the ACh binding site. D. The M2-pore region, emphasizing "rings" of conserved residues. Note that these pictures are highly speculative and many features depicted are still matters of debate. For example, the arrangement of the subunits, i.e., the positions of the β and δ subunits may be reversed; and the location of the actual "gate" of the channel is still uncertain.

1.4 The Agonist Binding Site in the nAChR

The agonist binding sites in nAChR are thought to be primarily associated with the extracellular region of the α subunits and reside at the interfaces of α/γ or α/δ (Figure 1.2D) (76-79). Binding of ACh to both binding sites acts cooperatively to activate the receptor (80). Upon activation, the channel opens and Na^+ and K^+ ions start to flow passively across the membrane. The first, and one of most essential issues which needs to be addressed in our effort to understand the structure-function relationships of nAChR is to identify the amino acid residues contributing to ACh binding and to discern their corresponding roles. In the absence of high-resolution structures, biochemical studies and site-directed mutagenesis have proven invaluable in studying ACh binding sites. Pioneering affinity and photoaffinity labeling studies performed with *Torpedo* nAChR have led to the realization of amino acid residues in four peptide "loops," three (loop A, B, and C) in the α subunit, and one (loop D) in the γ or δ subunit, that constitute the binding site (80). The labeling reagents used are: dimethylamino-benzene diazonium fluoroborate (81, 82), 4-(N-maleimido)benzyltrimethylammonium (MBTA) (83), nicotine (79), d—tubocurarine (84), lophotoxin (85, 86), and acetylcholine mustard (87). The identified residues are: αTrp 86 and αTyr 93 in loop A; αTrp 149 and αTyr 151 in loop B; αTyr 190, αCys 192, αCys 193, and αTyr 198 in loop C; γTrp 55 and γTrp 57 in loop D. All of the labeled residues in loops A, B, and C are conserved at homologous positions in all known α subunits from neuronal receptors and in all vertebrate species including humans (88). In fact, residues αCys 192 and αCys 193 form a vicinal disulfide bond that is unique to the α subunit and this feature is used to distinguish neuronal α's from non-α subunits. Three residues, αTrp 86, αTyr 151, and αTyr 198, are among the

highly conserved "structural canonical residues." The Trp residue in loop D also shows remarkable conservation, even in all neuronal α subunits, including α 7 and α 8 which are known to form functional homo-oligomers. Subsequent mutagenesis studies with neuronal α 7 nicotinic (82, 89, 90), muscle (91, 92), and *Torpedo* receptors (93) confirmed the functional importance of many of these residues in agonist and antagonist binding and ion channel activation. Additionally, in an elegant cross-linking study, Karlin has identified an anionic residue on the γ/δ subunits, γAsp 174/δAsp 180, that also influences agonist binding (94-96).

The remarkable feature of the ACh binding site is the predominance of aromatic residues. Given that ACh contains a positively charged quaternary ammonium group, it is truly surprising that affinity labeling studies failed to reveal any anionic residues near the binding site. However, in molecular recognition studies with cyclophane hosts, the Dougherty group at Caltech and others, especially the Collet and Schneider groups, have shown that aromatics can bind cations quite favorably in water (97-100). The fact that host P, designed and studied in our group, can bind the positively charged neurotransmitter ACh with affinity comparable to that of natural ACh receptors, in conjunction with the crystal structure of the phosphocholine binding antibody McPC603, prompted Dougherty and Stauffer to propose explicitly in 1990 that the binding of ACh by its natural receptors (such as ACh esterase and nAChRs) would be mediated primarily by cation-π interactions rather than by conventional interactions of the quaternary ammonium cation with carboxylate anions (101). In the following section, we will discuss the cation-π interaction and its relevance to ACh binding.

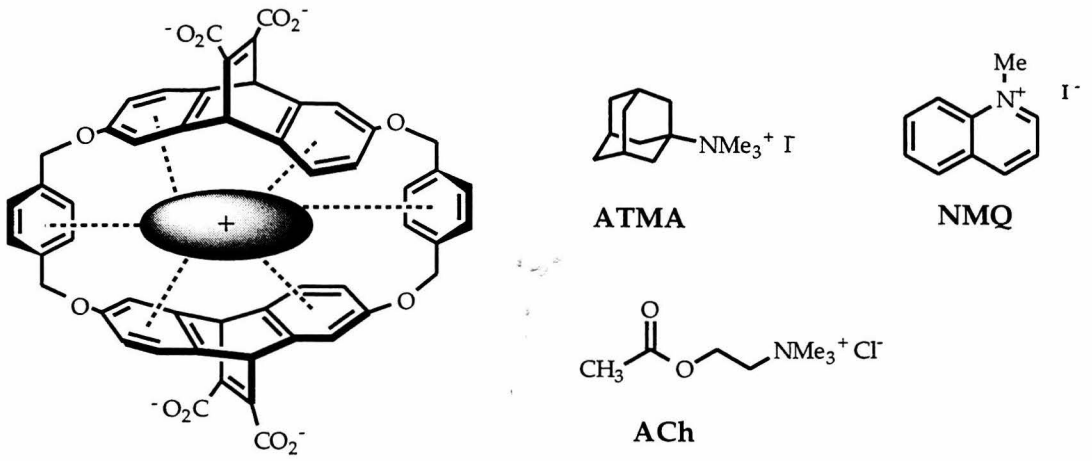

A. **Host P** B. **Guests**

Figure 1.3. Cation-π interactions in artificial receptor systems. A. The structure of host P. Note that the carboxylates are removed from the binding cavity, serving mainly as solubilizing groups. B. Representative cationic guests. Acetylcholine (ACh) binds to host P with similar affinity to its natural receptors.

1.5 The Cation-π Interaction

The cation-π interaction is a general noncovalent force, in which the face of an aromatic ring provides a region of negative electrostatic potential that can bind cations with considerable strength (Figure 1.4A) (97). In as early as 1981, Kebarle showed that in the gas phase, K^+ binds to benzene quite strongly with a binding enthalpy of 19 kcal/mol (102). In fact, it binds more strongly to benzene than it does to water. In biological contexts, the aromatic side chains of Phe, Tyr, and Trp can be expected to be involved in cation-π interactions, and a large body of evidence indicates a prominent role for cation-π interactions in structural biology in general (97, 103).

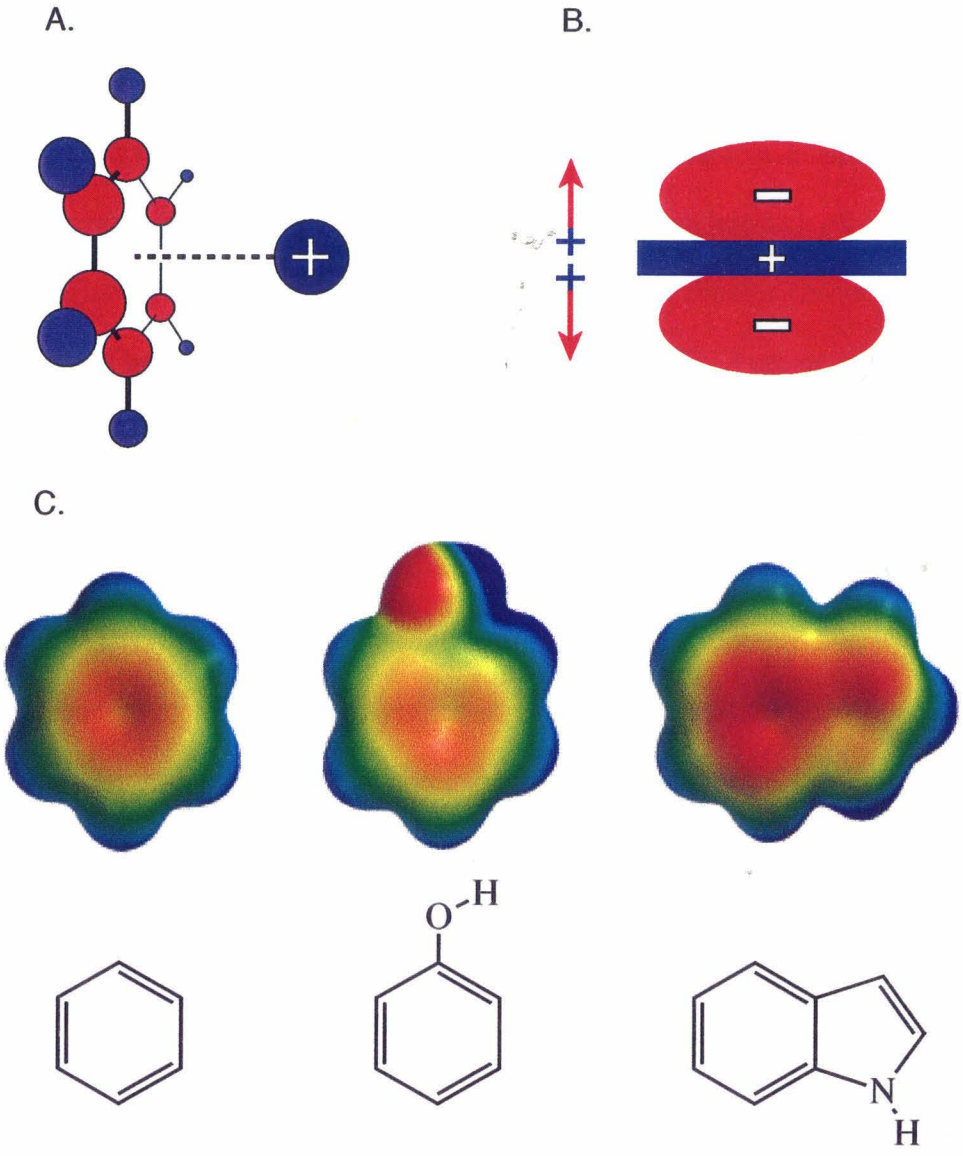

Figure 1.4. The cation-π interaction. A. Schematic representation of the cation-π interaction, in which simple and complex cations bind to the faces of aromatic rings. B. Illustration of the important role of electrostatics in cation-π interactions. The electrostatic interactions result from the large quadrupole moment of benzene and related aromatics, which provides a powerful binding surface for cations. C. The electrostatic potential surfaces of aromatics can serve as a predicative tool for examining their cation binding abilities. Shown here are the surfaces for the biologically relevant aromatics, corresponding to the side chains of Phe, Tyr, and Trp. It is clear that Trp provides the most intense and potent cation-π site in proteins. Color code: red, negative; blue, positive.

The nature of the cation-π interaction has been discussed in a number of publications (104, 105). Theoretical studies have indicated that a simple model of ion-quadrupole interaction is not appropriate. A complete quantitative description of this phenomenon would necessarily take into consideration of a number of other intermolecular forces, such as ion-dipole, ion-induced dipole, charge transfer, dispersion forces and in some cases hydrophobic interactions (106). Former group members Sandro Mecozzi and Anthony P. West, Jr., performed high level quantum mechanical calculations of cation-π interactions using Na^+ as a generic cation and found that, for simple aromatics, electrostatics can account for 40—60% of the total interaction energy, except in some selected systems where there is no electrostatic binding component. More interestingly, they found that across all the systems studied, electrostatics account for essentially 100% of the variation in cation binding to the aromatics. All other factors, such as polarizability-related terms, are absorbed into a constant term worth 11.6 kcal/mol when six-membered ring aromatics are considered (105). Based on these observations, they further demonstrated that it is a quite reliable method to qualitatively or even semi-quantitatively evaluate new aromatics as potential cation binders by simply considering their electrostatic surfaces (104). The physical underpinnings of the cation-π interaction are so well understood now that it is possible for one to predict with confidence how modifications of an aromatic system should affect its cation-π binding ability. Indeed, Sarah M. Ngola in our group observed that across a series of cationic guest molecules tested, the binding affinities to a host P analog which contains tetrafluorinated *p*-xylenyl linkers were 1.2 to 2.3 kcal/mol lower than those to host P. When guest molecule N-methylquinolinium was considered, as much as 60% of the decrease in binding affinity

could be attributed to the decreased cation-π binding ability of the two tetrafluorinated linkers (107).

The role of the cation-π interaction in ACh binding by its natural receptors was confirmed in less than a year after the Dougherty/Stauffer proposal. In 1991, Sussman *et al.* determined the X-ray structure of ACh esterase from *Torpedo*, which provided compelling structural evidence for the importance of cation-π interactions (Figure 1.5) (108). The structure revealed that 14 highly conserved aromatic residues define a large portion of a 20 Å deep "gorge," which guides ACh to the enzyme active site. Studies with inhibitors indicated that the ammonium group of these compounds (therefore that of ACh also) is bound by a tryptophan residue near the catalytic triad. In addition, the long-sought "peripheral anionic site" has also been identified as a tryptophan (109). Our work here focuses on another ACh binding site, the ACh binding site in the nicotinic acetylcholine recptor.

As discussed earlier, the large number of aromatic residues at the agonist binding site in nAChR makes cation-π interactions almost unavoidable in binding ACh. We envisioned that a combination of our knowledge of predicting the cation binding ability of aromatics with the ability to introduce unnatural amino acids into membrane proteins via the *in vivo* nonsense suppression method would allow the systematic evaluation of potential cation-π binding sites. In such studies, we will be directly applying the knowledge of classical physical organic chemistry along with modern computational methods to the complex neuroreceptor nAChR to try to determine the important roles of specific noncovalent interactions involved in agonist binding. These studies on a complex

neuroprotein in a living cell are essentially the same sort of studies of molecular recognition carried out in artificial receptor systems. We believe it is in this sense that we are doing "real" physical organic chemistry on the brain.

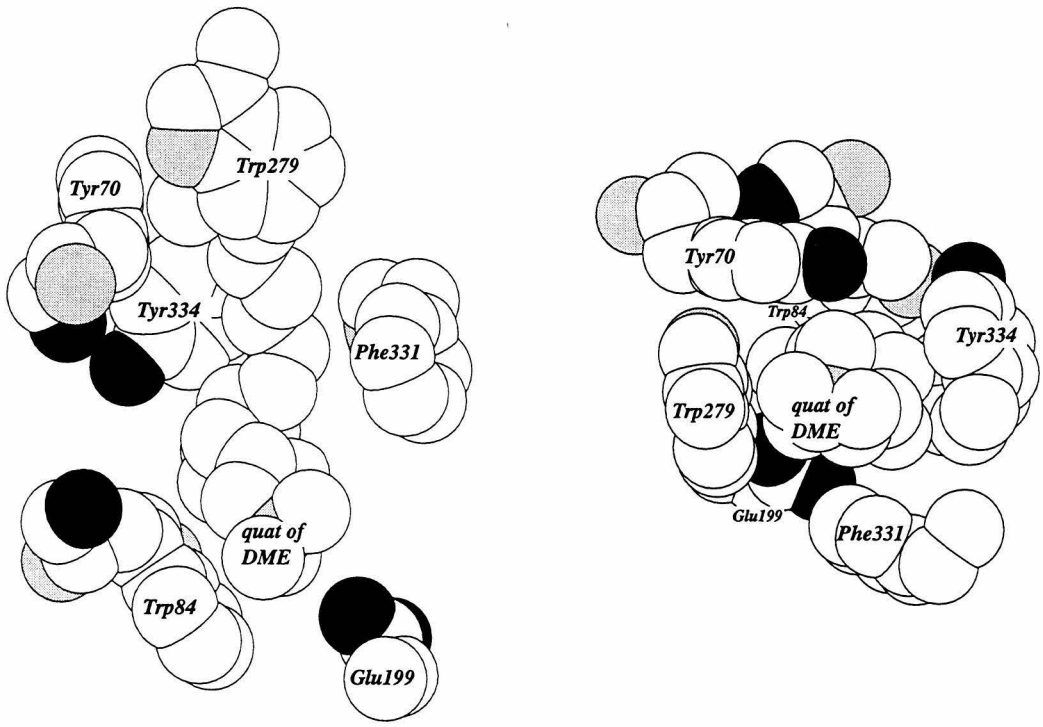

Figure 1.5. Two views of the acetylcholine esterase structure complexed with the bisquat decamethonium (DME). Coordinates are taken from the Brookhaven Protein Data Bank file 1ACL.(109) Code: carbon, white; nitrogen, light gray; oxygen, dark gray. Hydrogens are omitted. Left: Side-on view of the aromatic gorge. The active site is at the bottom, showing the quat of DME that is thought to mimic the quat of ACh, in close proximity to Trp84. Right: View looking down the aromatic gorge from the outside of the protein, showing the other quat of DME complexed to the "peripheral anionic site," Trp 279.

In summary, to do physical organic chemistry on the nAChR is to ask the following questions (1, 2):

- How is the agonist binding site designed to recognize ACh?
- What is the nature of the ion channel structure?
- What forces govern subunit-subunit assembly?
- What is the underlying structure that transduces local conformational changes induced by ACh binding to channel opening?

Our ability to answer these questions is important in understanding not only the fundamental structure-function relationships of nAChR, but also the pathological basis for the many nAChR related diseases (110, 111). New insights gained from these studies should also be applicable to other members of the ligand-gated ion channel superfamily.

This work is related to all the above questions, with a major emphasis on the agonist binding site. In Chapter 2, extensive mutagenesis studies on four tryptophan residues which are thought to be at the binding sites will be discussed. We will present clear evidence that only one residue - Trp 149 in the α subunit - contributes to ACh binding through a favorable cation-π interaction. This implies that the quaternary ammonium group of agonist ACh is in van der Waals contact with the indole sidechain of αTrp 149, providing the most precise structural information to date on this receptor. In Chapter 3, we report studies of constitutively active receptors with tethered agonists introduced by the nonsense suppression method at α 149. The potential broad usage of the tethered agonist approach will be discussed. In Chapter 4, a brief discussion of studies on the channel gating region is presented and efforts to probe a possible

inter-subunit hydrogen bond are reported. We also describe findings of long range energetic couplings between acidic residues near the binding sites and hydrophobic residues in the channel region, which has subtle implications in agonist binding-induced conformational changes that lead to channel gating. In Chapter 5, a description of the electrophysiological techniques used and a collection of syntheses of the dinucleotide dCA and numerous representative amino acids are documented. In Chapter 6, design and synthesis of a potential alkali metal cyclophane host to explore the scope of cation-π interactions is reported. In addition, the synthesis of an intermediate to a tetraamide host and HPLC separation of a tetraphosphate host P4P are described.

I should point out here that in all these studies, I have collaborated with many outstanding colleagues whose contributions are acknowledged in the proper contexts.

1.6 References

1. D. A. Dougherty, *Pure & Appl. Chem.* **69**, 1969-1977 (1997).
2. D. A. Dougherty, *J. Phys. Org. Chem.* **11**, 1-7 (1998).
3. J. H. van't Hoff, *Arch. Neerl. Sci. Exactes Nat.* **9**, 445 (1874).
4. J. A. Le Bel, *Bull. Soc. Chim. Fr.* **22**, 337 (1874).
5. J. Steiglitz, *Am. Chem. J.* **21**, 101 (1899).
6. J. F. Norris, *AM. CHEM. J.* **25**, 117 (1901).
7. J. F. Norris, Ingraham, J. N., and Sanders, W. W., *Am. Chem. J.* **25**, 54 (1901).
8. F. a. W. Kehrmann, F., *Chem. Ber.* **34**, 3815 (1901).
9. F. a. W. Kehrmann, F., *Chem. Ber.* **35**, 622 (1902).
10. A. Baeyer, V. Villiger, *Chem. Ber.* **35**, 1189, 3013 (1900).
11. M. Gomberg, *J. Am. Chem. Soc.* **22**, 757 (1900).
12. M. Gomberg, *Chem. Ber.* **35**, 3150 (1900).
13. R. W. L. Clarke, A. Lapworth, *J. Chem. Soc.* **91**, 694 (1907).
14. E. S. Wallis, F. H. Adams, *J. Am. Chem. Soc.* **55**, 3838 (1933).
15. E. Buchner, S. Hediger, *Chem. Ber.* **36**, 3502 (1903).
16. J. Allan, A. E. Oxforn, R. Robinson, J. C. Smith, *J. Chem. Soc* , 401 (1926).
17. T. M. Lowry, *J. Chem. Soc.* **123**, 822 (1923).
18. C. K. Ingold, E. H. Ingold, *J. Chem. Soc.*, 1310 (1926).
19. T. H. Lowry, K. S. Richardson, *Mechanism and Theory in Organic Chemistry* (Harper Collins Publishers, New York, NY, 1987).
20. R. G. W. Norrish, G. Porter, *Nature* **164**, 658 (1949).
21. E. D. Becker, G. C. Pimentel, *J. Chem. Phys.* **25**, 224 (1956).
22. A. H. Zewail, *Adv. Chem. Phys.* **101**, 892 (1997).
23. R. B. Woodward, R. Hoffmann, *The Conservation of Orbital Symmetry* (Verlag Chemie, Weiheim, 1970).
24. K. Fukui, *Acc. Chem. Res.* **4**, 57 (1971).

25. J.-M. Lehn, *Angew. Chem. Int. Ed. Engl.* **27**, 89-112 (1988).

26. J. M. Lehn, *Angew. Chem., Int. Ed. Engl.* **27**, 89-112 (1988).

27. D. J. Cram, *Angew. Chem. Int. Ed. Engl.* **27**, 1009-1020 (1988).

28. C. J. Pedersen, *Angew. Chem., Int. Ed. Engl.* **27**, 1021-1027 (1988).

29. D. H. R. Barton, *Experimentia* **6**, 316 (1950).

30. T. T. Tidwell, *Pure & Appl. Chem.* **69**, 211-213 (1997).

31. F. H. Westheimer, *Pure & Appl. Chem.* **69**, 285-286 (1997).

32. Z. W. Hall, Eds., *An Introduction to Molecular Neurobiology* (Sinauer Associates, Inc., Sunderland, MA, 1992).

33. B. Hille, *Ionic Channels of Excitable Membranes* (Sinauer Associates, Inc., Sunderland, MA, 1992).

34. J. G. Nicholls, A. R. Martin, B. G. Wallace, *From Neuron to Brain* (Sinauer Associates, Inc., Sunderland, MA, 1992).

35. C. J. Noren, S. J. Anthony-Cahill, M. C. Griffith, P. G. Schultz, *Science* **244**, 182-188 (1989).

36. J. Ellman, D. Mendel, S. Anthonycahill, C. J. Noren, P. G. Schultz, *Meth. Enzym.* **202**, 301-336 (1991).

37. M. W. Nowak, et al., *Science* **268**, 439-442 (1995).

38. M. W. Nowak, et al., *Methods in Enzymology*, (in press).

39. J. P. Gallivan, H. A. Lester, D. A. Dougherty, *Chem. Biol.* **4**, 739-749 (1997).

40. J. C. Miller, S. K. Silverman, P. M. England, D. A. Dougherty, H. A. Lester, *Neuron* (In press).

41. P. C. Kearney, et al., *Mol. Pharmacol.* **50**, 1401-1412 (1996).

42. P. M. England, H. A. Lester, N. Davidson, D. A. Dougherty, *Proc. Natl. Acad. Sci. USA* **94**, 11025 - 11030 (1997).

43. P. M. England, H. A. Lester, D. A. Dougherty, (manuscript in preparation).

44. M. H. Akabas, A. Karlin, *Biochemistry* **34**, 12496-12500 (1995).

45. A. Devillers-Thiéry, et al., *J. Membrane Biol.* **136**, 97-112 (1993).

46. R. M. Stroud, M. P. McCarthy, M. Shuster, *Biochemistry* **29**, 11009-11023 (1990).

47. B. Katz, R. Miledi, *Proc. R. Soc. Lond. B.* **196**, 59-72 (1977).

48. S. W. Kuffler, D. Yoshikami, *J. Physiol.* **244**, 703-730 (1975).

49. L. W. Role, *Curr. Op. Neurobiol.* **2**, 254-262 (1992).

50. P. B. Sargent, *Ann. Rev. Neurosci.* **16**, 403-443 (1993).

51. A. W. Bannon, et al., *Science* **279**, 77-81 (1998).

52. R. Gray, A. S. Rajan, K. A. Radciffe, M. Yakehiro, J. A. Dani, *Nature* **383**, 713-716 (1996).

53. J.-P. Changeux, et al., *Cold Spring Harbor Symp. Quant. Biol.* **61**, 343-362 (1996).

54. J. Lindstrom, *Mol. Neurob.* **15**, 193-222 (1997).

55. A. Karlin, *Curr. Opin. Neurobiol.* **3**, 299-309 (1993).

56. J. Machold, C. Weise, Y. Utkin, V. Tsetlin, F. Hucho, *Eur. J. Biochem.* **234**, 427-430 (1995).

57. A. Karlin, et al., *J. Biol. Chem.* **258**, 6678-6681 (1983).

58. D. A. Dougherty, *Chirality* **10**, 8-13 (1998).

59. N. Unwin, *J. Mol. Biol.* **229**, 1101-1124 (1993).

60. T. Maeno, C. Edwards, M. Anraku, *J. Neurobiol.* **8**, 173-184 (1977).

61. N. Unwin, *Nature* **373**, 37-43 (1995).

62. M. Noda, et al., *Nature* **299**, 793-797 (1982).

63. M. Noda, et al., *Nature* **301**, 251-255 (1983).

64. M. Noda, et al., *Nature* **302**, 528-532 (1983).

65. T. Claudio, M. Ballivet, J. Patrick, S. Heinemann, *Proc. Natl. Acad. Sci. U.S.A.* **80**, 1111 (1983).

66. K. W. Rickert, B. Imperiali, *Chem. Biol.* **2**, 751-759 (1995).

67. R. Huganir, A. Delcour, P. Greengard, G. Hess, *Nature* **321**, 774-776 (1986).

68. J. F. Hopfield, D. W. Tank, P. Greengard, R. L. Huganir, *Nature* **336**, 677-680 (1988).

69. R. L. Huganir, K. Miles, *Crit. Rev. Biochem. and Mol. Biol.* **24**, 183-215 (1989).

70. R. L. Huganir, P. Greengard, *Neuron* **5**, 555-567 (1990).

71. P. N. Kao, A. Karlin, *J. Biol. Chem.* **261**, 8085-8088 (1986).

72. A. Karlin, M. H. Akabas, *Neuron* **15**, 1231-1244 (1995).

73. P. Charnet, et al., *Neuron* **2**, 87-95 (1990).

74. M. H. Akabas, D. A. Stauffer, M. Xu, A. Karlin, *Science* **258**, 307-310 (1992).

75. H. Zhang, A. Karlin, *Biochemistry* **36**, 15856-15864 (1997).

76. P. Blount, J. P. Merlie, *Neuron* **3**, 349-357 (1989).

77. S. E. Pedersen, J. B. Cohen, *Proc. Natl. Acad. Sci. USA* **87**, 2785-2789 (1990).

78. C. Czajkowski, A. Karlin, *J. Biol. Chem.* **266**, 22603-22612 (1991).

79. R. E. Middleton, J. B. Cohen, *Biochemistry* **30**, 6987-6997 (1991).

80. J.-L. Galzi, J.-P. Changeux, *Neuropharmacology* **34**, 563-582 (1995).

81. M. Dennis, et al., *Biochemistry* **27**, 2346-2357 (1988).

82. J. L. Galzi, et al., *J. Biol. Chem.* **265**, 10430-10437 (1990).

83. P. N. Kao, et al., *J. Biol. Chem.* **259**, 11662-11665 (1984).

84. D. C. Chiara, J. B. Cohen, *FASEB J.* **6**, A106-A106 (1992).

85. S. N. Abramson, W. Fenical, P. Taylor, *Drug Develop. Res.* **24**, 297-312 (1991).

86. S. K. Choi, K. Nakanishi, et al., *Chemistry & Biology* **2**, 23-32 (1995).

87. J. B. Cohen, S. D. Sharp, L. W.S., *J. Biol. Chem.* **266**, 23354-23364 (1991).

88. N. Le Novere, J. P. Changeux, *J. Mol. Evol.* **40**, 155-172 (1995).

89. J.-L. Galzi, et al., *FEBS Lett.* **294**, 198-202 (1991).

90. P.-J. Corringer, et al., *J. Biol. Chem.* **270**, 11749-11752 (1995).

91. G. F. Tomaselli, J. T. McLaughlin, M. E. Jurman, E. Hawrot, G. Yellen, *Biophys. J.* **60**, 721-727 (1991).

92. S. M. Sine, P. Quiram, F. Papanikolaou, H.-J. Kreienkamp, P. Taylor, *J. Biol. Chem.* **269**, 8808-8816 (1994).

93. M. E. O'Leary, M. M. White, *J. Biol. Chem.* **267**, 8360-8365 (1992).

94. C. Cazjkowski, C. Kaufmann, A. Karlin, *Proc. Natl. Acad. Sci. USA* **90**, 6285-6289 (1993).

95. C. Czajkowski, C. Kaufmann, A. Karlin, *Proc. Natl. Acad. Sci. USA* **90**, 6285-6289 (1993).

96. M. D. Martin, A. Karlin, *Biochemistry* **36**, 10742-10750 (1997).

97. D. A. Dougherty, *Science* **271**, 163-168 (1996).

98. P. C. Kearney, et al., *J. Am. Chem. Soc.* **115**, 9907-9919 (1993).

99. A. Collet, J.-P. Dutasta, B. Lozach, J. Canceill, *Top. Curr. Chem.* **165**, 104-129 (1993).

100. H.-J. Schneider, D. Güttes, U. Schneider, *J. Am. Chem. Soc.* **110**, 6449-6454 (1988).

101. D. A. Dougherty, D. A. Stauffer, *Science* **250**, 1558-1560 (1990).

102. J. Sunner, K. Nishizawa, P. Kebarle, *J. Phys. Chem.* **85**, 1814-1820 (1981).

103. J. C. Ma, D. A. Dougherty, *Chem. Rev.* **97**, 1303-1324 (1997).

104. S. Mecozzi, A. P. West, Jr., D. A. Dougherty, *J. Am. Chem. Soc.* **118**, 2307-2308 (1996).

105. S. Mecozzi, A. P. West, Jr., D. A. Dougherty, *Proc. Natl. Acad. Sci. USA* **93**, 10566-10571 (1996).

106. S. Mecozzi, *Ph.D. Thesis* (California Institute of Technology, 1996).

107. S. M. Ngola, D. A. Dougherty, *J. Org. Chem.*, (submitted).

108. J. L. Sussman, et al., *Science* **253**, 872-879 (1991).

109. M. Harel, et al., *Proc. Natl. Acad. Sci. USA* **90**, 9031-9035 (1993).

110. J. Lindstrom, *Mol. Neurobiol.* **15**, 193-222 (1997).

111. M. J. Ackerman, D. E. Clapham, *N. Engl. J. Med.* **336**, 1575-1586 (1997).

Chapter 2

Physical Organic Chemistry on the Nicotinic Acetylcholine Receptor: αTrp 149 is the Cation-π Site for ACh Binding

2.1 Introduction

In Chapter 1, it was noted that there are as many as four tyrosines and four tryptophans near the agonist binding site (Figure 1.2C) in the nAChR and the potential importance of cation-π interactions in ACh binding were discussed. In this chapter, we describe studies aimed to reveal such cation-π site(s) in the nAChR by utilizing a broad spectrum of methods. In such endeavors, we combined the principles of physical organic chemistry in high-precision modifications of chemical structures and properties with the versatility of the *in vivo* nonsense codon suppression method and the unparalled sensitivity of modern electrophysiological techniques.

In our early efforts, postdoctoral fellow Mark W. Nowak and former group member Patrick C. Kearney applied the *in vivo* nonsense suppression method to evaluate three conserved tyrosines at the agonist binding site of the α subunit (1, 2). They found that the hydroxyl group of αTyr 93 functions as a hydrogen bond donor, while the hydroxyl group of αTyr 198 is mostly a steric place-holder. α 190 was shown to be a very sensitive position, many mutations produced either receptors with much elevated EC_{50} values or no detectable functional receptors. Studies with agonists ACh, tetramethylammonium (TMA) and nicotine suggested these agonists all interact similarly with αTyr 93 or αTyr 198. Although these are interesting observations, it seems that none of the tyrosine residues is the primary cation-π interaction site for ACh. The intriguing possibility, then, is that one of the tryptophans at the binding site may be primarily responsible for cation-π interactions (3).

Theoretical studies of the cation-π interaction and surveys of protein structures clearly indicated that Trp represents the most potent cation-π binding site among the natural amino acids (4, 5, 6). A quick examination of the electrostatic potential surfaces (Figure 1.4) of the corresponding aromatics of Phe (benzene), Tyr (phenol), and Trp (indole) reveals that the Trp sidechain (indole) provides a much larger and more intense region of negative electrostatic potential. Indeed, in the crystal structure of the ACh esterase, the only known structure of a natural ACh binding protein, Trp 84 near the active site is believed to be in contact with the quaternary ammonium group of ACh (7, 8, 9). Complex structure of the esterase with decamethonium also identified Trp 279 as the "peripheral anionic site" (Figure 1.5) (10). Recent biochemical studies confirmed the important roles of these aromatic residues (11, 12).

A little surprisingly, perhaps, only limited functional studies have been reported on the binding site tryptophans in nAChR. White *et al.* and Changeux *et al.* have studied mutants of *Torpedo* and α 7 receptors, respectively, and they found a significant role for γTrp 55/ δTrp 57 in both ACh and *d*-tubocurarine binding (13, 14). Changeux *et al.* also found a Phe mutation for αTrp 148 (aligned with αTrp 149 in muscle) in α 7 causes a 91-fold increase in EC_{50} (15). In a study with receptor α subunit peptide fragments, Fraenkel used NMR NOE methods to establish contacts between the quaternary ammonium group of ACh and Trp 184 (16, 17, 18). Based on these findings, we initiated extensive mutagenesis studies using the nonsense suppression method on the four different ACh binding site tryptophans of the mouse muscle nAChR, αTrp 86, αTrp 149, αTrp 184, and γTrp 55/δTrp 57. We found that at one and only one site -

αTrp 149 - EC_{50} correlates strongly with the cation-π binding ability of the aromatic sidechain. We take this as clear evidence that the αTrp 149 sidechain is in van der Waals contact with the quaternary ammonium group of ACh, engaging in a strong cation-π interaction.

2.2 αTrp 149 Interacts Uniquely with ACh

A few critical points should be discussed before we describe any experimental details. As mentioned earlier, we use electrophysiological techniques to evaluate functional receptors. In most of this thesis work, we rely on measurements of EC_{50} values - the agonist concentration required to elicit half maximal response - as the functional probe for specific mutational effects. A word of caution should be given. In the study of complex allosteric proteins such as nAChR, EC_{50} is a composite value, an empirical measure of apparent ligand sensitivity which reflects both agonist binding and channel gating. However, to first order approximation, EC_{50} changes caused by mutations often correlate well with differences in free energy changes ($\Delta\Delta G°$) in receptor activation (19). In our studies, we believe that EC_{50} values reveal mostly binding changes since none of the residues under present investigation is implicated in channel gating (see below). It is also very important to note here that at all sites and for all derivatives, receptor responses display hallmarks of functional nAChR molecules: desensitization with prolonged exposure to agonist, and dose-response relations with Hill coefficients between one and two.

Another important issue that needs to be highlighted is the use of additional βLeu9'Ser mutations for residues that give receptors with very high EC_{50} values. In fact, the EC_{50} for Phe (and others discussed later, such as 5-CN-Trp and 4,5,6,7-F_4-Trp) at α 149 is too large to be accurately measured directly, because at the ACh concentrations required to cover the dose-response relation, ACh itself also becomes an effective channel blocker. As in previous work (2), we have compensated for this by introducing a Leu9'Ser mutation in the M2 region of the β subunit (residue 262). The M2 9' residue is thought to lie some 50 Å from the binding site (Figure 1.2B), and a Leu9'Ser mutation in the β subunit lowers EC_{50} by a consistent factor of ca. 40, most likely by increasing the equilibrium constant for the conformational change that opens the channel subsequent to agonist binding (20). The validity of using the β Leu9'Ser mutation is supported by three entries in Table 2.2 (Trp, 5-Br-Trp, and 5-F-Trp) in which the ratio of EC_{50} values with and without the 9' mutation is the same. This observation also has additional important implications. In conjunction with studies discussed in Chapter 4, we reason that αTrp 149 and βLeu 9' are independent of each other in channel activation, and αTrp 149 has minimal effects in channel gating, and therefore mutations at this site reflect mostly changes in ACh binding affinities. This gives us confidence in using EC_{50} as the probe for cation-π interactions.

We validated our experimental approach by incorporating wild type Trp at the four tryptophan positions using the *in vivo* nonsense suppression with tRNA-Trp. Similar dose responses and identical EC_{50} values to that of wild type were observed (Table 2.1). As a first screen for cation-π site(s), we then suppressed the *amber* stop codon, TAG, one at a time, at the four Trp positions with tRNA-Phe. Note that we are

introducing simultaneously two mutations into the receptor, one at each binding site, because there are two α subunits and when γ and δ are concerned, we use both γ55 and δ57 TAG mutants. We measured EC_{50} values for all the Phe mutants (Table 2.1). At positions α 86 and α 184, the EC_{50} values are 70 μM and 86 μM, respectively, which are within a factor of two-fold higher than that of wild type (50 μM). At γ55/δ57, the effect is bigger but still only *ca.* six-fold.

sidechain[a]	**α 86**	**α 184**	**γ55/δ57**
Trp	50.0±1.0	50.0±1.0	50.0±1.0
5-Br-Trp	53.0±4.1	48.0±1.3	23.0±1.0
5-CN-Trp	61.0±4.0	46.0±3.0	25.0±1.4
4,5,6,7-F_4-Trp	62.4±2.0	45.3±2.1	92.0±6.9
Phe	70.0±3.5	86.0±3.7	286±9.3
2-Np-Ala	81.3±4.7	81.0±2.5	207±7.6
7-N-Trp	—[b]	—	43.0±3.6
N-Me-Trp	—	—	78.0±3.2
Bta	—	—	152±3.1

Table 2.1. EC_{50} (μM) (provided with standard error) for selected Trp mutants at α86, α184, and γ55/δ57 showing that all three sites are substantially insensitive to the electronic properties of the Trp sidechain. Note that the Hill coefficients in these studies are all in the range 1.5 - 2.0. a. See Figure 2.3 for sidechain structures. b. not determined.

However, the Phe mutation at α 149 caused an increase in EC_{50} by over 100-fold. This is in agreement with Changeux's result on neuronal α 7 receptors (15). Without revealing any details about these different Trp sites, the Phe mutation results already clearly indicated a unique role for αTrp 149 in ACh binding. Consistent with this notion, Tyr mutation at α 184 generated a receptor with EC_{50} of 91 μM, but at α 149, it caused a much higher increase in EC_{50}.

2.3 None of αTrp 86, αTrp 184, and γTrp 55/δTrp 57 Interacts Strongly with ACh

After the initial observation on the Phe mutants, we decided to look further for cation-π binding site(s) by incorporating more Trp analogs. In our design and selection of Trp analogs, we tried to maximize changes in sidechain cation binding abilities while minimizing steric perturbations. It should be emphasized here that in such efforts, we turned to theory and high level quantum mechanical calculations for chemical insights and quantitative guidances. At the early stage of the project, my research advisor Dennis A. Dougherty provided electrostatic potential surfaces for a number of aromatics. Later on, our group member Justin P. Gallivan calculated the electrostatic surfaces of many side chain aromatics and the Na^+ binding energies to these aromatics that are relevant in the present study. The methods we used are as described previously (4, 5). All the available Na^+ binding energies are listed in Table 2.2.

It is well established that strongly electron-withdrawing groups such as cyano (CN) and fluoro substantially weaken the cation-π interaction (21). Fluorine is a widely used hydrogen surrogate that can provide a negligible steric perturbation (22, 23, 24), so

direct comparison of fluorinated Trps with the wild type is justified. In considering the cyano group, modeling shows that 5-Br-Trp and 5-CN-Trp are quite similar in size, but they differ considerably in cation-π binding ability, making this also a useful comparison (Figure 2.1). Such a comparison is much preferable than, for example, 5-CN-Trp versus wild type Trp, where both sterics and electronics are changing.

At three sites - α 86, α 184, or γ 55/δ 57 - 5-Br-Trp and 5-CN-Trp receptors were almost identical and were not substantially different from wild type, ruling out a strong cation-π interaction at these sites. In fact, 5-CN-Trp at γ 55/δ 57 produced a receptor with an EC_{50} that is half of wild type, which lies in the opposite direction if cation-π interaction were operative at this site. These data are illustrated in Table 2.1 and Figure 2.2.

Probably more compelling is the result from the 4,5,6,7-F_4-Trp mutations at these sites (Figure 2.2). The cation binding ability of 4,5,6,7-F_4-Trp over the 6-ring is dramatically decreased compared to wild type Trp, as shown in quantum mechanical calculations (Table 2.2). However, while at α 86 and α 184, 4,5,6,7-F_4-Trp had wild type behavior, at γ 55/δ 57, it is only slightly worse (< 2-fold) than wild type, providing convincing evidence that none of these Trp residues is the primary cation-π site. The results for 4,5,6,7-F_4-Trp also support the notion that fluoro substitution does not cause a strong steric perturbation.

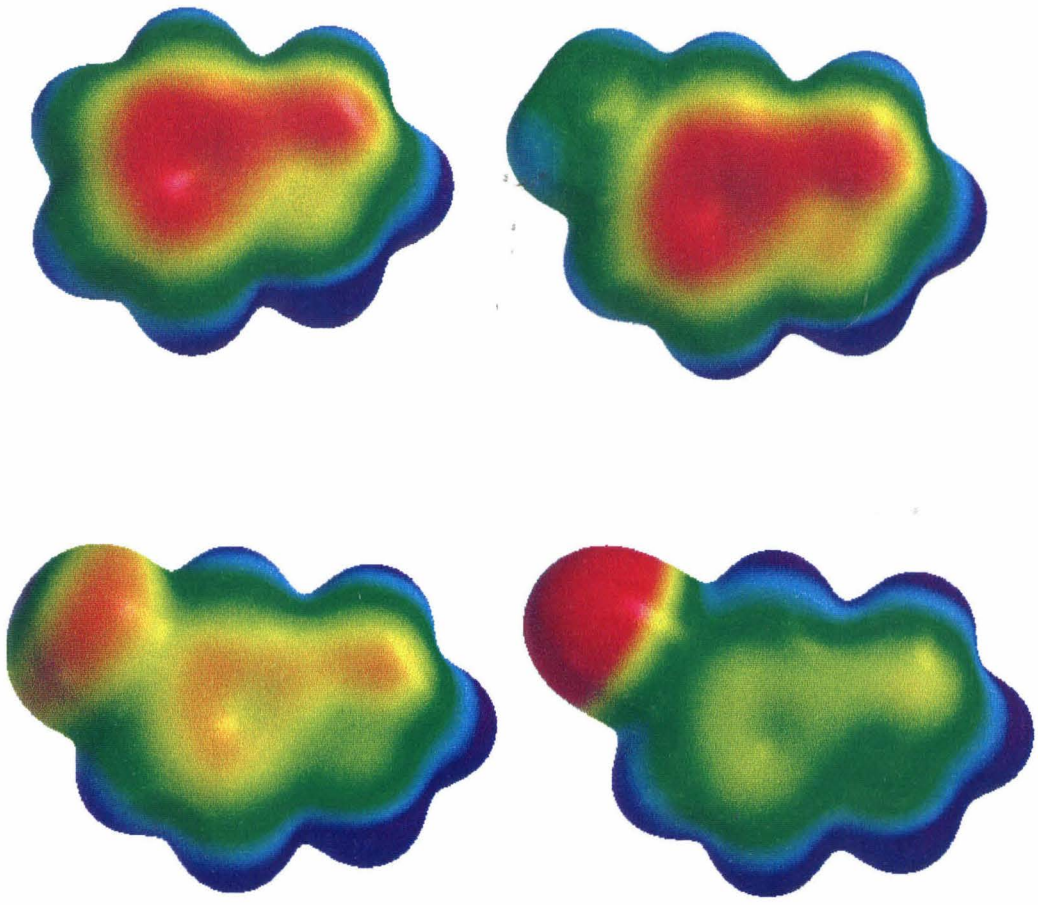

Figure 2.1. The electrostatic potential surfaces for sidechains of Trp (upper left), 5-Me-Trp (upper right), 5-Br-Trp (lower left), and 5-CN-Trp (lower right). Color code: red, negative; blue, positive. It is quite clear that 5-Br-Trp, and 5-CN-Trp are similar in size but differ considerably in cation-π binding ability. 5-Me-Trp resembles wild type Trp electronically while being isosteric to both 5-Br-Trp and 5-CN-Trp.

A. **Mutations at α86**

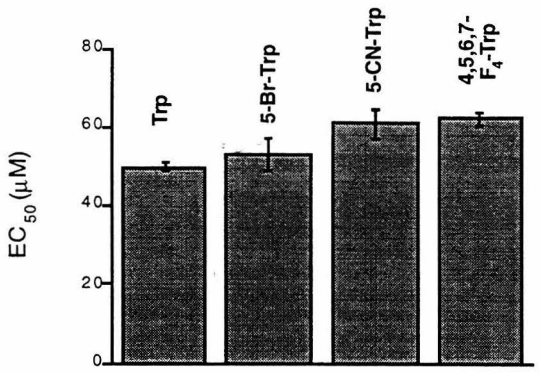

B. **Mutations at α184**

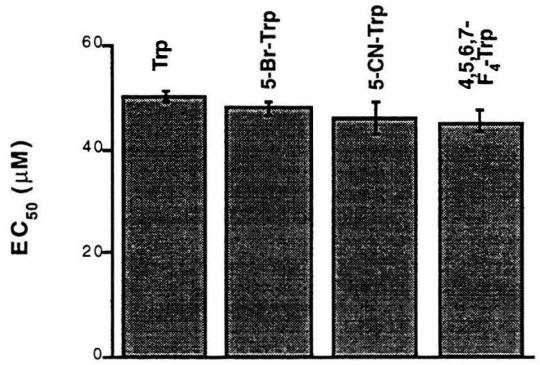

C. **Mutations at γ55δ/57**

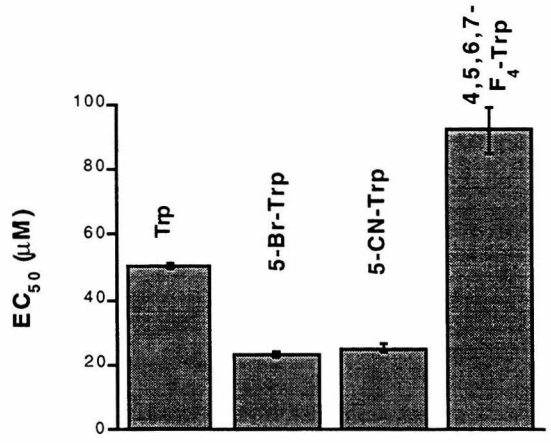

Figure 2. EC_{50} (μM) values for mutants at α86, α149, and γ55/δ57 showing none of these sites is the primary cation-π site for ACh binding (see also Table 2.1 for data).

In addition, we have incorporated other amino acids at these sites (Table 2.1). Together, these data suggest that at sites α 86, α 184, and γ 55/δ 57 in nAChR, Trp is contributing primarily hydrophobic interactions in ACh binding and channel activation.

2.4 αTrp 149 is the Cation-π Binding Site in nAChR

At αTrp 149, however, a very different pattern is seen. 5-CN-Trp gives an EC_{50} that is much greater than wild type and, more importantly, much greater than 5-Br-Trp (Table 2.2), consistent with a role of cation-π interaction at this site. To confirm that this is not a steric effect, we determined that 5-Me-Trp, which is sterically similar to 5-CN-Trp and 5-Br-Trp, but resembles wild type Trp in a cation-π interaction, shows wild type behavior (Table 2.2). The 5-Br-Trp and 5-Me-Trp results suggest that the 5-position of αTrp 149 can accommodate significant steric perturbations, thus providing an ideal position in the indole ring system to explore substituent effects.

Suspecting that cation-π interactions may be important, we studied αTrp 149 more extensively. We successfully incorporated 12 more Trp analogs, besides the ones already discussed above. All the sidechain structures of these residues can be found in Figure 2.3, and the syntheses of these amino acids are documented in Chapter 5. Although every one of these residues are designed to tune side chain cation-π binding abilities, some of them, such as 1-naphthylalanine (1-Np-Ala), 1-N-methyltryptophan (1-N-Me-Trp), and 3-benzothienylalanine (3-Bta), can also serve as probes for hydrogen bond donor capability of the pyrrole N-H of Trp. The EC_{50} values for all these mutant receptors are listed in Table 2.2.

sidechain[a]	cation-π binding[b]	EC_{50}[c,f]	EC_{50}[d,f]
Trp	32.6	1.2±0.0	50±1.0
5-F-Trp	27.5	4.7±0.1	200±7.4
5,7-F_2-Trp	23.3	13±1.1	(550)[e]
5,6,7-F_3-Trp	18.9	34±1.1	(1400)[e]
4,5,6,7-F_4-Trp	14.4	65±2.6	(2700)[e]
5-Br-Trp	27.8	2.0±0.0	88±6.6
5-CN-Trp	21.5	114±3.6	(4750)[e]
5-Me-Trp	33.4	—[g]	49±4.6
4-F-Trp	27.9	—	56±4.0
6-F-Trp	27.4	—	48±3.4
1-Np-Ala	28.9	—	51±1.4
2-Np-Ala	28.9	—	82±3.1
7-aza-Trp	26.0	—	130±5.0
Bta	26.9	—	174±3.5
N-Me-Trp	33.7	—	95±3.4
5-NH_2-Trp	36.4	—	278±5.0

Table 2. EC_{50} (μM) and cation-π binding ability (kcal/mol) for various Trp mutants at position α149. a. See Figure 2 for sidechain structures. b. The cation-π binding is defined as the negative of the binding energy (kcal/mol) of a generic probe cation (Na^+) to the appropriate aromatic ring using ab initio, HF 6-31G** calculations as described previously (4,5). This provides a broadly applicable, quantitative indicator of cation-π binding ability for a series of closely related aromatics. Since the 6-31G** basis set is not available for Br, the 6-311G** basis set was used for 5-Br-Trp, and then the value was corrected based on a linear correlation (R = 0.997) between binding energies for a collection of ten aromatics determined with the two different basis sets. c. For receptors with a βLeu9'Ser mutation - see text. d. For receptors that are otherwise wild type. e. Obtained by multiplying the entries of the adjacent column by a constant factor of 42, to

compensate for the βLeu9'Ser mutation - see text. f. Hill coefficients are generally in the range 1.3 - 1.8, but for the highly inactivated structures (5-CN-Trp and 4,5,6,7-F_4-Trp with β9' Leu/Ser mutations) values as low as 1.0 can be seen. g. not determined.

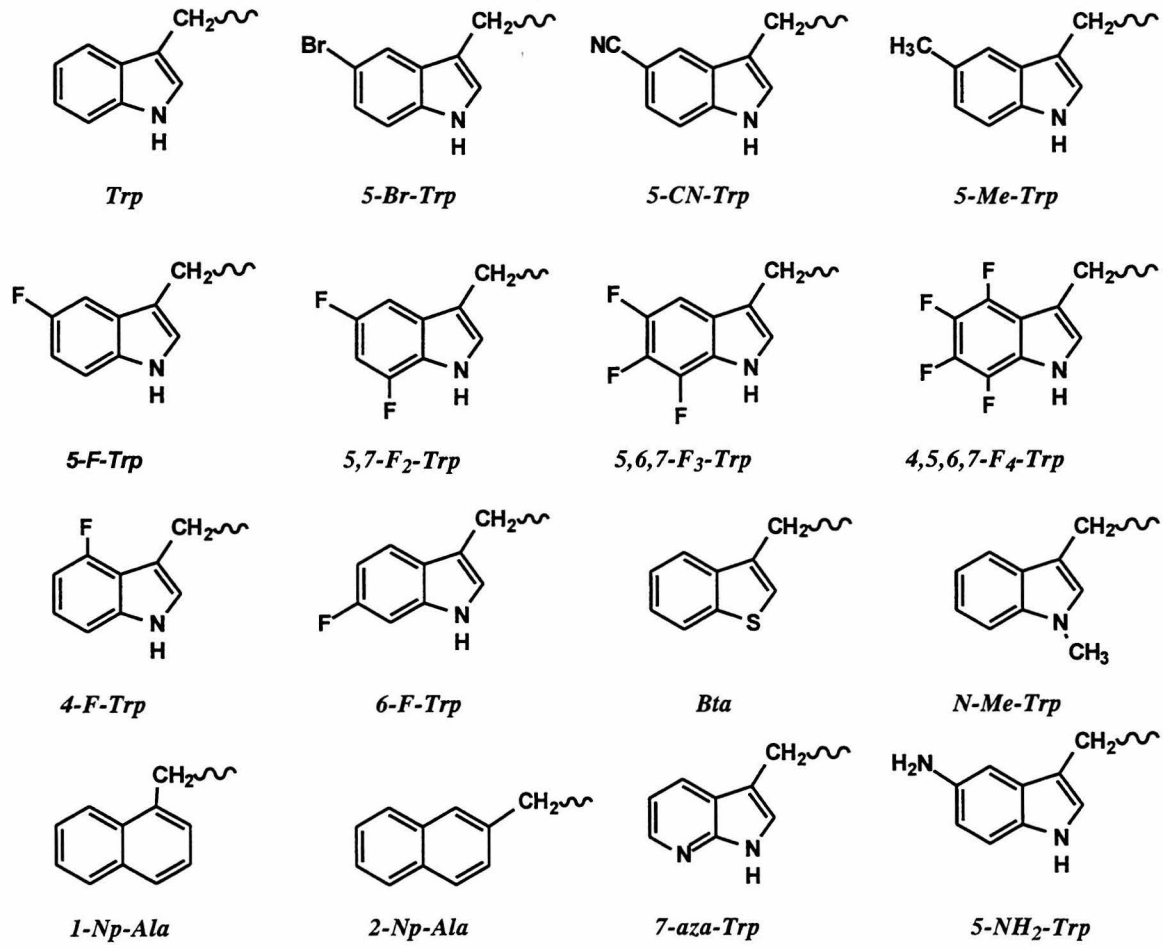

Figure 2.3. Structures of Trp derivatives incorporated by the nonsense suppression method. Non-obvious abbreviations: Bta - benzothienylalanine; 1-Np-Ala, - 1-napthylalanine.

While the results with 5-CN-Trp were suggestive, the most intriguing data come from studies of the fluorinated Trp derivatives. Beginning with 5-F-Trp and moving on to di-, tri-, and tetrafluoro derivatives produces a series of closely related compounds with substantial electronic but minimal steric changes (see Table 2.2 for Na^+ binding energies and Figure 2.4 for their side chain electrostatic potential surfaces). Within such a series, the ever-present concerns that site-directed mutagenesis has led to major structural reorganizations are minimized. This level of control over structural perturbations represents a substantial advantage of the nonsense suppression method.

In Figure 2.5A, representative ACh-evoked current traces for wild type Trp and mutant 5, 7-F_2-Trp are shown. In Figure 2.5B, we plotted the dose-response fits for Trp and four fluorinated Trp derivatives, 5-F-Trp, 5, 7-F_2-Trp, 5, 6, 7-F_3-Trp, 4, 5, 6, 7-F_4-Trp. It is clear that progressive fluorination at position α 149 leads to a systematic increase in EC_{50} (see also Table 2.2).

In fact, Figure 2.6 shows that the relationship is quite compelling. Over a range of nearly two orders of magnitude in EC_{50}, a linear relationship is seen between log(EC_{50}) and the quantitative cation-π binding ability of the sidechain. To the extent that EC_{50} can be considered as proportional to a binding constant in this particular situation, log(EC_{50}) is the appropriate quantity to compare to the cation-π binding energy. The EC_{50} change on going from Trp to 4,5,6,7-F_4-Trp corresponds to over 2 kcal/mol of binding energy. This is a substantial quantity for weakening (but not removing) of a single noncovalent contact, and it requires that the ACh and the Trp sidechain are interacting directly. We

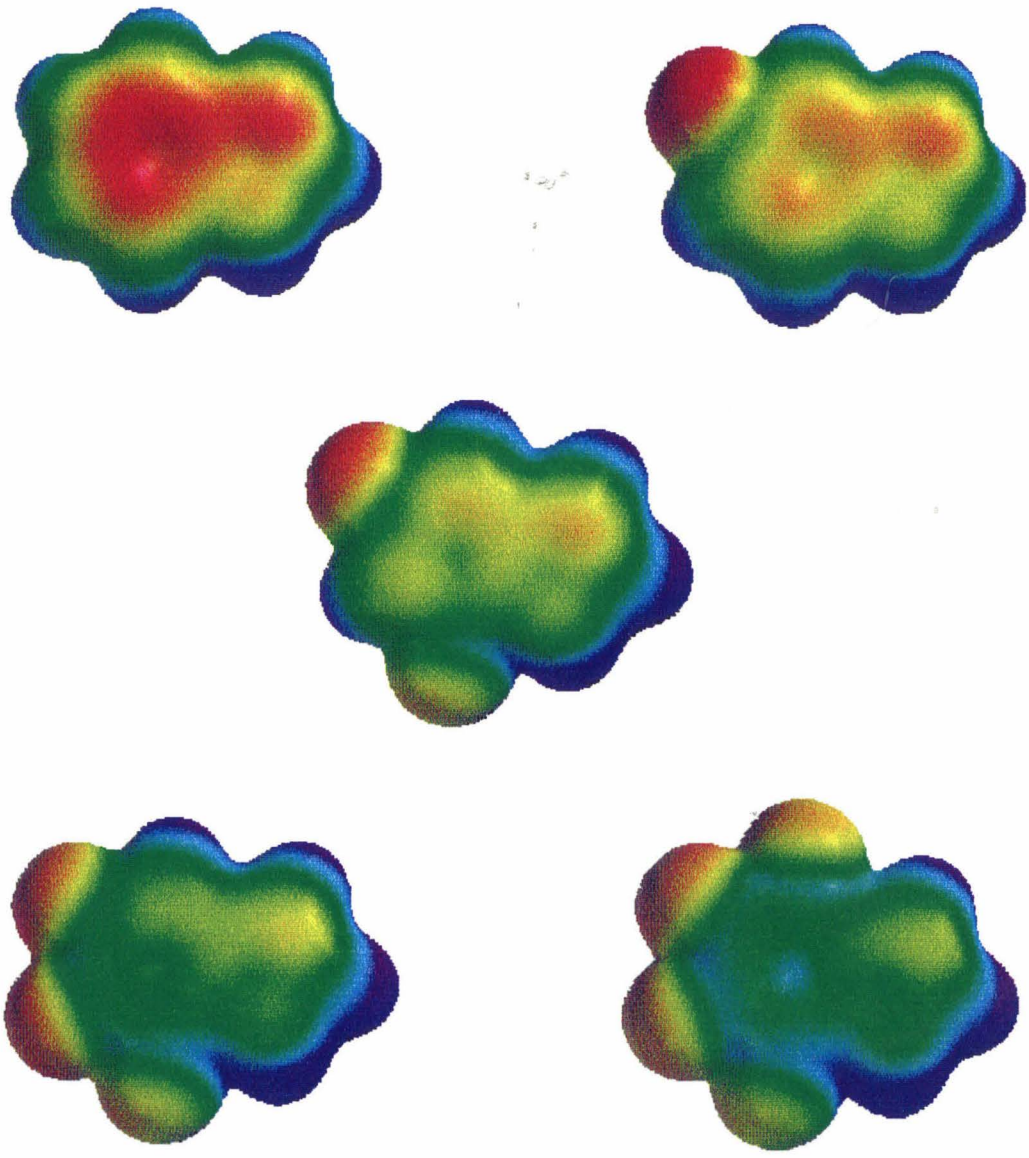

Figure 2.4. The electrostatic potential surfaces for sidchains of Trp (upper left), 5-F-Trp (upper right), 5,7-F_2-Trp (center), 5,6,7-F_3-Trp (lower left), and 4,5,6,7-F_4-Trp. Color code: red, negative; blue, positive. Note that the trend of decreasing cation binding ability of the aromatics correlates well with progressive fluorination.

A.

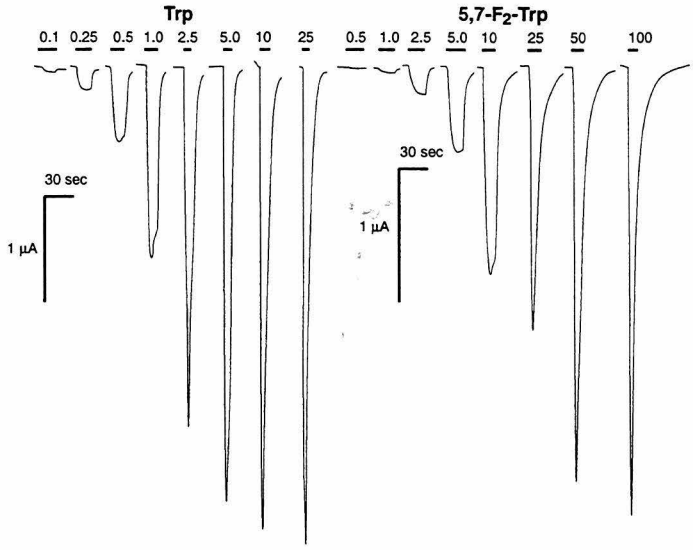

B.

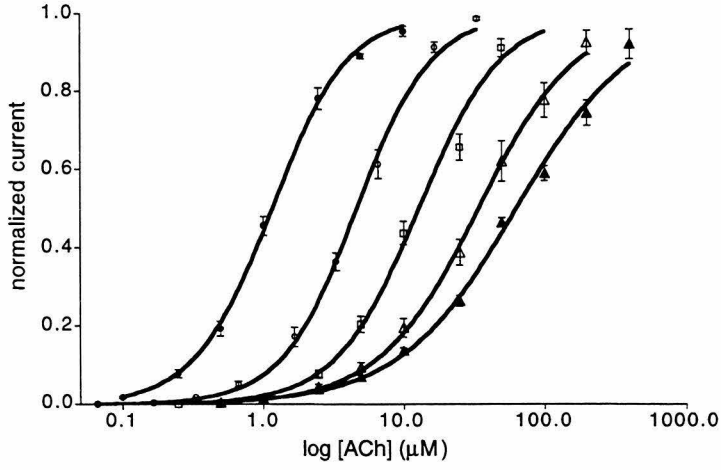

Figure 2.5. A) Representative dose-response measurements for two Trp derivatives at α149, Trp and 5,7-F_2-Trp. B) Dose-response fits for: (left to right) Trp; 5-F-Trp; 5,7-F_2-Trp; 5,6,7-F_3-Trp; 4,5,6,7-F_4-Trp. EC_{50} values are given in Table 2.

note that Figure 2.6 correlates two very different measurements. On one axis are the results of quantum mechanical calculations on small molecule, gas phase complexes; while the other axis shows results from measurements on a MW 290,000 ion channel protein in a living cell. The clear correlation indicates that we have isolated an important interaction in the receptor - a cation-π interaction at αTrp 149.

Inclusion of all the data in Table 2.2 produces a similar plot (Figure 2.7, correlation coefficient R = 0.90). Although the range spanned by the additional entries is not large, for most of the residues, a decrease in cation-π binding implies an increase in EC_{50}. There are a few outliers, as expected for a much broader range of structural variation. The EC_{50} value for 5-NH_2-Trp is much higher than expected, and the differences among the various monofluoro tryptophans are not easily rationalized. These could indicate specific interactions in the receptor, and the 5-NH_2-Trp result in particular is under further investigation in relation to the possibility that the amine is protonated in the receptor.

We consider the data of Table 2.2 and Figure 2.6 to provide convincing evidence that the quaternary ammonium group of ACh makes close contact with the side chain of αTrp 149 in the nAChR. Note that the maximum in cation-π binding occurs over the six-membered ring (6-ring) of Trp, and the calculated cation-π binding energies of Table 2.2 and Figure 2.6 involve such a geometry, so the quaternary ammonium of ACh must be positioned over the 6-ring of αTrp 149 (Figure 2.8). Since the aromatic rings of Phe and Tyr align with the 5-ring of Trp - poorly positioned for a binding interaction - one might expect them to perform poorly at α 149, and this is apparently so. Changeux

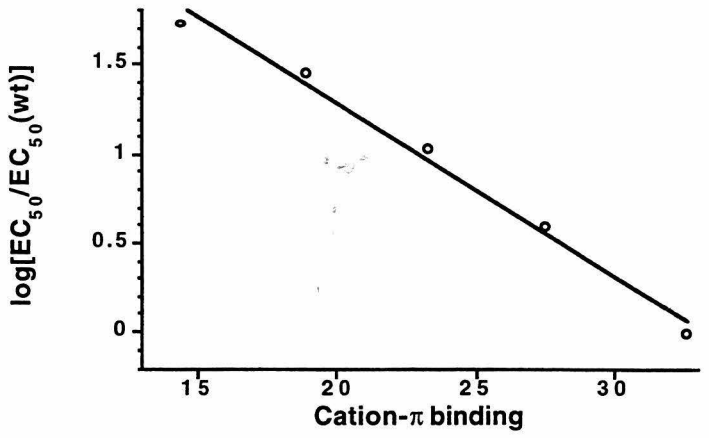

Figure 2.6. Plot of log[EC_{50}/EC_{50}(wild type)] vs. quantitative cation-π binding ability at α149 for the same residues as in Figure 2.5B. Data are from Table 2.2. The data fit the line y = 3.2 - 0.096x, with a correlation coefficient R = 0.99. Note that the values on the x axis refer to isolated molecules in the gas phase, and so the absolute magnitudes of the binding energies are not directly comparable to data from the nAChR, but trends in the data are.

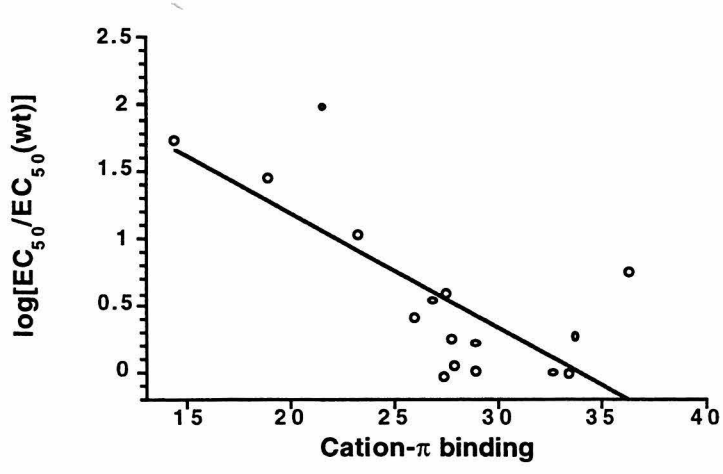

Figure 2.7. Plot of log[EC_{50}/EC_{50}(wild type)] vs. quantitative cation-π binding ability at α149 for all the residues shown in Figure 2.3. Data are from Table 2.2. The data fit a linear line with a correlation coefficient R = 0.90. Note that the two major outliers are 5-NH_2-Trp and 5-CN-Trp.

has found that an analogous Trp-to-Phe mutation in the α 7 neuronal nAChR markedly increased EC_{50} (15). We found that the same mutation at α 149 in the muscle-type receptor increases EC_{50} roughly 100-fold (see section 2.2), consistent with the model that the quaternary ammonium group of ACh is positioned over the 6-ring of αTrp 149.

The model proposed here provides the most precise information to date on the location of the quaternary ammonium group of ACh when bound to the nAChR. It suggests that any means of positioning such a cationic group in close proximity to α 149 might produce an active receptor. In classic experiments, tethered agonists were introduced into the nAChR by attaching structures containing quaternary ammonium groups to the cysteines produced by reducing the highly conserved Cys192-Cys193 disulfide of the α subunit, leading to the conclusion that the quaternary ammonium group interacts with a moiety within 9Å of the disulfide (25, 26, 27). We applied a similar strategy at position α 149 by incorporating the unnatural amino acid Tyr-O3Q (Figure 2.8).

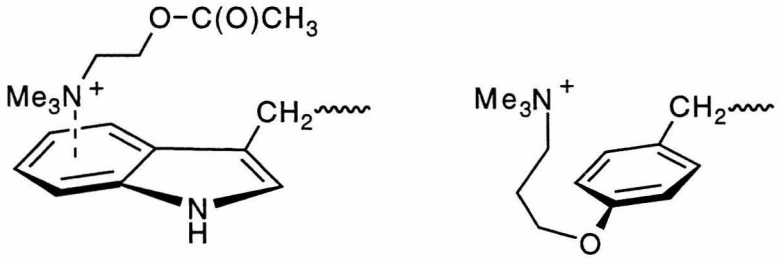

Figure 2.8. Left: schematic of the quaternary ammonium of ACh positioned over the 6-ring of αTrp149. Right: structure of Tyr-O3Q, showing that the tethered quaternary ammonium can be positioned in roughly the same location as the quaternary ammonium of ACh.

Modeling clearly shows that the quaternary ammonium of Tyr-O3Q can achieve the same position as that proposed in the binding of ACh by αTrp 149 (Figure 2.8). Indeed, incorporation of Tyr-O3Q at α 149 produces a constitutively active receptor. Considering size limitations for this chapter and the potentially broad applications of this novel approach, we will report our preliminary results from tethered agonist studies and discuss its future directions in Chapter 3.

2.5 The Role of αTrp 149 in Binding TMA, Nicotine, and *d*-Tubocurarine

In an attempt to probe the role of αTrp 149 in binding other agonists, we initiated studies to evaluate the effects of the various fluorinated Trp mutants in muscle receptors on both tetramethylammonium (TMA) and nicotine. Recall that TMA is a partial agonist while nicotine is a potent full agonist for the nAChRs. Our previous studies at two Tyr sites in α subunit, both agonists establish similar modes of interactions to those of ACh (2).

In this study, we found that TMA screens wild type Trp, and three fluorinated Trp analogs, 5-F-Trp, 5, 7-F_2-Trp, and 5, 6, 7-F_3-Trp, very similarly to that of ACh. It is important to note that we needed to introduce two Leu9'Ser mutations - one each in β and δ - because of the high EC_{50} values for TMA. Shown in Figure 2.9 is a plot of Log(EC_{50}) values for TMA against those of ACh for the corresponding mutants (Data are shown in Table 2.3). The linear correlation with a slope of 0.83 and a correlation coefficient of 0.999 suggests that TMA also binds to αTrp 149 via a cation-π interaction. However, 4, 5, 6, 7-F_4-Trp is an outlier for such a correlation. It is perplexing that its

EC_{50} (262 μM) is some five-fold lower than expected (1340 μM). One possible interpretation is that the cation binding ability of the 6-ring of 4, 5, 6, 7-F_4-Trp is diminished so much that the 5-ring pyrrole now can compete favorably for binding TMA. However, when ACh binds to nAChR, the ammonium group may be held over the 6-ring by interactions established between other sites of the receptor and the ester group of the agonist molecule. This implies that a different binding geometry could be experienced by TMA with 4, 5, 6, 7-F_4-Trp at α 149. This subtle structural reorganization may compensate for the decrease in 6-ring cation binding ability, rendering a receptor with normal-like EC_{50} for TMA.

sidechain	ACh[a]	TMA[b]	Nicotine[a]
Trp	1.2±0.0	47.6±1.7	45.3±0.6
5-F-Trp	4.7±0.1	155.4±3.5	129.8±4.8
5,7-F_2-Trp	13.0±1.1	312.7±8.0	172.3±5.7
5,6,7-F_3-Trp	34.0±1.1	788.6±22.7	187.8±11.4
4,5,6,7-F_4-Trp	65.0±2.6	262.2±11.6	136.4±5.0

Table 2.3. EC_{50} (μM) values for different agonists, ACh (from Table 2.2), tetramethylammonium (TMA), and (-)-nicotine. a. One βLeu9'Ser mutation is also introduced (see text). b. Leu9'Ser mutations are introduced in both the β and δ subunits (see text).

Nicotine showed a quite different pattern. In this set of experiments, one β Leu9'Ser mutation is introduced for reasons discussed earlier. We found that nicotine

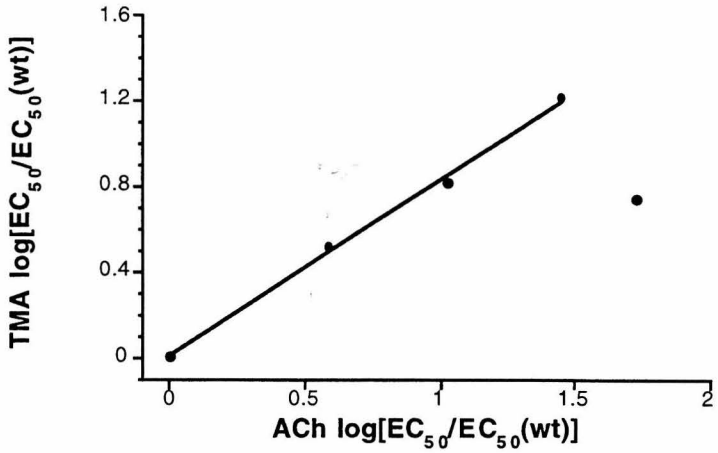

Figure 2.9. Plot of log[EC_{50}/EC_{50}(wt)] for TMA vs. log[EC_{50}/EC_{50}(wt)] for ACh for receptors bearing Trp, 5-F-Trp, 5,7-F_2-Trp, 5,6,7-F_3-Trp at α149, and 4,5,6,7-F_4-Trp. Data are from Table 2.3. The data (without 4,5,6,7-F_4-Trp) fit the line y = 0.001 + 0.83x, with a correlation coefficient R = 0.999.

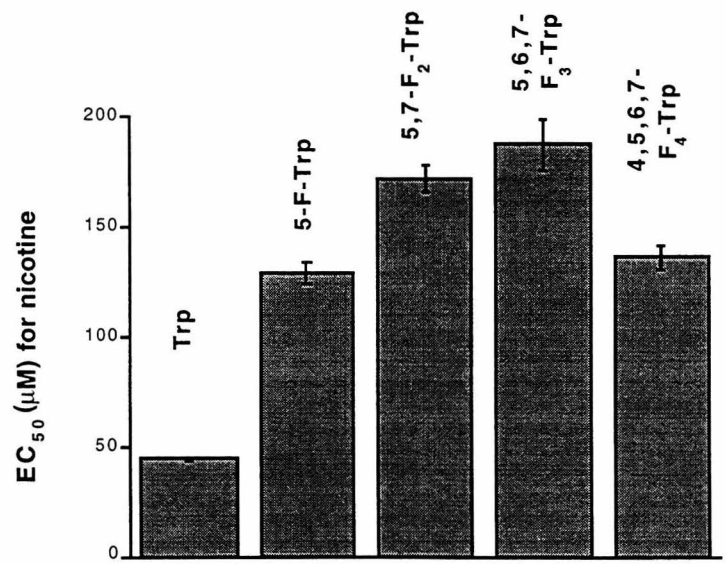

Figure 2.10. EC_{50} (μM) values for (-)-nicotine with receptors containing Trp, 5-F-Trp, 5,7-F_2-Trp, 5,6,7-F_3-Trp, and 4,5,6,7-F_4-Trp at α149. All the mutations caused a three-four fold increase in EC_{50} values, which are within a factor of 2 from each other (see data in Table 2.3).

was relatively insensitive to mutations at α 149, in contrast to what we saw for ACh. The EC_{50} values for the four fluorinated Trp mutants are very similar to each other and are less than four-fold higher than wild type (Table 2.3). This is illustrated in Figure 2.10. In Changeux's study, it was found that the Phe mutation at α 149 caused an increase of 300-fold in EC_{50} for nicotine (15). However, in this study, same mutation caused only a less than ten-fold increase. This seeming discrepancy adds to the already complicated pharmacology of muscle and neuronal nAChR molecules (28).

We also tested the role of αTrp 149 in *d*-Tubocurarine (dTC) binding. We measured the IC_{50} values - the inhibitor concentration required to block half of maximal agonist-induced current - for wild type and three mutants, 5-F-Trp, 6-F-Trp, and 4, 5, 6, 7-F_4-Trp. As shown in Figure 2.11, all these receptors produced almost identical IC_{50}'s, disputing a role for cation-π interactions in binding dTC at this site. Given that γTrp 55/δTrp 57 are implicated strongly in binding dTC, we also tested if these residues can achieve cation-π interactions. However, same IC_{50}'s were obtained for 5-Br-Trp and 5-CN-Trp receptors, inconsistent with such a notion. All the data are summarized in Table 2.4.

Thus far, we have presented some preliminary pharmacological experiments on the muscle nAChR. Further investigations are currently being carried out by postdoctoral fellow Hong Dang in the Lester group on the many interesting and complex issues of muscle and neuronal nAChR pharmacology (28).

sidechain	α149	γ55/δ57
Trp	29.7±1.2	29.7±1.2
6-F-Trp	26.8±1.5	—
5-F-Trp	21.2±0.6	—
4,5,6,7-F_4-Trp	23.5±1.2	—
5-Br-Trp	—[a]	13.7±0.8
5-CN-Trp	—	18.0±1.2

Table 2.4. IC_{50} (nM) of dTC for various mutant receptors. These data were obtained at a constant [ACh] (15 μM). a. not determined.

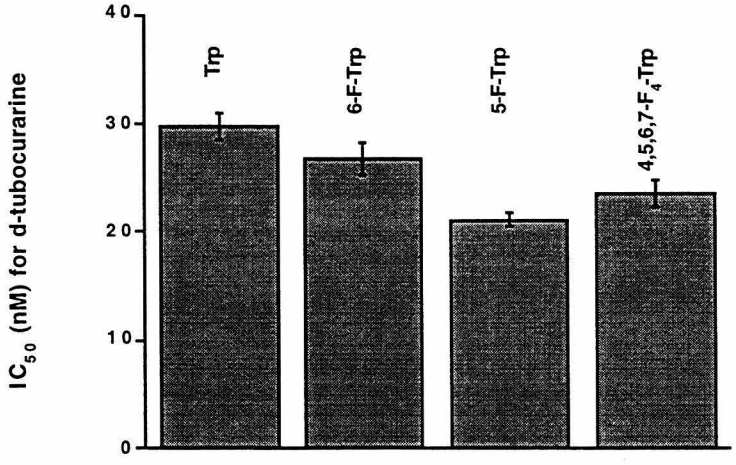

Figure 2.11. IC_{50} (nM) values for receptors containing mutations at α149. Data are from Table 2.4. The Hill coefficients are in the range from 0.75 to 1.0.

2.6 Conclusions and Discussion

We conclude that, based on above observations, αTrp 149 is the primary cation-π binding site for ACh in the nAChR. When ACh binds, the quaternary ammonium group makes van der Waals contact with the 6-ring of the indole side chain. This represents the most precise structural information to date on this complex neuroreceptor. To further support this model, we produced constitutively active nAChR molecules by incorporating an amino acid containing a quaternary ammonium group, Tyr-O3Q, at this site (see Chapter 3). We highlight again that we applied a wide array of methods, ranging from high level quantum mechanical calculations and fine tuning of chemical structures to unnatural amino acid incoporation in *Xenopus* oocytes and electrophysiological recordings. The level of precise structural modification and the isolation of a specific noncovalent interaction in the complex, multisubunit nicotinic receptor presented above is clearly analogous to the sort of physical organic chemistry studies in superamolecular systems. Our result convincingly demonstrated the power of our approach to the study of the many important neuroproteins. We anticipate that this field, physical organic chemistry on the brain, will become ever more fascinating.

We discuss a technical issue regarding the unnatural amino acid incorporation method here. A major setback at the beginning of the project was the contradictory observation between conventional mutagenesis and the nonsense suppression method. While conventional Ala and Leu mutants at α 149 yielded no functional receptors, the suppression method produced wild type-like receptors (in terms of EC_{50}) when tRNA-Ala and tRNA-Leu were used. While suppressed Leu mutants always gave small

currents, the expression levels were quite variable for the suppressed Ala mutant on a day-to-day basis. In general, higher currents could be observed when a large amount of tRNA-Ala was used. To substantiate the conventional results, we made the conventional mutants, along with side-by-side positive controls, using a few different methodologies and confirmed the cDNA constructs by DNA sequencing. We also tested the "translational pausing" hypothesis (29) by introducing both a conventional Ala mutation at α 149 and a TAG mutation at α 151 (which would pause translation to some extent). Rescue of wild type Tyr at α 151, if successful, would provide the α 149 Ala mutant. Not surprisingly but frustratingly, we observed no functional responses, providing further evidence for the validity of conventional Ala mutant. This apparent contradiction still remains to be settled. In order to justify our results for all the suppressed studies, we performed side-by-side comparative experiments. While minimizing the tRNA-Ala suppression to background level, we were still able to produce receptors with several μA maximal currents by injecting with same amount of corresponding tRNA's. The EC_{50} values for these receptors, wild type Trp, 5-Br-Trp, 5-F-Trp, 5,7-F_2-Trp, and 5,6,7-F_3-Trp, which cover the wide range of mutations we have studied, were identical to those determined previously. We thus believe that the remaining controversy is not detrimental to our studies.

It should be mentioned that we have also tried to incorporate pentafluoro-Phe, cyclohexylalanine, homo-Tyr, and 5-MeO-Trp (to test the limit of steric tolerance at the 5-position of indole) at α 149, but we either failed to detect functional responses or observed very small responses.

The present work has general implications on the study of ligand-gated ion channels. We notice that in nAChR's, the aligned position for α 149 is highly conserved as a Trp in all muscle and neuronal α subunits. In non-α subunits, however, the analogous residue is not Trp, generally being Tyr, Gln, and Leu in β, γ, and δ, respectively. It is therefore not a "structural, canonical residue", as has been suggested for Trp86, Tyr151, and Tyr198 (30). The aligned position in 5-HT_3 (serotonin) receptors is also Trp, while it is Tyr in GABA and glycine receptors. It will be interesting to see if these aligned residues in other ligand-gated ion channels are also cation-π binding sites.

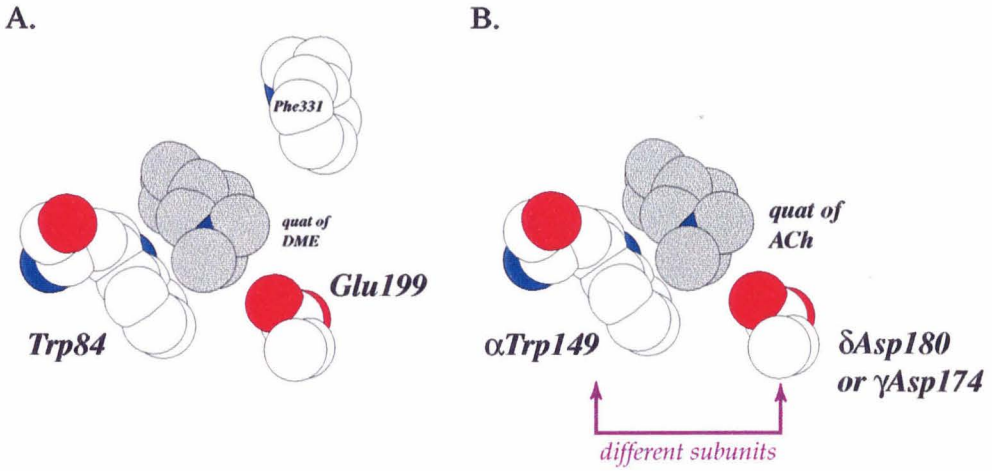

Figure 2.12. An agonist binding site model by analogy to acetylcholine esterase. A. X-ray structure of acetylcholine esterase complexed with decamethonium. B. A highly speculative presentation which presumes that δAsp180 and/or γAsp174 are in close contact with the quaternary ammonium group of bound ACh.

It is also interesting to speculate the role of carboxylate (s) in agonist binding. As revealed in the high resolution structure of acetylcholine esterase, the quaternary ammonium group of ACh makes van der Waals contact with Trp84, as in the model proposed here. Further away, but probably contributing to binding, is the carboxylate of Glu199 (Figure 2.12A) (7, 8, 9). The primary carboxylate implicated in the nAChR is δAsp180/γAsp174, based on work by Karlin. If the binding arrangement in the nAChR is similar to that of the esterase, then αTrp 149 lies very close to δAsp180/γAsp174, and therefore must be at the interface between two subunits (Figure 12B). (This model offers a simple explanation for the result with 5-NH_2-Trp at α 149). Further work to test this model using the suppression methodology is underway.

2.7 References

1. M. W. Nowak, et al., *Science* **268**, 439-442 (1995).

2. P. C. Kearney, et al., *Mol. Pharmacol.* **50**, 1401-1412 (1996).

3. J. C. Ma, D. A. Dougherty, *Chem. Rev.* **97**, 1303-1324 (1997).

4. S. Mecozzi, A. P. West Jr., D. A. Dougherty, *J. Am. Chem. Soc.* **118**, 2307-2308 (1996).

5. S. Mecozzi, A. P. West Jr., D. A. Dougherty, *Proc. Natl. Acad. Sci. USA* **93**, 10566-10571 (1996).

6. D. A. Dougherty, *Science* **271**, 163-168 (1996).

7. J. L. Sussman, et al., *Science* **253**, 872-879 (1991).

8. J. L. Sussman, I. Silman, *Curr. Opin. Struct. Bio.* **2**, 721-729 (1992).

9. M. L. Raves, et al., *Nature Struct. Biol.* **4**, 57-63 (1997).

10. M. Harel, et al., *Proc. Natl. Acad. Sci. USA* **90**, 9031-9035 (1993).

11. A. Ordentlich, et al., *J. Biol. Chem.* **268**, 17083-17095 (1993).

12. I. Schalk, L. Ehret-Sabatier, F. Bouet, M. Goeldner, C. Hirth, *Eur. J. Biochem.* **219**, 155-159 (1994).

13. M. E. O'Leary, G. N. Filatov, M. M. White, *Am. J. Physiol.* **266**, C648-C653 (1994).

14. P.-J. Corringer, et al., *J. Biol. Chem.* **270**, 11749-11752 (1995).

15. P.-J. Corringer, et al., *J. BIOL. CHEM.* **270**, 11749-11752 (1995).

16. Y. Fraenkel, J. M. Gershoni, G. Navon, *FEBS Lett.* **291**, 225-228 (1991).

17. Y. Fraenkel, J. M. Gershoni, G. Navon, *Biochemistry* **33**, 644-650 (1994).

18. Y. Fraenkel, D. E. Shalev, J. M. Gershoni, G. Navon, *Crit. Rev. Biochem. Mol. Biol.* **31**, 273-301 (1996).

19. M. D. Martin, A. Karlin, *Biochemistry* **36**, 10742-10750 (1997).

20. C. Labarca, et al., *Nature* **376**, 514-516 (1995).

21. S. Mecozzi, *Ph.D. Thesis* (California Institute of Technology, 1997).

22. I. Ojima, J. R. McCarthy, J. T. Welch, Eds., *Biomedical Frontiers of Fluorine Chemistry* , vol. 639 (American Chemical Society, Washington D. C., 1996).

23. R. Filler, in *Organofluorine Compounds in Medicinal Chemistry and Biomedical Applications* R. Filler, Y. Kobayashi, L. M. Yagupolskii, Eds. (Elsevier Science Publishers, The Netherlands, 1993), vol. 48, pp. 1-22.

24. R. Filler, Y. Lobayashi, L. M. Yagupolskii, Eds., *Organofluorine Compounds in Medicinal Chemistry and Biomedical Applications*, vol. 48 (Elsevier Science Publishers, The Netherlands, 1993).

25. I. Silman, A. Karlin, *Science* **164**, 1420-1421 (1969).

26. C. Czajkowski, C. Kaufmann, A. Karlin, *Proc. Natl. Acad. Sci. USA* **90**, 6285-6289 (1993).

27. L. D. Chabala, H. A. Lester, *J. Physiol.* **379**, 83-108 (1986).

28. A. Karlin, P. N. Kao, M. DiPaola, *Trends Pharmacol. Sci.* **7**, 304-308 (1986).

29. R. F. Collins, M. Roberts, D. A. Phoenix, *Biochem. Soc. Trans.* **23**, 76S (1995).

30. J.-L. Galzi, J.-P. Changeux, *Neuropharmacology* **34**, 563-582 (1995).

Chapter 3

Introducing A Tethered Agonist into the nAChR

3.1 Introduction

In Chapter 2, we provided convincing evidence that the quaternary ammonium group of ACh makes van der Waals contact with the 6-ring of the indole side chain of αTrp 149 in the nAChR. This precise structural information suggests that any means of tethering a cationic ammonium group in close proximity to α 149 should produce a constitutively active receptor.

In classic experiments, tethered agonists have been shown to a very valuable approach to the study of nAChR structure and function. By reducing the binding site Cys 192-Cys 193 disulfide of the α subunit, Karlin introduced tethered ACh (with bromoacetylcholine, BrACh) and phenyltrimethylammonium (PTA) (with the *p*-nitrophenyl ester of *p*-carboxyphenyltrimethylammonium iodide, NPTMB) and produced constitutively active receptors (1, 2). Lester *et al.* also produced a photoswitchable, constitutively active channel using a similar approach with the reagent Q-Br (3, 4, 5).

We envisioned the *in vivo* nonsense suppression method provides a powerful and more versatile alternative for introducing tethered agonists at many different sites in intact nAChR. By varying tether lengths and tethered functional groups, we can at least start to map out the global layout of the receptor binding site. At many positions, valuable high-resolution geometrical constrains could be obtained, from which we could build a detailed structure of the binding site. Additionally, we could incorporate tethered photocleavable and photoisomerizable agonists, photocleavable channel blockers.

Incorporation of these residues at positions not directly associated with agonist binding site or channel "gate" domain will provide useful information on the relative spatial relationship between functionally distant regions of the receptor. These aspects of the receptor structure, and new insights from other complimentary studies, should facilitate computer modeling for achieving a more realistic atomic-scale receptor structure.

It should be pointed out that at the fore-front of this project, we recognized that our approach differs from the previous tethered agonist studies in that agonist-like functionalities are introduced directly into the receptor while it is being made in living cells. Mark W. Nowak and I first touched upon the tethered agonist project about four years ago, but we were soon forced to stop working on it, simply because we had not seen any encouraging results (we were not sure what to look for; we often wished that the oocytes injected with various amino acids bearing a quaternary ammonium group would die due to the production of constitutively active channels).

Another technical point worth mentioning is that making the NVOC protected cyanomethyl ester of amino acids having a cationic ammonium group was not trivial. After numerous futile efforts, we finally devised a general scheme for the synthesis of this class of unnatural amino acids. Details can be found in Chapter 5.

3.2 Introducing Tyr-O3Q at α 149

We applied our strategy at position α 149, incorporating the unnatural amino acid Tyr-O3Q (Figure 3.1). Model clearly shows that the quaternary ammonium group of

Tyr-O3Q can achieve the same position as that proposed in the binding ACh in the bound nAChR (Figure 2.10). Indeed, we observed constitutively active receptors when Tyr-O3Q is incorporated at α 149, supporting our cation-π binding model at this site. This finding opens the possibility that many unnatural amino acids bearing a cationic sidechain group can be incorporated into neuroproteins using the nonsense suppression method, allowing broad applications of the tethered agonist approach.

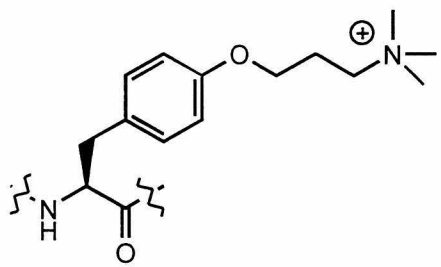

1

Figure 3.1. The chemical structure of Tyr-O3Q.

As shown in Figure 3.2, in the absence of added ACh, standing inward currents in standard Ringer solution (500 - 3000 nA) and substantially reduced resting membrane potentials are consistently seen in *Xenopus* oocytes expressing the mutant channel with Tyr-O3Q at α 149. Exposure of the oocytes to channel blockers such as QX-314 and TMB-8 immediately and reversibly reduces the standing inward current and leads to more typical resting membrane potentials. Substitution of the Na^+ and K^+ ions by much larger organic cation N-methyl-D-glucoamine (NMDG) in Ringer solution also reversibly decreases the standing currents to comparable level as affected by the channel blockers.

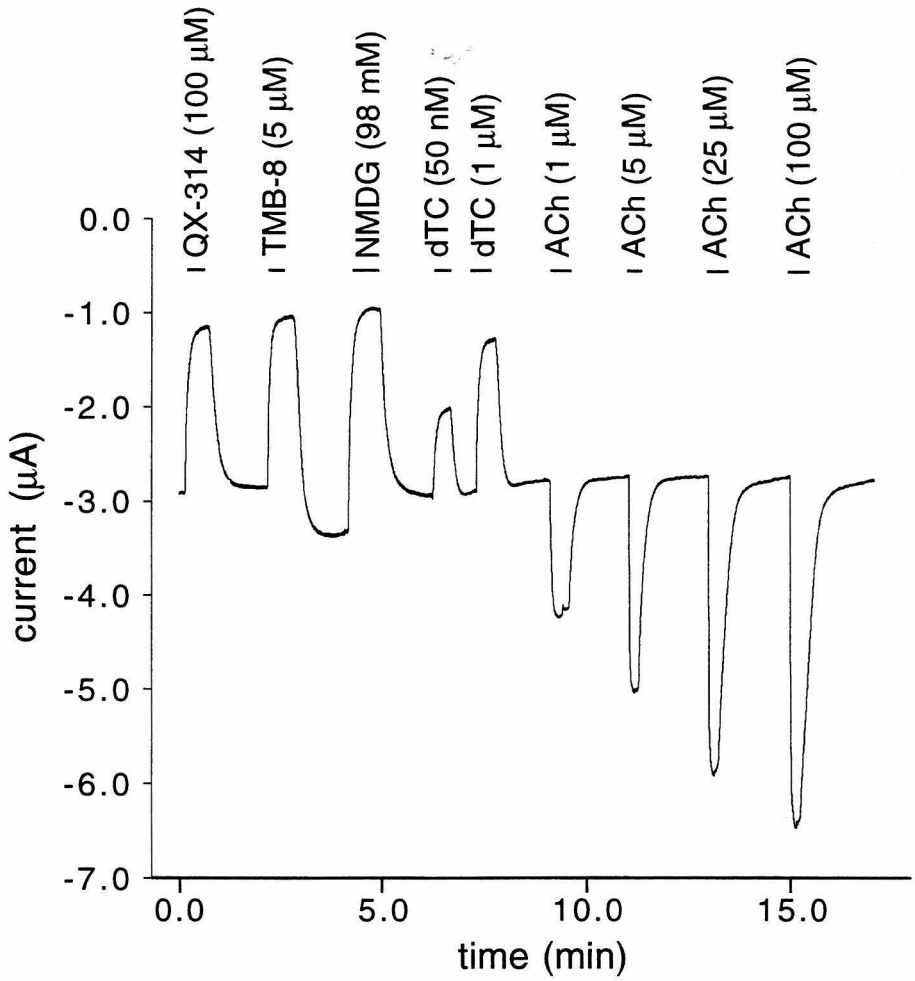

Figure 3.2. Behavior of the nAChR with Tyr-O3Q incorporated at α149, and a Leu9'Ser mutation in M2 of the β subunit. The initial current of almost -3 µA is the leak current that is inherent to the mutant channel. The leak current is substantially, but not completely, elminated by channel blockers such as QX-314 and TMB-8 or the well-known antagonist curare (dTC). Application of ACh leads to increased currents.

We note that the tethered quaternary ammonium appears to be a fairly weak agonist, as standing currents are observed only when a Leu9'Ser mutation is incorporated into the M2 region of the β subunit. While a Leu9'Ser mutation in a single subunit of muscle receptors increases the sensitivity to ACh and decreases desensitization, by itself it does not activate receptors (6). Without a Leu9'Ser mutation, normal cell resting membrane potentials (-40 to -50 mV) and leakage currents (-20 to -70 nA at -80 mV) were seen. We also point out that with two Leu9'Ser mutations, one each in β and δ, standing current levels were still in the range similar to those with only the β Leu9'Ser mutation. Therefore, we carried out the following studies using just one Leu9'Ser mutation in the β subunit.

3.3 ACh Induces Additional Inward Currents

We tested the idea that the tethered quaternary ammonium group is a partial agonist when compared to ACh itself and other features of the ACh molecule are presumably required for full activation of the nAChR. Indeed, application of ACh produces additional inward currents (Figure 3.2), in agreement with the hypothesis. Not surprisingly, however, EC_{50} for added ACh is at least five-fold greater than the normal value of 1.2 μM (Table 2.2), suggesting that the tethered agonist restricts ACh access to the agonist binding site. This is different from observations in the tethered agonist study with Q-Br, in which addition of carbamylcholine, a potent full agonist of nAChR, could not induce further channel activation, a fact that may be attributable to the steric size of the Q-group (3).

3.4 α-Bungarotoxin and *d*-Tubocurarine Block Standing Currents

To verify that the currents are at least largely from constitutively active nAChR molecules, we exposed the oocytes expressing such mutant channels to high concentrations of ACh (25 - 100 μM) for a long period of time. We found that such treatments led to desensitization of both the standing currents and the responses to further ACh applications (data not shown). We further evaluated the effect of α-bungarotoxin, a specific, high affinity competitive antagonist for nicotinic receptors (7). As shown in Figure 3.3, we can see that prolong exposure to 125 nM α-bungarotoxin leads to channel blockade by as much as 30% of all the standing currents, or 50% of that blockable by TMB-8 in this study. More interestingly, the blocking effect can be reversed after washing with the standard Ringer's solution for ca. 5 minutes. In control experiments, wild type or other mutant receptors with neutral residues at α 149 can all be completely irreversibly blocked by the same treatment with α-bungarotoxin. This is not surprising; it has been shown that α-bungarotoxin binding to nAChR can be inhibited to certain extent in the presence of added agonist ACh or antagonist *d*-tubocurarine (dTC) (8, 9). By tethering a quaternary ammonium at the binding site, one should expect the binding affinity of α-bungarotoxin to be reduced. In previous studies, Karlin and co-workers found that tethering ACh at or near the binding could reduce α-bungarotoxin binding by as much as 50% (10, 11), in agreement with our results.

We also found that dTC can block the standing currents. At 50 nM, a value near its K_i for wild type receptor (12), dTC can inhibit about half of the TMB-8 blockable current. At 1 μM, it almost blocks as much as TMB-8 does (Figure 3.2). This implies

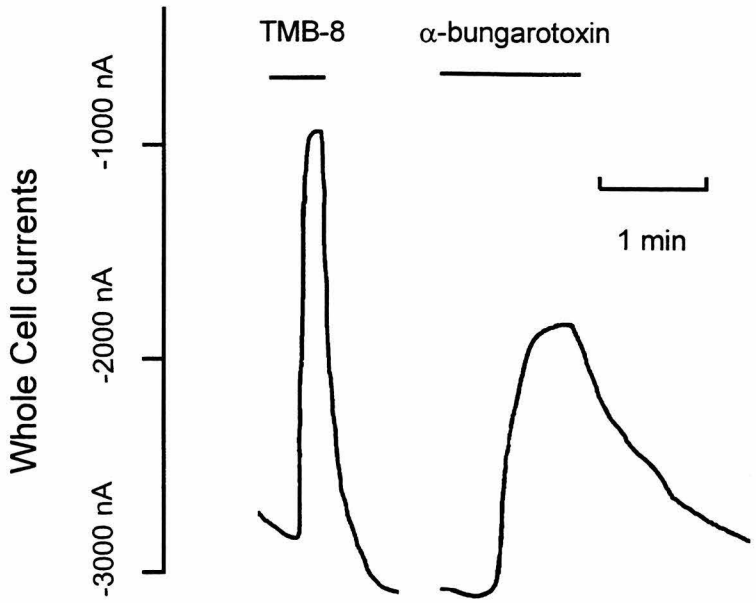

Figure 3.3. α-Bungarotoxin blocks the standing currents of nAChRs with Tyr-O3Q incorporated at α149, and a Leu9'Ser mutation in M2 of the β subunit. Note that the blocking effect can be reversed within minutes by washing the oocytes with the standard Ringer's solution.

that IC_{50} for this mutant receptor is much greater than wild type. In Karlin's study, he found that dTC should be added at a concentration that is 400-fold of its K_i for wild type in order to reverse the tethered agonist-induced depolarization (equivalent of current in our studies) (1). This result suggests that dTC binding site does not overlap with the cation-π site or that the tethered quaternary group can be displaced by dTC. Considering the intrinsic flexibility in protein binding sites and the available data on ACh/dTC binding to nAChR, one might favor the later possibility (1).

3.5 Single Channel Studies of the Constitutively Active Receptor

Since high level expression (ca. 3 μA) of the mutant receptors could be achieved, we performed cell-attached patch clamp studies. Postdoctoral fellow Yinong Zhang at the Lester and Zinn laboratories measured the single channel conductances and analyzed mean channel open times. The actual single channel trace in shown in Figure 3.5. We found that the slope conductance for this mutant channel was 43 pS, identical to that of wild type. This result provided very strong evidence that the macroscopic standing currents were due to the nAChR containing Tyr-O3Q at α 149. The open time distribution was best described by two exponentials with time constants of 0.38 ms, 67% and 1.44 ms, 33%, respectively.

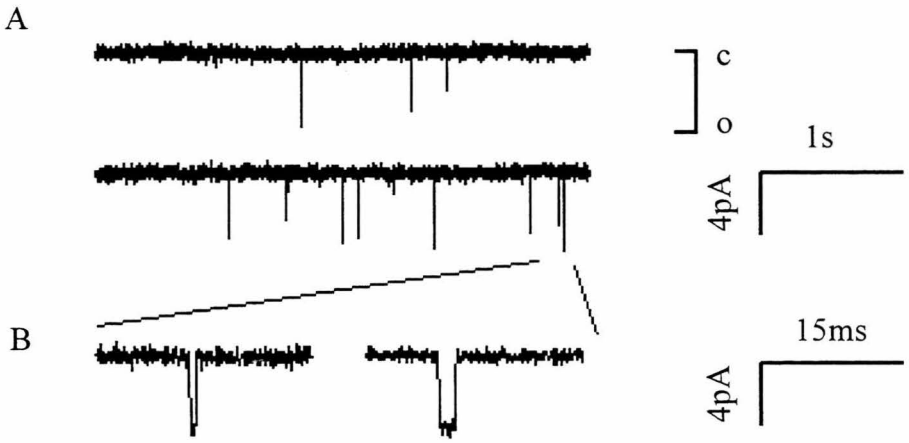

Figure 3.4. Examples of single channel recordings from oocytes expressing nAChRs with Tyr-O3Q incorporated at α149, and a Leu9'Ser mutation in M2 of the β subunit. Single channel records are shown at low (A) and high (B) time resolution. The pipette potential was held at +80 mV. Recordings were made at room temperature with an Axopatch-1D amplifier and analyzed with pCLAMP software (Axon Instruments, Foster City, CA). Single-channel currents were filtered at 5 kHz and stored on a digital data recorder (Neurodata DR-384, Neurodata Instruments Corp., New York). The data were played back and re-digitized at 20 kHz.

3.6 Conclusion and Future Directions

We conclude that these initial findings clearly establish that positioning a quaternary ammonium group near the region normally occupied by αTrp149 can be enough to activate the receptor. In a more general sense, we have demonstrated that it is possible to introduce tethered agonists into the nAChR. We expect much broader and more extensive applications of the tethered agonist approach in addressing many interesting structural issues of this prototypical ligand-gated channel.

Given our encouraging result with Tyr-O3Q at α 149, more experiments should be performed to further characterize the mutant receptor. Voltage-step experiments will reveal the voltage dependence of these mutant channels, providing additional information to determine if essentially all the standing currents are from constitutively active nAChRs. In this regard, experiments with calcium chelators would also be informative in that contributions, if any, of calcium-activated endogenous chloride channel currents in oocytes would be uncovered.

Further work includes incorporation of Tyr-O3Q around the agonist binding site. For example, we should incorporate this residue at the other three Trp sites as well as the Tyr sites in the α subunit in order to probe more residues that are possibly in close proximity to the quaternary ammonium group. Other tethered agonists should also be explored. As shown in Figure 3.5, two very interesting residues, one bearing a quaternary ammonium group (ε-trimethyllysine, **2**), and the other a carbamylcholine moiety (Lys-carbamylcholine, **3**), have already been made and are awaiting to be exploited. A

perhaps more interesting direction that should be taken is to vary the tether length of Tyr-O3Q systematically and create a series of tethered agonists (for example, **8**, **9**, **10** shown in Figure 3.5). Incorporating these novel residues into nAChR would provide detailed and valuable atomic-scale information. This project is now being actively pursued by first year graduate student Lintong Li in our lab.

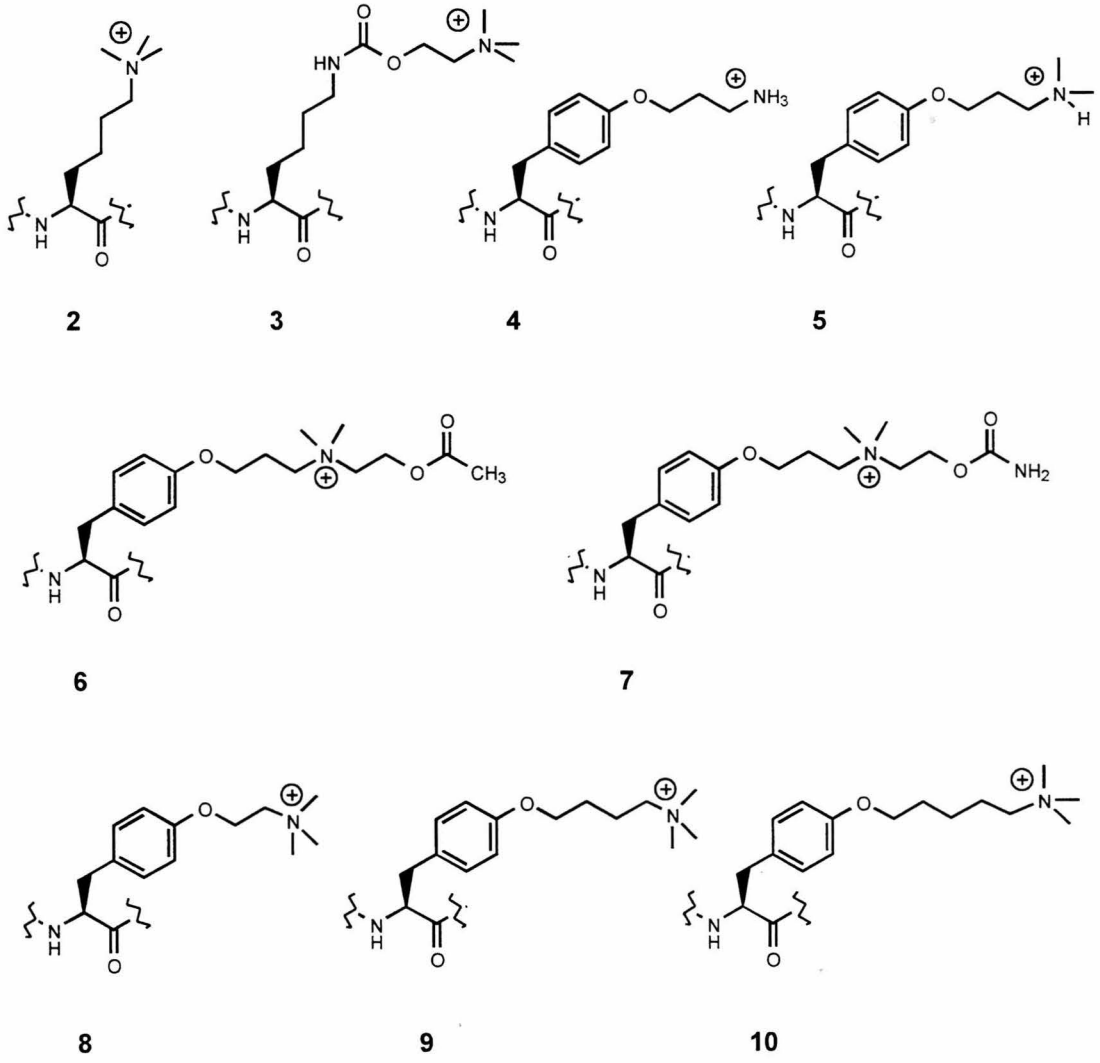

Figure 3.5. The chemical structures of potential tethered agonists.

In Chapter 2, we discussed the intriguing possibility that there is a carboxylate anion near the quaternary ammonium group of ACh in bound receptor. Residue **4** (Figure 3.5) seems to be a very promising candidate for crosslinking studies. Incorporation of this amino acid into nAChR presents an alternative method to Karlin's elegant study that identified γD174/δD180. Also, we noted the complicated pharmacology of the nicotinic receptors in Chapter 2. Residues such as **5** (Figure 3.5) can be used to probe important site(s) in both muscle and neuronal nAChRs that interact with the pyrolidinium group of nicotine. It is clear now that this powerful approach allows many structural questions to be investigated.

3.7 References

1. I. Silman, A. Karlin, *Science* **164**, 1420-1421 (1969).

2. A. Karlin, *J. Gen. Physiol.* **54**, 245-264 (1969).

3. H. A. Lester, M. E. Krouse, M. M. Nass, N. H. Wassermann, B. F. Erlanger, *J. Gen. Physiol.* **75**, 207-232 (1980).

4. H. A. Lester, et al., *Ann. N.Y. Acad. Sci.* **346**, 475-490 (1980).

5. H. A. Lester, M. E. Krouse, J. M. Nerbonne, N. H. Wasserman, B. F. Erlanger, *Light-activated compounds as probes for nicotinic acetylcholine receptors*. N. J. M. Birdsall, Ed., Drug Receptors and Their Effectors (MacMillan, London, 1981).

6. C. Labarca, et al., *Nature* **376**, 514-516 (1995).

7. S. G. Blanchard, et al., *Biochemistry* **10**, 1875-1883 (1979).

8. C. Czajkowski, C. Kaufmann, A. Karlin, *Proc. Natl. Acad. Sci. USA* **90**, 6285-9 (1993).

9. M. Martin, C. Czajkowski, A. Karlin, *J. Biol. Chem.* **271**, 13497-13503 (1996).

10. V. N. Damle, A. Karlin, *Biochemistry* **17**, 2039-2045 (1978).

11. D. A. Stauffer, A. Karlin, *Biochemistry* **33**, 6840-6849 (1994).

12. M. W. Nowak, et al., *Science* **268**, 439-442 (1995).

Chapter 4

Couplings Between Distant Regions in the nAChR: Acidic Residues Near the Agonist Binding Site and Hydrophobic Ones in the Channel Pore

4.1 Introduction

In this chapter, we will focus our attention on the channel gating region of the nAChR, which is situated some 50 Å away from the agonist binding site (Figure 1.2B). An important goal in the study of ion channel gating is to relate functional measurements to the structures of side chains thought to move during channel opening and closing. These include residues located directly at the channel "gate" and those implicated in conformational changes that link agonist binding event to the channel gating event.

It is particularly appropriate to study the role of a leucine residue which is highly conserved in the M2 domain of nearly all known subunits of nAChRs. In one numbering system, the leucine residues align at the 9' position in the M2 region (Figure 4.1) (1). There is evidence that these residues, as well as nearby residues at 6' and 10', contribute to the conduction pathway (1-4). In one interpretation of structural data at 9 Å resolution, the five 9' sidechains (one each from the two α, the β, the γ, and the δ subunits) form an axial constriction that prevents current flow through the closed channel. Channel opening is accompanied by movements of these 9' leucine residues, removing the physical block to conduction (5). Other models also posit a crucial role in gating for 9' residues (6).

It has been shown by Labarca *et al.* that a Ser mutation at this position consistently decreases EC_{50} by about ten-fold and that the effects are multiplicative in multiple Leu9'Ser mutations (7). To a first approximation, this suggests that each leucine governs gating in an independent and symmetrical manner. However, detailed analysis of

A.

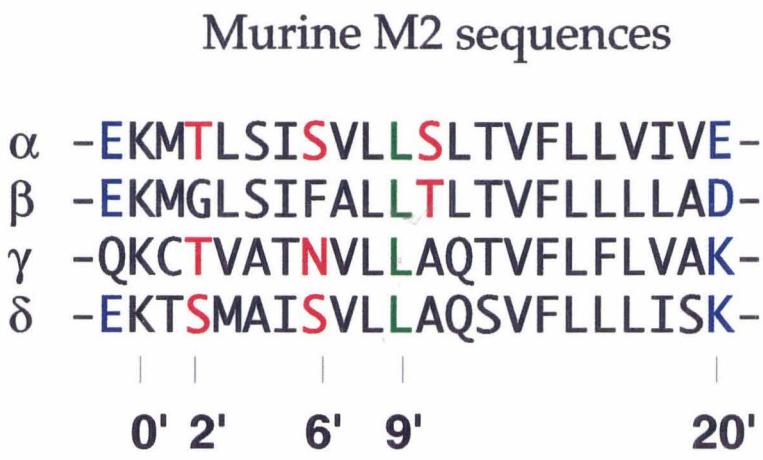

B.

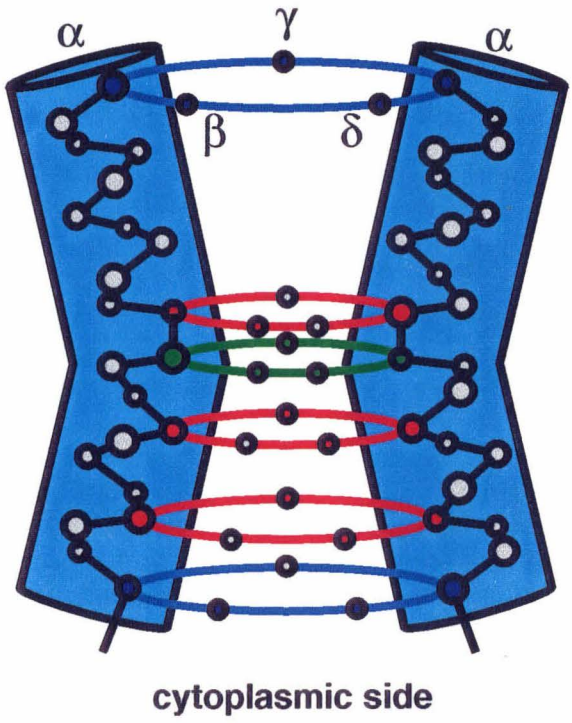

Figure 4.1. A. Sequences of the M2 region for the four subunits of the mouse muscle nAChR. B. A model for the channel "gate" formed by leucine residues at 9' position (green) (5).

these data indicates that individual mutations are not identical, as though some subunit pairs have a special relationship.

Moving away from the gating region, we are also interested in finding residues that couple agonist binding events to channel opening and closing. One acidic residue, δAsp 180 (and the aligned γAsp 174), seems to fit such a role. In Karlin's elegant crosslinking studies, this residue is shown to be 9 Å away from the binding site disulfide bond, and it is likely to interact with the cationic quaternary ammonium group of bound ACh (8-11). In another study with adult muscle nAChR, Auerbach showed that the aligned residue in adult muscle receptor, εD 175, is strongly involved in channel gating (12). In our earlier studies, we established that the side chain hydroxyl group of binding site residue αTyr 93 is a hydrogen bond donor to an as yet unknown functional group from the receptor (13, 14). There is an interesting possibility that a hydrogen bond is formed between αTyr 93 and δAsp 180 (likewise between αTyr 93 and γAsp 174). Note that this putative hydrogen bond is a high precision structure which necessitates both residues at subunit interfaces (Figure 4.2).

Patrick C. Kearney initiated a detailed study of possible interactions among the leucine residues at 9' positions in the M2 region using the in vivo nonsense suppression method (15). My most significant contribution to this project was the realization and synthesis of two pairs of diastereomeric amino acids: O-methylthreonine/*allo*-O-methylthreonine (O-Me-Thr/*allo*-O-Me-Thr) and

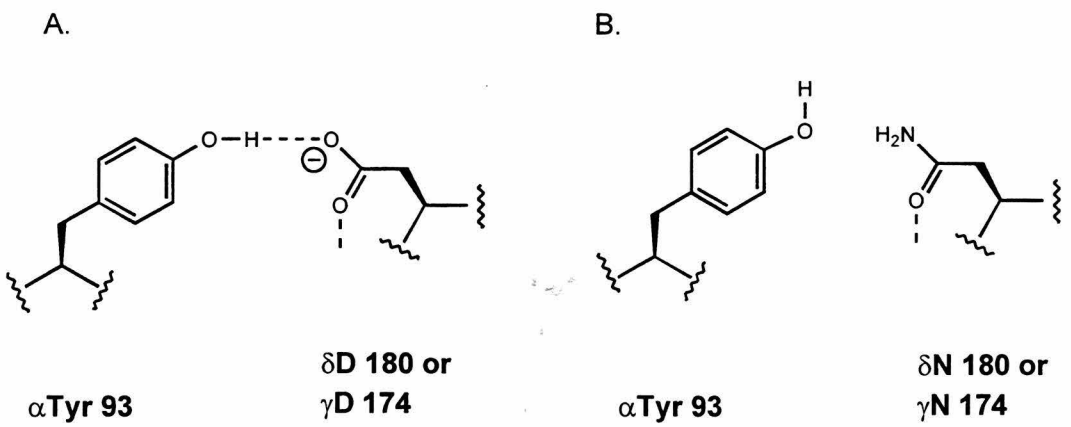

Figure 4.2. A) The putative hydrogen bond between αTyr 93 and δAsp 180/γAsp 174. Note that this model places these residues at the subunit interfaces. B) The presumed disruption of the putative hydrogen bond by Asp-to-Asn mutation in both δ and γ subunits.

isoleucine/*allo*-isoleucine (Ile/*allo*-Ile). Their structures are shown in Figure 4.3 and their synthesis is reported in Chapter 5. Since this work has been published, we simply note here that the incorporation of these pairs of amino acids indicated that increased hydrophilicity in the side chains at the 9' position consistently increases the sensitivity to ACh, confirming earlier findings with Ser mutations at this position. More interestingly, the incorporation of the Ile/*allo*-Ile pair, whose side chains share identical size and hydrophobicity and differ only in the placement of a methyl versus an ethyl group, revealed subtle local asymmetry at the 9' position in the δ subunit. An additional Leu9'Ser mutation in β essentially obliterated this distinction, suggesting a special pairing relationship between the β and δ subunits. This systematic study which allowed the precise dissection of contributions from side chain size, hydrophobicity/hydrophilicity, and chirality to channel activation - the correlation of

structure and function - can be viewed as a classical example of physical organic chemistry on the brain.

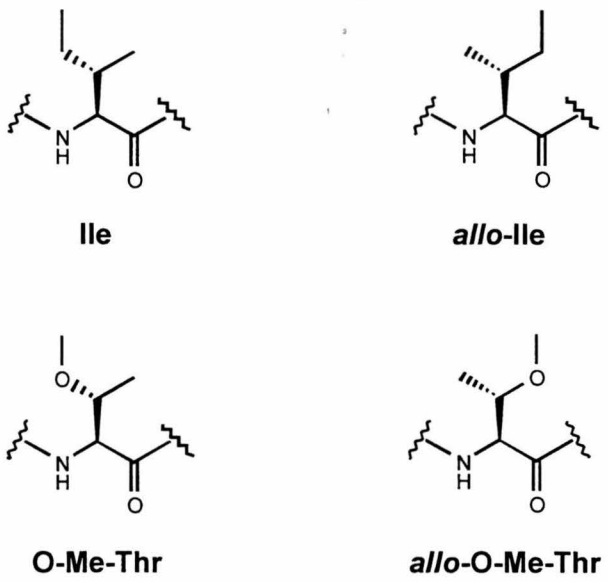

Figure 4.3. The diastereomeric pairs of amino acids: Ile/*allo*-Ile and O-Me-Thr/*allo*-O-Me-Thr. Note that residues in the same column are isosteric in size but different in side chain hydrophobicities.

In the following sections, we will present our finding of distant energetic couplings between γD 174/δD 180 near the binding site and leucines at the 9' position in the channel gating domain. In addition, studies on the putative hydrogen bond between αY 93 and γD 174/δD 180 at subunit interfaces will be discussed.

Before we go on, a technical issue should be discussed. We employed a "double-mutant cycle" approach in these studies, in which changes in EC_{50} values serve

as tests for coupling between pairwise mutations (16-19). There are evident ambiguities in applying such analyses to multisubunit allosteric proteins such as the nAChR (20). However, as discussed in Chapter 2, to a first approximation, EC_{50} changes (on a logarithmic scale) caused by mutations often correlate well with differences in free energy changes ($\Delta\Delta G°$) in receptor activation. In a double-mutant cycle, changing each individual residue can be expected to significantly change the EC_{50}, but not necessarily to the same degree. If the two residues under study are interacting strongly with each other, simultaneously mutating them to disrupt the set of forces in-between would produce a receptor with an EC_{50} that is different from a predicted value derived directly from effects caused by the individual mutations. That is, the difference in free energy change for the double mutant channel activation (compared to wild type) would be different from the simple addition of those of the two individual mutants. Therefore, if the ratio of changes in EC_{50} (compare to wild type) are not multiplicative (i.e., not additive on the logarithmic scale) in double mutant cycles, one would expect some sort of interactions or distant energetic couplings between the two residues. However, if they are multiplicative, a lack of strong interaction, if any, can be inferred.

4.2 Coupled Effects Between Leu9' in M2 and γD174/δD180

We used the double-mutant cycle strategy to examine possible distantly coupled effects between γD174/δD180 and the highly conserved leucine residue at the 9' position in the M2 domain. Leu9'Ser (denoted L9'S) mutations in all four subunits were introduced and separately combined with Asp-to-Asn (denoted D-to-N hereafter) mutations at γ 174 and/or δ 180. We note here that we will identify receptors by their

specific mutations from now on, e.g., γD174NδD180N represents the receptor that bears D-to-N mutations in both γ and δ subunits at the designated sites. The measured macroscopic EC_{50} values for various combined mutants are shown in Table 4.1. All the receptors were tested with ACh, with maximum currents in the range of 1.5-5 μA and Hill coefficients in the range between 1.3 and 1.9.

Pore Mutation	Binding Site Mutation			
	Wild-type	δD180N	γD174N	γD174NδD180N
α_2L9'S	0.50±0.01 μM **1**	3.10±0.05 μM **1**	7.9±0.3 μM **1**	47.3±0.8 μM **1**
βL9'S	1.22±0.02 μM **2.4**	78±1 μM **25**	62±2 μM **7.8**	~307±4 μM **~6.5**
γL9'S	4.5 μM **9.0**	31.5±0.5 μM **10**	76±2 μM **9.6**	~244±4 μM **~5.1**
δL9'S	1.00±0.05 μM **2**	15.7±0.5 μM **5.1**	19.6±0.1 μM **2.5**	~137±5 μM **~2.9**
Wild-type	49±3.0 μM **98**	~267±6 μM **~86**	~207±5 μM **~26**	~360±3 μM **~7.6**

Table 4.1. EC_{50} values for receptors with combinations of L9'S, δD180N and γD174N mutations. Each EC_{50} value was averaged from 3-5 oocytes for each receptor. The standard error estimates were provided, except those for the γL9'S receptors, which were adapted from (7). The EC_{50} values that were larger than 100 μM may contain systematic errors due to open-channel blockade and receptor desensitization. Therefore, they were indicated with the "~" symbol. The values in bold are normalized to those with the α_2L9'S mutations (the top row).

We found that the D-to-N mutations decrease ACh sensitivity. Receptors with a γD174N or δD180N mutation give EC_{50} values that are about fivefold higher than wild type; while the double mutant γD174NδD180N had an EC_{50} value of 360 μM, more than sevenfold higher than wild-type (Table 4.1, bottom row). The dose-response relations for wild type and γD174NδD180N are shown in Figure 4.4. These results suggested that at positions γD 174 and δD 180 acidic residues facilitate channel opening more than neutral ones.

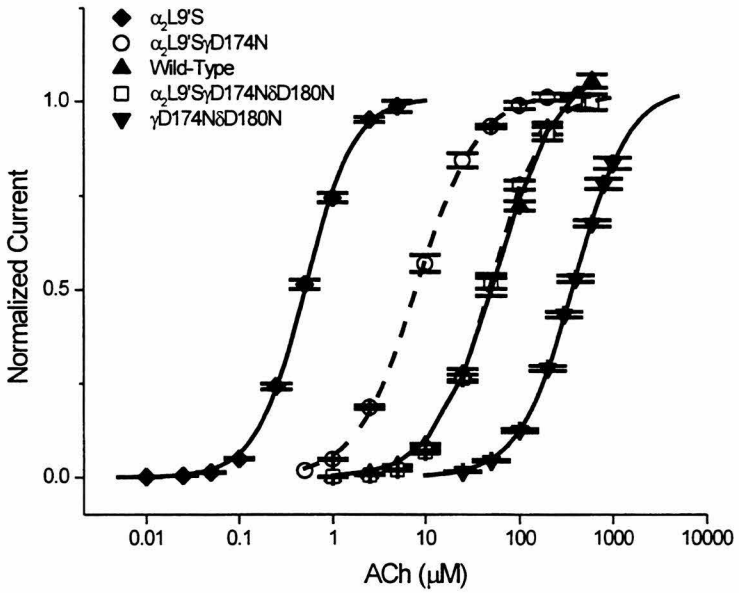

Figure 4.4. Dose-response relations for wild type and mutant receptors. The membrane potential was held at -80 mV. The data shown are averages of at least five oocytes for each receptor. The standard errors are given. The smooth lines are the Hill equation fits to the data (see Chapter 5 for details).

It has been well established that L9'S mutations increase the receptor sensitivity to ACh (decrease EC_{50}), opposite to γD174N and δD180N mutations (7). But the effects of these mutations were not all independent of each other, since the EC_{50} changes of double mutants were not always multiplicative of the corresponding single mutant values. The α_2L9'S receptor, for example, has an EC_{50} of 0.5 μM, 100-fold lower than wild type (Table 4.1 and Figure 4.4). The γD174NδD180N mutant, on the other hand, has an EC_{50} of 360 μM, more than sevenfold higher than wild type. When α_2L9'S and γD174NδD180N were combined, a multiplicative effect would have predicted an EC_{50} of about 3.6 μM, yet 47 μM was actually observed. This is also true for L9'S in β, γ, and δ subunits. For all the mutant receptors containing γD174NδD180N, a factor of 10 to 20 is consistently seen between the expected EC_{50} values and the experimentally determined ones, indicating coupled effects between these residues. The couplings are weaker for receptors bearing only one D-to-N mutation. The double mutants γ(L9'S, D174N), δ(L9'S, D180N), and δL9'SγD174N as well as α_2L9'SγD174N displayed EC_{50} values only about fourfold higher than expected. Interestingly, γL9'SδD180N and α_2L9'SδD180N have EC_{50} values almost exactly as expected. Therefore, these pairs of mutations are likely to be independent of each other.

4.3 βL9' Couples Most Strongly with γD174 and/or δD180

L9'S mutation in the β subunit causes a 40-fold decrease in EC_{50} (Table 4.1, see also ref. (7)). In the present study, we found that γD174N or δD180N increased EC_{50} by about 5-fold. If assuming that γD174N or δD180N is independent of βL9'S in channel activation, an EC_{50} of ca. 6 μM would be expected for double mutant βL9'SδD180N or

βL9'SγD174N. The actual observations, however, were 78 μM and 62 μM, respectively. The 10-fold deviation from prediction is the biggest among mutant receptors with only one D-to-N mutation, indicating the distant coupling between βL9'and γD174 and/or δD180 is the strongest, corresponding to about 1.5 kcal/mol in free energy change of channel activation. In addition, the predicted EC_{50} for mutant βL9'SγD174NδD180N is 9 μM, 33-fold lower than the actual value of 307 μM, consistent with a special role for βL9'S in such long range couplings.

Shown in Figure 4.5 are log-log plots of EC_{50} values normalized to those of the corresponding receptors without γD174N or δD180N mutations (e.g., the EC_{50} for βL9'S γD174N is adjusted to that of βL9'S). Such a comparison clearly shows that the receptor with βL9'S has the largest normalized EC_{50} value, whether it is γD174N, δD180N, or γD174NδD180N, revealing strong distant coupling between βL9'and γD174 and/or δD180.

Another interesting observation can be illustrated by ratios shown in the bold numbers from Table 4.1, which are the EC_{50} values normalized to those in the top row, which are for receptors bearing α_2L9'S. For the receptors bearing γL9'S, the four normalized EC_{50} values were 9.0, 10, 9.6, and 5.1, within a factor of two of each other. The receptors bearing δL9'S behaved similarly. However, for receptors with βL9'S, the four numbers are 2, 25, 7.8, and 6.5, varying by as much as 10-fold. This implies that similar modes of distant coupling can be found for αL9', γL9', and δL9', while βL9' couples to γD174/δD180 differently. This can also be visualized clearly in Figure 4.5A.

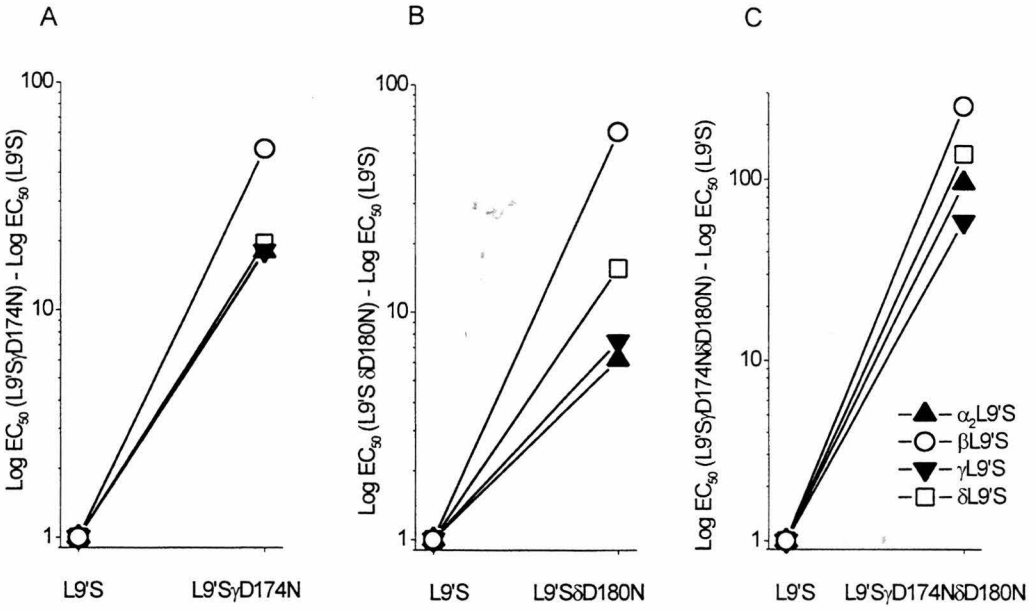

Figure 4.5. Comparisons of EC_{50} values before and after the introduction of γD174N and/or δD180N mutations to the L9'S mutations. The values for receptors containing D-to-N mutations are normalized to those of receptors having only the corresponding L9'S mutations, e.g., the EC_{50} for βL9'S γD174N is adjusted to that of βL9'S. A. Receptors with the γD174N mutation. B. Receptors with the δD180N mutation. C. Receptors with the γD174NδD180N mutations.

In summary, we found that the effects of γD174N and/or δD180N mutations were not independent of the L9'S mutations in most combinations of mutations. The aspartic acid residues near the binding site are energetically coupled, over a distance of about 50 Å, to the highly conserved leucines at the 9' position in the M2 pore region, and the coupling is the strongest for the leucine in the β subunit.

4.4 Single-Channel Analysis of αL9'SγD174N and αL9'SγD174NδD180N

To understand the kinetic changes underlying the inter-dependence between the γD174/δD180 residues and the leucine 9' residues, we examined the single-channel behavior of the receptors with mutations at these sites. Former Lester group graduate student Haiyun Zhang generated single channel data and performed initial data analysis. Graduate student Jun Li in the same lab is responsible for the extensive single channel data analysis and modeling presented herein (21, 22).

We have chosen to examine receptors containing α_2L9'S, based on the fact that the agonist binding site is primarily associated with this subunit. We focused on four receptors: wild type, α_2L9'S, α_2L9'SγD174N and α_2L9'SδD180NγD174N. The first two receptors have been described in more detail elsewhere (21).

The single-channel chord conductances were measured at -100 mV. They were 76 ± 1 pS (n = 24) for α_2L9'SγD174N, 76 ± 2 pS (n =10) for α_2L9'SγD174NδD180N, and 79 ± 2 pS (n =11) for α_2L9'S (Table 2). They were, however, about 20% larger than that of the wild type, 64.6 ± 0.7 pS (n =17). One interesting similarity among the mutant receptors is that they often enter rather brief (<1 ms) subconductance states before entering the main conductance state (data not shown), although the subconductance states accounted for less than 1% of the integrated conductance. In this study we have treated them as closed. Figure 4.6A shows examples of single channel openings for the wild type and the three mutant receptors. The corresponding open- and closed-time histograms are shown in Figures 4.6B and 4.6C.

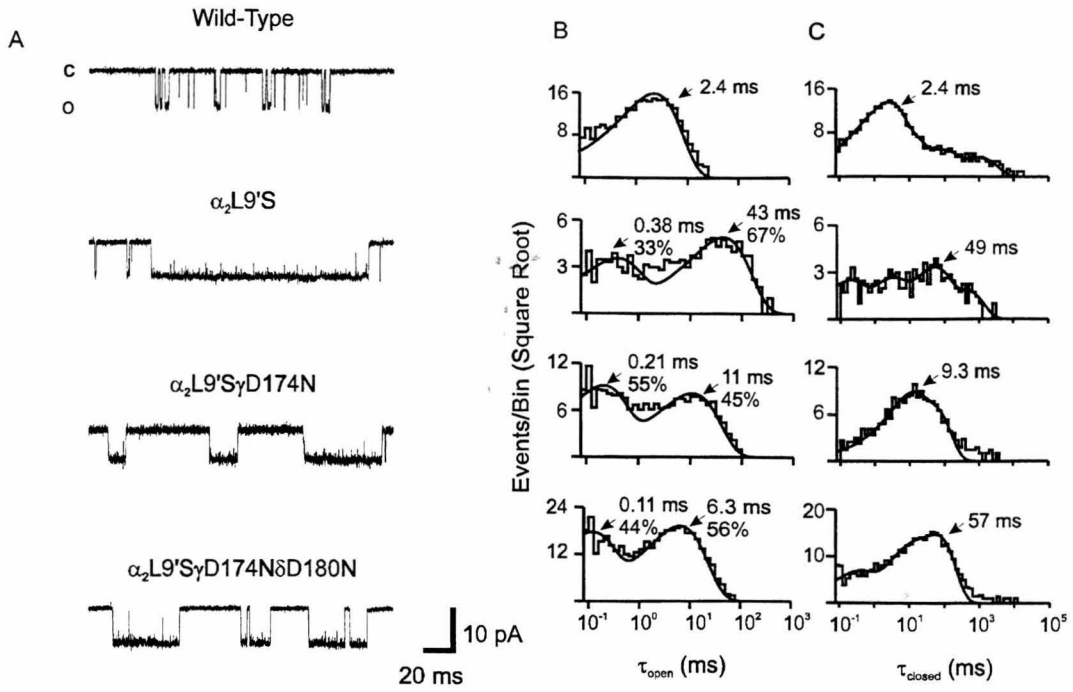

Figure 4.6. Examples of single-channel openings and open-time histograms. A. Continuous current traces. B and C. Open- and closed-time histograms for the patches shown in A. The data are binned with a logarithmic time scale and are plotted on a square-root events-count axis, so that the apparent peaks correspond to the open-time exponential components. The solid lines are exponential fits to the binned data. The time constants of exponential components are indicated by arrow (see Chapter 5 for details).

The dose-response relations are shown in Figure 4.7. The P_{open} values were derived from within bursts. The EC_{50} value from these dose-response relations is 28 μM for α_2L9'SγD174NδD180N, 31 μM for the wild type, and 0.46 μM for α_2L9'S, differing less than twofold from their corresponding macroscopic values. We did not plot the dose-response for α_2L9'SγD174N due to insufficient data.

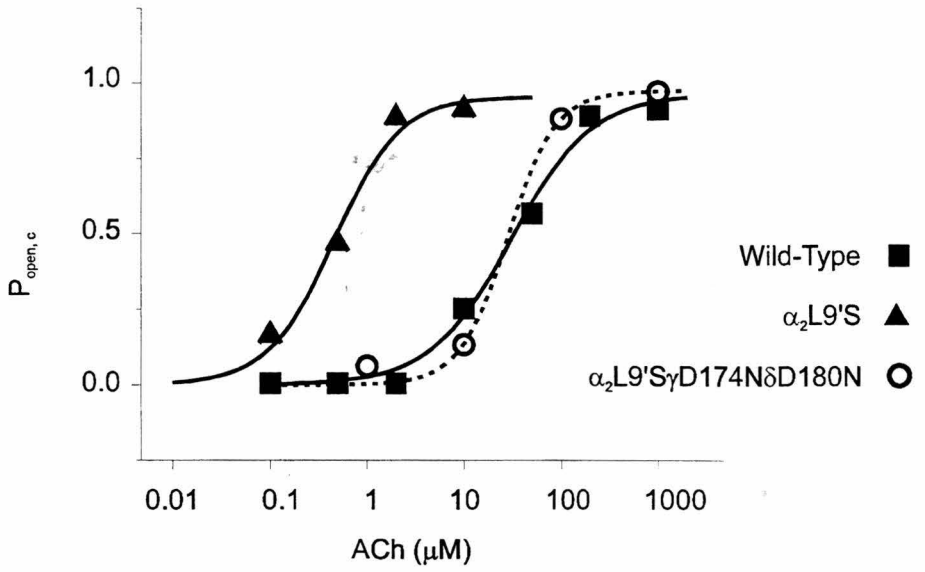

Figure 4.7. Single-channel dose-response relations for the wild-type (squares), α_2L9'SγD174NδD180N (open circles) and α_2L9'S (triangles) receptors. The open probabilities within bursts (P_{open}) were averaged over 1 to10 patches at each ACh concentration. The solid lines were the Hill equation (see Chapter 5) fits to the data, with EC_{50} values of 31, 0.46, and 28 μM, and Hill coefficients of 1.1, 1.3, and 1.8 for the wild-type, α_2L9'S, and α_2L9'SγD174NδD180N receptors, respectively.

Throughout the range of ACh concentrations tested (2-1000 μM), the distributions of open times of the wild-type AChR were fitted by a single-exponential function. The time constant, 1-2.5 ms, does not vary with concentration. This observation indicates that a single open state is sufficient to account for the kinetic behavior of wild-type nAChR. In the absence of ACh, we were unable to observe spontaneous openings of the wild-type receptors, inconsistent with observations made by Jackson and coworkers (1986). In this study, we only compare the wild type and mutant receptors at mid-range concentrations (P_o: 38%-86%) where, for the wild-type receptor, the number of unliganded and

monoliganded openings are negligible (while this is not the case for the three mutant receptors, see below). For this reason we will fit the wild-type receptor data to the model shown in Figure 4.8A, where only the doubly liganded receptor (A_2R) will open.

A

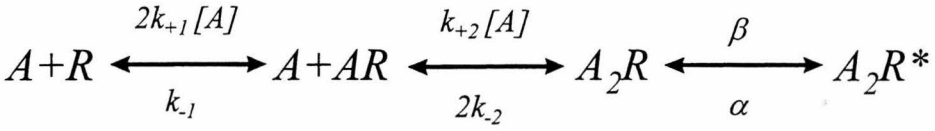

B

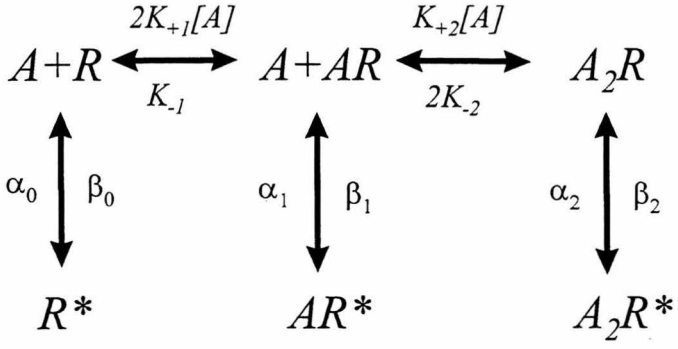

Figure 4.8. Kinetic models used for the wild-type (A) and the three mutant receptors (B): α_2L9'S, α_2L9'SγD174N, and α_2L9'SγD174NδD180N.

The distributions of closed times of wild-type AChR are fitted to the sum of several exponential terms. At low concentrations of ACh such as 2 μM, the dominant component is of 100-300 ms. At higher concentrations, there is an overall shift toward shorter closings, so that at concentrations around or greater than the macroscopic EC_{50} value, a relatively small number of long closed events separate a far greater number of shorter closed events into groups, causing the "bursting" pattern of opening. These burst data sets were analyzed as described in Chapter 5.

Although we have not been able to observe spontaneous openings of the wild-type receptors, all three mutant receptors, α_2L9'S, α_2L9'SγD174N, and α_2L9'SγD174NδD180N, do open spontaneously. Their open-time distributions contain a single exponential component, with a time constant of 0.2-0.25 ms. This pattern is similar among these three mutants, and consistent between patches. Within the limits of our analysis, these brief openings also have the same current amplitude as the longer ones (data not shown). In contrast to the spontaneous openings, the ACh-induced openings for all three mutant receptors contain an additional, longer (tens of ms) component, as can be seen in the representative histograms in Figure 4.6B.

Even though the durations of the spontaneous openings showed little variability between patches and between mutant receptors, the closed times between spontaneous openings vary greatly between patches. The mean closed times of seven patches of α_2L9'SγD174NδD180N, for example, cover the range of 14.5-200 ms. This variability is due in part to the presence of multiple channels in the patch. Because the exact number of channels in the patch is not known, we chose for each receptor the longest closed time

as its representative value and used it to calculate the lowest spontaneous open frequency. As shown in Table 4.2, the spontaneous closed time defined by this method is 5000 ms for α_2L9'S, 757 ms for α_2L9'SγD174N, and 200 ms for α_2L9'SγD174NδD180N.

Mutation	wild-type	α_2L9'S	α_2L9'SγD174N	α_2L9'SγD174NδD180N
γ(pS)	64.6±0.7	79±2	76±1	76±2
τ_{os}(ms)	--	0.25	0.2	0.2
$\alpha_0(s^{-1})$	--	4000	5000	5000
τ_{cs}(ms)	--	5000	757	200
$\beta_0(s^{-1})$	--	0.2	1.32	5
L_0	$3.0\times10^{-7*}$	5×10^{-5}	2.6×10^{-4}	1.0×10^{-3}

Table 4.2. Comparison of wild type and mutant receptors. γ is the single-channel chord conductance measured at -100 mV. τ_{os} is the mean open time of the spontaneous channel openings; α_0 is the corresponding closing rate, calculated as the inverse of τ_{os}. The spontaneous opening rate β_0 is calculated as the inverse of the mean closed time τ_{cs} between the spontaneous openings. L_0 is the gating equilibrium constant of spontaneous openings, calculated as β_0/α_0; the L_0 value for wild-type receptor is adapted from Jackson's work (23) as denoted by *.

Table 4.2 shows not only the spontaneous open and closed times, but also their inverse values: α_0 and β_0, respectively, which are the rate constants governing the transitions between the closed and open states of the unliganded receptor (R and R* in

Figure 8B). In this way the spontaneous activities for the three mutant receptors unequivocally specified their α_0's and β_0's. These two rate constants were therefore fixed in all the subsequent maximum-likelihood fittings. Moreover, because the unliganded receptors can open, it is plausible to assume that the monoliganded receptors will also be able to open. A monoliganded-open state (AR*) was therefore always included in Figure 4.8B, which is the model used for all three mutant receptors. This model is different from that shown in Figure 4.8A, in that the latter does not allow opening transition from either the unliganded or the monoliganded receptors.

The event series that we chose for fitting were first illustrated in Figure 4.9, which showed the open and closed time histograms superimposed with smooth curves representing their fitting by sums of exponential functions. In Figure 4.10, the same histograms are superimposed with the distribution predicted by the model shown in Figure 4.8, with parameters estimated via the maximum likelihood algorithm (Chapter 5). These parameters are shown in Figure 4.11. The units are $\mu M^{-1}s^{-1}$ or s^{-1} where applicable. The equilibrium constants, obtained by taking the ratio of the forward and reverse rate constants of each transition, are shown in Table 4.3.

Our resolution of 80 μs allows rates up to 12500 s^{-1} to be experimentally determined. In fitting the wild-type data, β was fixed to 25000 s^{-1}, higher than our resolution, but in accordance to the previous results by Zhang *et al.* (12). β values for mutant receptors, on the other hand, were treated as free parameters because we have no grounds to make *a priori* guesses. To ensure that we are not severely underestimating β values due to limited experimental resolution, we focused on recordings of mid-to-high

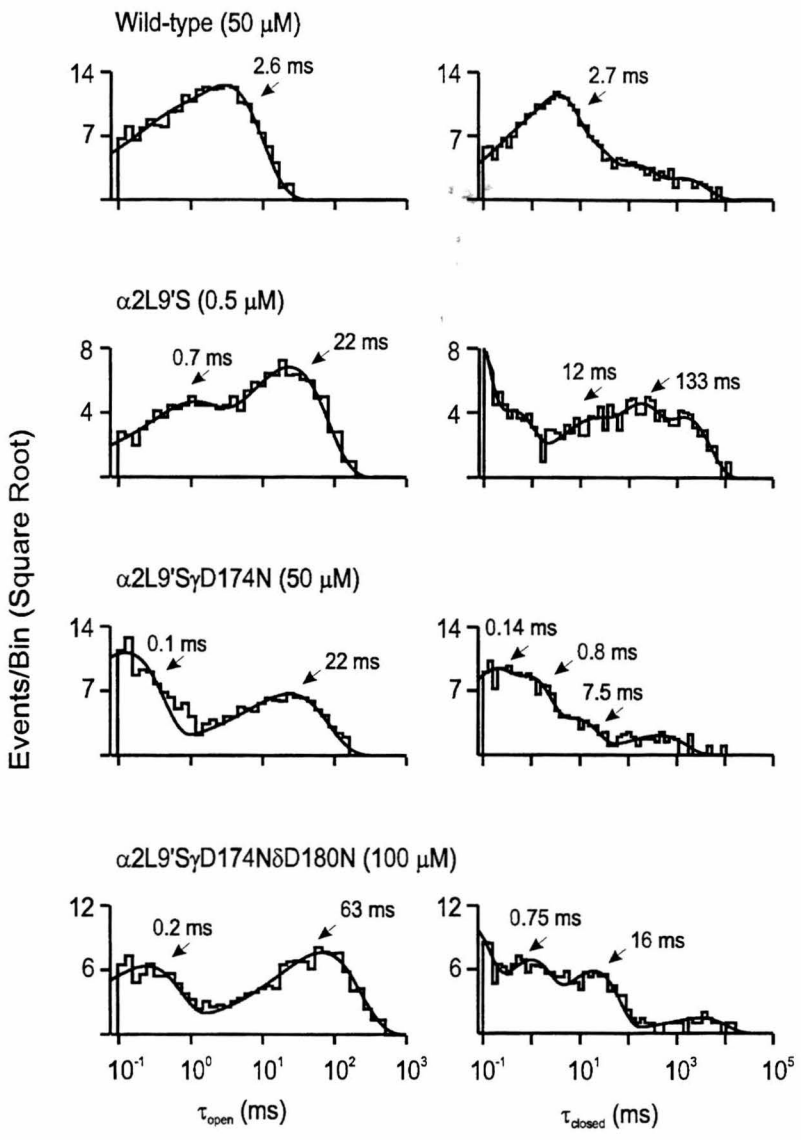

Figure 4.9. The open and closed-time histograms for the event series analyzed for the four receptor types. The smooth lines were the fittings by sums of exponential functions. The time constants and the corresponding fractional areas for major components were indicated by arrows.

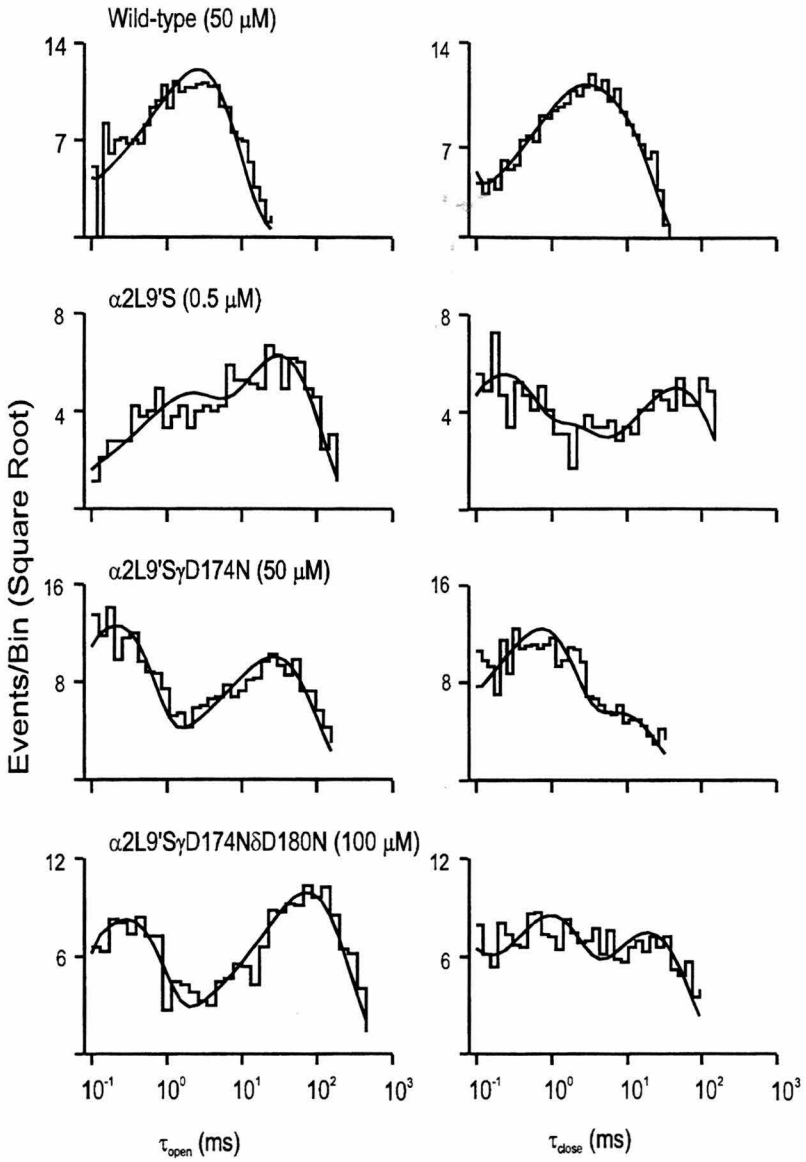

Figure 4.10. The same histograms as in Figure 10 superimposed with the appropriately normalized dwell-time probability density functions calculated from the maximum likelihood estimates of kinetic models.

open probabilities. The concentration and open probability of the recordings that gave rise to the results in Figures 4.10 and 4.11 were: for αL9'S, 0.5 μM, 51%; for α_2L9'SγD174N, 50 μM, 86%; and for α_2L9'SγD174NδD180N, 100 μM, 84%. The same parameters for the wild type were: 50 μM, 38%. The results showed that only the β_2 of α_2L9'SγD174NδD180N approaches our temporal resolution.

	K_{a1} $(=k_{-1}/k_{+1})$ (μM)	K_{a2} $(=k_{-2}/k_{+2})$ (μM)	L_0 $(=\beta_0/\alpha_0)$	L_1 $(=\beta_1/\alpha_1)$	L_2 $(=\beta_2/\alpha_2)$
Wild-type	22.7	1882	--	--	32
α_2L9'S	3.2	4.8	5×10^{-5}	0.16	70.8
α_2L9'SγD174N	122	51	2.6×10^{-4}	0.36	28.8
α_2L9'SγD174N δD180N	529	1264	1×10^{-3}	0.09	413

Table 4.3. Equilibrium constants of wild type and mutant receptors.

The results in Figure 4.11 and Table 4.3 indicate that the α_2L9'S mutation affected the binding affinities more strongly than they affected the gating constants. The affinities of both binding sites were higher than the wild-type values, with the differences at sevenfold and ~400-fold at the first and the second binding site, respectively. Meanwhile L_2 was not changed much (about twofold, Table 3), associated with an eight-fold reduction of β_2. The mild effects on gating constants were especially striking in light of the vast difference between the L_0

Wild-type (50 μM)

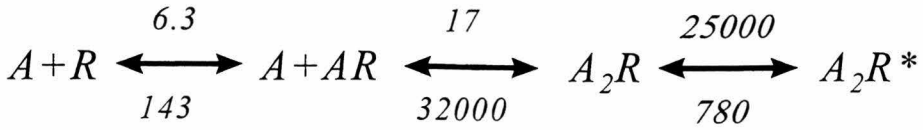

α2L9'S (0.5 μM)

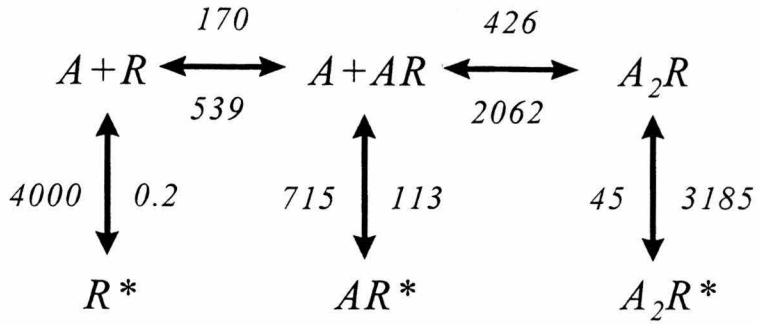

α2L9'SγD174N (50 μM)

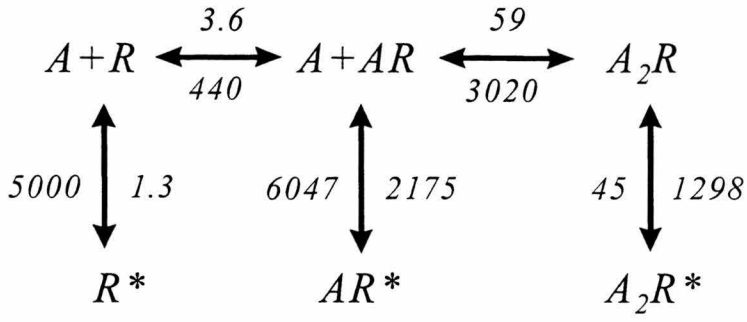

α2L9'SγD174NδD180N (100 μM)

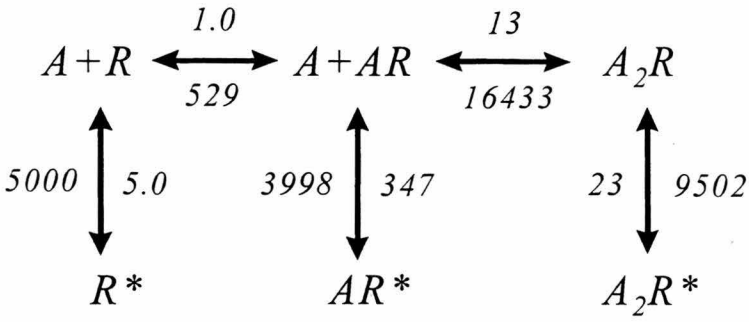

Figure 4.11. The rate constants for individual kinetic transitions estimated using the maximum-likelihood method.

value of wild type (3.0×10^{-7}(23), and that of α_2L9'S (5×10^{-5}, 167-fold greater than the wild-type, Table 4.2). It was also in contrary to the common belief that mutations at the 9' position of M2 affect primarily gating processes due to their proximity to the pore and a much greater distance to the ACh binding sites.

To test how the 80 μs temporal resolution underestimates β, and contributes to the apparently small effects on gating, we first refitted the wild-type data to Scheme 4.1 while allowing β to take the maximum value we have observed: 10778 s^{-1} (by fitting the wild-type data at 1 mM, P_{open}=91%). The resulting K_{a1}, K_{a2}, and L(=β/α) were, respectively, 24 μM, 869 μM, and 21, not significantly different from the results in Table 4.3, which came from fixing β at 25000 s^{-1}, but still different from the α_2L9'S results primarily in binding affinity rather than in gating constants.

Next we refitted the α_2L9'S data while fixing β_2 at 25000 s^{-1}, to test the effect of assuming that opening rate was unchanged from the wild-type value, on the gating and binding parameters were affected. The resulting K_{a1}, K_{a2}, L_1, and L_2 were, respectively, 11 μM, 4.7 μM, 0.82 and 212, showing about 400-fold higher affinity at the second binding site than the wild-type, while only a seven-fold greater gating constant for the doubly-liganded receptor.

The α_2L9'SγD174N receptor has an EC_{50} value intermediate to those of the wild-type and α_2L9'S. According to the data in Table 4.3, this can be mainly attributed to the changes in binding affinities, while the gating constants were only moderately different from either wild-type or α_2L9'S. 50 μM was the highest concentration we have tested for

α_2L9'SγD174N, and for the three representative recordings made at this concentration the β_2 values were (in s^{-1}): 884, 1298, and 3331, none approaching the resolution limit of our recording. Therefore, it is unlikely that the mildly affected gating parameters are artifacts resulting from our 80 μs temporal resolution.

The α_2L9'SγD174NδD180N receptor has its EC_{50} restored from 0.5 μM of α_2L9'S to 50 μM of the wild-type, by having lower affinities at both binding sites than α_2L9'S. Its L_2 is roughly 13 times greater than wild-type (413 vs. 32), but this effect, which favors a lower EC_{50} value, was offset by the 23-fold lower affinity at the first binding site (529 vs. 22.7 μM).

In summary, we have found through maximum-likelihood modeling that all three mutations, α_2L9'S, γD174N, and δD180N, affected both the ligand binding and channel gating, with greater effects on agonist binding affinity.

4.5 Strong Interaction Between αY 93 and δD 180 or γD 174 Is Unlikely

In order to probe the putative hydrogen bond between γAsp 174/δAsp 180 and αTyr 93 (αY 93 hereafter), we also used the double mutant cycle method. We first introduced D-to-N mutations at γ 174/δ 180. The replacement of an anionic carboxylate by a neutral amide group changes the hydrogen bond acceptor characteristics (Figure 4.2). To complete the double-mutant cycle, we then introduced the *amber* stop codon, TAG, at α 93 and suppressed the TAG mutation with five aminoacyl tRNA's, including wild type Tyr. The incorporation of these amino acids makes it possible to

fine-tune side-chain properties. Previously, we had shown that these mutations at α 93 produce a range of different EC_{50}'s, all higher than wild type (13, 14). To study with double-mutants, we necessarily needed again to take advantage of the Leu9'Ser mutation in the M2 region, this time in the α subunit (denoted α_2L9'S) (see Chapter 2). This mutation, occurring twice in the receptor, decreased the EC_{50} roughly by 100-fold (Table 4.1). We showed that the mutant receptor containing α_2L9'S and D-to-N mutations at γ174 and δ180 indeed has an EC_{50} value in the experimentally measurable range (Table 4.1). We point out that, when combined with αY93TAG mutations, receptors are expected to contain a total of six mutations [α_2(Y93TAG, L9'S)γD174NδD180N].

To substantiate the viability of the nonsense codon suppression method in such complex systems, we first rescued wild type Tyr at α 93 with tRNA-Tyr. The receptor obtained was indistinguishable from receptor containing wild type αY93 and α_2L9'SγD174NδD180N in all aspects (data not shown).

Having validated this approach, we then suppressed α93TAG with four other aminoacyl tRNAs: tRNA-Phe, tRNA-4-MeO-Phe, tRNA-4-COOH-Phe, and tRNA-Homo-Tyr. These residues are designed to perturb the putative hydrogen bond in different ways. Phe (phenylalanine) removes the hydroxyl group completely, 4-MeO-Phe (4-methoxy phenylalanine) removes the hydrogen bond donor capability, Homo-Tyr (homo-tyrosine) partially releases the side chain constraints and adjusts the hydroxyl group positions, and 4-COOH-Phe (4-carboxy phenylalanine) furnishes a hydroxyl group with a lower pK_a and sub-optimal positioning.

The observed maximal current amplitudes for Phe, 4-COOH-Phe, and Homo-Tyr mutants were lower than those for wild type and 4-MeO-Phe. The EC_{50} values were measured and listed in the lower row of Figure 4.12A.

A EC_{50} values (μM) for mutant receptors suppressed with various aminoacyl tRNA's:

	Tyr	4-COOH-Phe	4-MeO-Phe	Phe	Homo-Tyr
α_2Y93TAG*	50	149	388	429	459
α_2(Y93TAG, L9'S) γD174NδD180N	47	180	445	634	754

B

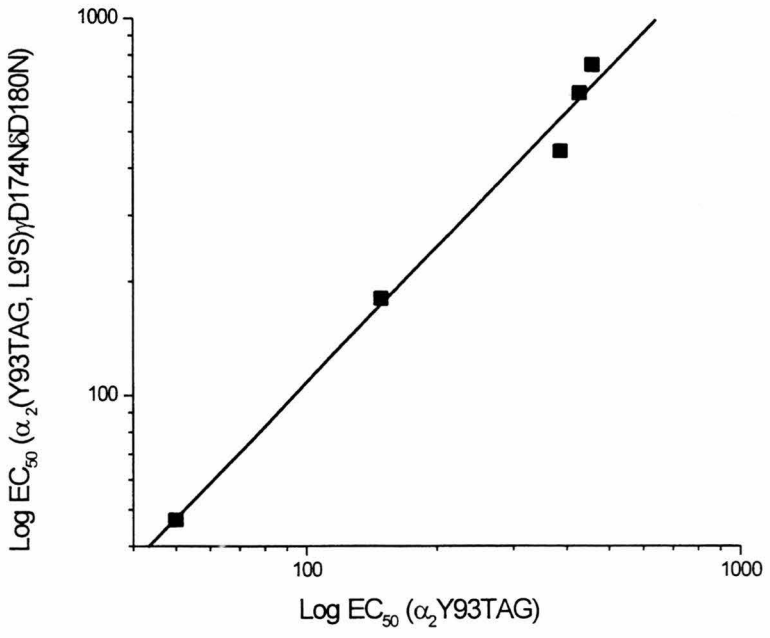

Figure 4.12. Comparison of EC_{50} values for receptors with α_2(Y93TAG, L9'S)-γD174NδD180N to α_2Y93TAG -only mutations. A. EC_{50} values for receptors suppressed with five different aminoacyl tRNA's. * Data were taken from Kearney et al. (14). B. Plot of the EC_{50} values for α_2(Y93TAG, L9'S)γD174NδD180N versus those for α_2Y93TAG in log-log scale. The straight line is the linear least-square fit, with R = 0.99±0.07 and slope = 1.19±0.07.

Comparison of these values to those of same mutations at α93TAG but without α_2L9'SγD174NδD180N clearly showed that the EC_{50} shifts exhibited by the four Tyr analogs at α 93 were largely reproduced, suggesting independent effects on channel activation from α_2Y93 and γD174/δD180 residues.

The result with the Phe mutation is quite revealing. If one assumes that γD174N/δD180N mutations significantly disrupt the putative hydrogen bond between γD174/δD180 and αY93 (and the α_2L9'S mutations have no such effects), then additional Phe mutation at α93 should increase, if at all, the EC_{50} to a smaller extent than that seen in receptors without α_2L9'SγD174NδD180N. However, the experimental result showed that additional Phe mutations shifted the EC_{50} for α_2L9'SγD174NδD180N by 14-fold, comparable to that seen before, arguing against such a notion. Other mutations follow the same pattern. This can be visualized again in Figure 4.5B, in which EC_{50} values of the α_2(Y93TAG, L9'S)γD174NδD180N receptors are plotted versus those with only the α_2Y93TAG mutations in a logarithmic-logarithmic scale. A linear fit with a slope of 1.2 and a correlation coefficient of 0.99, implies a lack of strong interaction between the residues in question. It is therefore unlikely that there is a hydrogen bond between αY93 and γD174/δD180, assuming that the D-to-N mutation significantly disrupted the side chain hydrogen bond acceptor ability at γ174 or δ180.

4.6 Discussion

One of the valuable methods to study direct interactions or coupled effects between two amino acids within a protein or protein complex is the "double mutatnt cycle" method (16, 17). If two residues are coupled together to contribute to channel activation, the combined effect in the double mutant is expected to be different from the mere addition of the effects caused by single mutations. These effects are reflected in changes of the macroscopic EC_{50} values in our studies. Hence one could reduce the "independent vs. coupled" problem into a question of whether the EC_{50} changes multiply in the combined double mutation.

The present study focuses on the function of two aspartic acid residues (γD174 and δD180) at the extracellular domains of the γ and δ subunits. We tested the possible long range couplings between γD174/δD180 and the well-characterized 9' leucine in the M2 transmembrane domains (21). The non-multiplicity of changes in EC_{50} values in these mutation combinations indicated remote couplings between the γD174/δD180 and the L9' residues. The coupling is strongest for the L9' in the β subunit.

Our single channel data lends support to earlier suggestion that γD174 and δD180 are involved in the conformational changes that correspond to transitions to higher affinity states, such as the open or desensitized states. Karlin has shown that the D-to-N mutations have greater effects on agonist binding affinity than on competitive antagonists (11). In addition, in single channel studies with adult nAChR, Zhang *et al.* found that the εD175N mutant receptor has an opening rate β of ~ 2000 s^{-1}, 30-fold lower than the wild-

type value (12). This effect accounts for most of the observed dose-response shift. Recently, Chen *et al.* have demonstrated remote energetic coupling between αD200, which is presumably near the ligand-binding site, and S12' in the M2 of δ subunit in adult mouse ACh receptor (24). In the present work, we found that the γD174N/δD180N mutations affected both the ligand binding process and the gating process, with the binding having the greatest effect.

Subunit-subunit interactions are crucial for agonist binding, receptor assembly and conformational changes during gating. We tested a putative hydrogen bond between the tyrosine residue at the α subunit (αY93) and aspartic acid at the γD174 and δD180. We have established earlier that αY93 is a potential candidate for hydrogen bond donor (13, 14) and is possibly close to γD174 and δD180 (9). Based on the double mutant cycle data, we found that γD174 or δD180 is unlikely the hydrogen bond acceptor of αY93. However, we note that although the D-to-N mutation changes the hydrogen bonding characteristics, it does not totally eliminate the hydrogen bond acceptor capability. As such, we consider our data presented here is inconclusive, and further work is needed to clarify this issue.

To sum up, we emphasize that in order to understand the working mechanisms of allosteric proteins such as nAChR, it is of importance to study the distant couplings which underlie the structures of allosteric transitions. We conclude that the present work, together with others' work discussed above, supports a role for γD 174 and δD 180 in allosteric structural changes that bridge agonist binding and channel gating.

4.7 References

1. P. Charnet, et al., *Neuron* **2**, 87-95 (1990).

2. J. Giraudat, M. Dennis, T. Heidmann, J.-Y. Chang, J.-P. Changeux, *Proc. Natl. Acad. Sci. USA.* **83**, 2719-2723 (1986).

3. R. J. Leonard, C. Labarca, P. Charnet, N. Davidson, H. A. Lester, *Science* **242**, 1578-1581 (1988).

4. M. H. Akabas, D. A. Stauffer, M. Xu, A. Karlin, *Science* **258**, 307-310 (1992).

5. N. Unwin, *Nature* **373**, 37-43 (1995).

6. A. Karlin, M. H. Akabas, *Neuron* **15**, 1231-1244 (1995).

7. C. Labarca, et al., *Nature* **376**, 514-516 (1995).

8. C. Czajkowski, C. Kaufmann, A. Karlin, *Proc. Natl. Acad. Sci. USA* **90**, 6285-9 (1993).

9. C. Czajkowski, C. Kaufmann, A. Karlin, *J. Biol. Chem.* **270** (1995).

10. M. Martin, C. Czajkowski, A. Karlin, *J. Biol. Chem.* **271**, 13497-13503 (1996).

11. M. Martin, A. Karlin, *Biochemistry* **36**, 10742-10750 (1997).

12. Y. Zhang, A. Auerbach, *Soc. Neurosci. Abst.* **21**, 1582 (1995).

13. M. W. Nowak, et al., *Science* **268**, 439-442 (1995).

14. P. Kearney, et al., *Mol. Pharmacol.* **50**, 1401-1412 (1996).

15. P. C. Kearney, H. Zhang, W. Zhong, D. A. Dougherty, H. A. Lester, *Neuron* **17**, 1221-1229 (1996).

16. A. Horovitz, *Proc. Royal Soc. London series B Biol. Sci.* **259**, 85-87 (1995).

17. A. Horovitz, *Folding & Design* **1**, R121-126 (1996).

18. P. Hidalgo, R. Mackinnon, *Science* **268**, 307-310 (1995).

19. R. Ranganathan, J. H. Lewis, R. Mackinnon, *Neuron* **16**, 131-139 (1996).

20. J.-P. Changeux, *Biochem. Soc. Trans.* **23**, 195-205 (1995).

21. H. Zhang, *Ph. D. Thesis* (California Institute of Technology, 1997).

22. J. Li, *Ph. D. Thesis* (California Institute of Technology, 1998).

23. M. B. Jackson, *Biophys. J.* **49**, 663-672 (1986).

24. J. Chen, A. Auerbach, *Biophys. J.* **72**, ppTUP64-TUP64 (1997).

Chapter 5

Methods in Electrophysiology and Preparation of Mutants and Amino Acids

In previous chapters, we have discussed structure-function studies on the nicotinic receptor at a chemical scale. In this chapter, we will document the electrophysiological methods we used in these studies and report the preparation of the mutant receptors and the numerous natural and unnatural amino acids.

5.1 Two Electrode Voltage Clamp and EC_{50} Measurements

Macroscopic (whole cell) current measurements were conducted at 20°C in a bath solution containing (in mM) 96 NaCl, 2 KCl, 1 $MgCl_2$, 5 HEPES and 1 μM Atropine (pH 7.4). We utilized a two-electrode voltage-clamp amplifier (GeneClamp 500, Axon Instruments, Foster City, CA) controlled by pCLAMP6 software (Axon Instruments). For steady-state current measurements, the membrane potential was held at -80 mV. All dose-response data are from 3-5 oocytes and are reported as mean ± standard error. The dose-response relations were fitted to the Hill equation

$$I = I_{\max} / \left\{1 + (EC_{50} / [A])^{n_H}\right\},$$

where I is the current induced by the agonist at concentration [A]; $I_{\max}$ is the maximal current; EC_{50} is the agonist concentration required to elicit half of the maximal response; and n_H is the Hill coefficient. This fitting used the least-squares procedures in Origin 4.1 (Microcal Software, Northampton, MA). When IC_{50}'s are measured at given agonist concentrations, the data are fitted to a similar equation where EC_{50} is substituted by IC_{50} and n_H by $-n_H$.

5.2 Single-Channel Recording and Analysis

Single-channel recordings were performed at 20°C on excised outside-out patches. Both the pipette solution and the bath solution contained (in mM): 150 KCl, 2 $MgCl_2$, 10 HEPES, and 10 EGTA (pH 7.4). The membrane potential was held at -100 mV unless otherwise indicated. Data were recorded using a GeneClamp 500 patch-clamp amplifier (Axon Instruments) with a headstage-resistor of 50 GΩ. Data were sampled at 44 kHz by a Neuro-Corder Digitizing Unit (Model DR384, NeuroData Instruments Corp., New York, NY) and stored on videotape. The Neuro-Corder employs a pre-digitizing, anti-aliasing brickwall type filter (rolloff is 70 dB within 1.5 KHz) of 22 KHz (-3 dB frequency). During analysis, data were played back, converted to analog form by the Neuro-Corder, and redigitized at 50 kHz with FETCHEX of the pCLAMP6 programs (Axon Instruments), via a DIGIDATA1200 interface (Axon Instruments).

The data were subjected to a 5 kHz digital Gaussian filter in FETCHAN of pCLAMP6, and idealized. The resulting event-list files (.evl) were converted into ASCII form, and selected for further analysis by (1) discarding files that were apparently non-stationary, judged by inspection of the opening probability, the open times, or the closed times and (2) discarding files with fewer than 1000 events. For the selected files, open time- and closed time-histograms were constructed in PSTAT of PLCAMP6, and were fitted in PSTAT with sums of exponential functions using the Levenberg-Marquardt method with weighting by function. In this study we used the fitting results mainly as a

descriptive measure of data, while the kinetic rate constants were estimated using the maximum-likelihood method (see below).

For files that show apparent bursting behavior, the critical duration that delimits the bursts needs to be determined. Two methods have previously been used: (1) to choose the delimiter as five times the duration of the "major component" of the closed-time histogram (1); (2) to choose the delimiter so that the number of shorter events misclassified as long equals the number of long events misclassified as short (2, 3). The first method cannot be applied to about half of our files, in which either the "major component" in the closed-times histogram is too broad (or skewed) to be fit by one exponential function, or there are simply several "major" components. The second method is only feasible when there are three (or less) clearly separated components: when there are three components, for example, typically one can define a BURST-delimiter between the short and the medium components, and a CLUSTER-delimiter between the medium and the long components. But many of our files have four or five components; additionally, there are large patch-to-patch variations in terms of the number of components, their locations, or their relative weights. For these reasons the two traditional methods mentioned above were no longer adequate. We placed special emphasis on the empirical testing procedure in which a series of "delimiter" values were chosen, and for each value the average number of closings in the putative bursts, or the average duration of these bursts, was individually calculated, and plotted against the corresponding delimiter (4). This plot was constructed in PSTAT, and the delimiter was determined on a file-to-file basis. In this study we did not make the distinction between "burst" and "cluster." Instead for all burst data set a single class, "burst," was defined.

The closed intervals shorter than the delimiter were hitherto regarded as INTRAburst intervals, while those longer than it became INTERburst closings. Following common practice, we categorically define interburst closings as representing the "desensitized" state(s), to be contrasted to the events within burst, which represent transitions among the "activatable" states. Because we know very little about the desensitized states, the goal of our analysis is to study the activatable states.

Since the delimiter selects the "activatable" states out of the original, contiguous event-sequence, choosing a proper delimiter becomes critically important for all subsequent analyses. In principle one should apply the kind of model that matches the complexity inherent in data; but because the data are transformed by the delimiter, the process of determining delimiter should reflect our hypotheses as to what constitutes plausible models. For instance, if a delimiter were chosen such that there are three exponential components left in the intraburst closed-time histogram (by being shorter than it), the data would call for three closed states, which would be consistent with the knowledge that AChR has two ligand-binding sites. According to this reasoning, for files having >3 closed-time components, we typically selected the delimiter so that the shortest 1-3 components (depending on their relative weights) were retained as within the bursts.

For each event-list file in ASCII format, we rewrote every closed time longer than the delimiter into segment titles, so that each burst is contained in a segment. The last opening of each segment was deleted, so that each burst had an equal number of openings as closings. Bursts having eight or less events were also discarded. Proper file format was followed so that the final dwell-time files (.dwt) were compatible with the

maximum-interval-likelihood program (MIL). MIL is for estimating, with a correction for missed events, the kinetic parameters from idealized single-channel records. The Windows 95-version of MIL was kindly provided by Drs. Feng Qin, Anthony Auerbach and Fred Sachs (Department of Biophysical Sciences, State University of New York at Buffalo, Buffalo, NY 14214).

By passing pulses through the NeuroCorder-filter-computer combination, we verified that openings as brief as 80 μs were resolved, and this value was used (1) as the lower limit of the closed-time histograms when fitting them to exponential functions, and (2) as the "dead time" in MIL for missed-event correction.

Single-channel dose-response relations were fitted to the Hill equation:

$$P_{open,c} = P_{open_{\max}} / \left\{1 + (EC_{50} / [A])^{n_H}\right\},$$

where $P_{open,c}$ is the channel open probability within burst in response to agonist at concentration [A]. $P_{open_{\max}}$ is the maximal $P_{open,c}$ at saturating agonist concentrations. EC_{50} is the concentration that activated 50% of the maximal response. n_H is the Hill coefficient. The fitting used least-squares procedures in Origin 4.1.

The parameters were reported as mean ± standard error where applicable.

5.3 Mutagenesis, mRNA Synthesis, tRNA Synthesis and Oocytes Microinjections

All the mutations involved in these studies were introduced into the cDNAs of the corresponding subunits of mouse muscle nAChR. The L9'TAG and L9'S mutations were generated using the Clontech Transformer Kit (Clontech, Palo Alto, CA) (5). Others were generated using the Quickchange kit (Stratagene, La Jolla, CA) or the PCR-cassette method. The expression vector is pAMV, which is optimized for oocyte expression. mRNAs were prepared by *in vitro* transcription of the linearized cDNA plasmid using the Ambion Magic Message Machine Kit (Ambion, Austin, TX). The stop codon in the δ subunit was mutated from TAG to TGA to avoid complications (6).

The genes for our original modified yeast $tRNA^{Phe}$ CUA (MN3) and *Tetrahymena thermophila* $tRNA^{Gln}$ CUA having a G at position 73 (THG73) were constructed from eight overlapping synthetic DNA oligonucleotides and cloned into pUC-19 giving the plasmids pMN3 and pTHG73, respectively (6, 7). The genes each contained an upstream T7 RNA polymerase promoter and a downstream Fok I restriction site. Template DNA for transcription of tRNA lacking the 3'-terminal C75 and A76 was prepared by digesting the plasmid DNA with Fok I restriction endonuclease. *In vitro* transcription of the linearized DNA template and purification of the truncated MN3 and THG73 RNA products were performed as previously described. The full length aminoacyl-tRNA were prepared as follows: the NVOC-protected dCA amino acids were ligated to the MN3 or THG73 Fok I runoff transcripts using T4 RNA ligase. The ligation efficiency as judged by electrophoresis on high resolution 8% denaturing polyacrylamide gel was approximately 90% for MN3 transcripts and only 10-30% for THG73 transcripts (8).

Stage V-VI *Xenopus* oocytes were injected with 50 nl of the appropriate mixture of mRNAs and tRNAs where necessary. Prior to microinjection, the ligated NVOC-aminoacyl-tRNA was deprotected by irradiating the sample for 5 min with a 600 W Xenon lamp equipped with WG-335 and UG-11 filters (Schott). For conventional mutants, no tRNAs were needed and, in general, the concentration ratio is 2:1:1:1 for α:β:γ:δ and a total of 0.08 - 3 ng of mRNA were injected. For mutants containing TAG mutations, the ratio for the corresponding subunit(s) was increased 4-10 times higher due to the concern of suppression efficiency. For example, the ratio for receptor bearing one TAG mutation in each of the α subunit was 20:1:1:1 or 100:1:1:1(α:β:γ:δ). The total amount of mRNA used usually was in the range of 3-16 ng. The deprotected aminoacyl-tRNAs were often injected in the amount of 25 ng, but occasionally lower amounts down to 3 ng or higher up to 75 ng were injected for some unnatural aminoacyl-tRNAs (9). The injected oocytes were incubated at 18°C in a modified Barth's solution supplemented with 50 mg ml^{-1} Gentamicin, 2.5 mM pyruvate and 0.6 mM theophylline. In addition, horse serum (1-4%) (HyClone Laboratories, Inc., Logan, UT) was added to the incubation solution to improve the viability of oocytes (10). Electrophysiological measurements were performed 18-96 hours after injection.

5.4 General Procedures for Synthesis of Aminoacyl dCA (dCA-AA)-Synthesis of dCA-Phe

The dinucleotide dCA was prepared as reported previously (11) with a few modifications: 1) the dinucleotide coupling, oxidation and deprotection with p-toluenesulfonic acid were done in one pot; 2) the desalting of dCA was accomplished by redissolving it in Millipore water, freezing, and lyophilization to obtain a fluffy material; 3) the tetra-n-butylammonium salt of the dinucleotide was formed by mixing the proper amount of tetra-n-butylammonium hydroxide (1M in MeOH) with a solution of dCA in water. Freezing and lyophilization provided a white fluffy solid which was then stored at -80°C. It remains fully reactive after one year of storage.

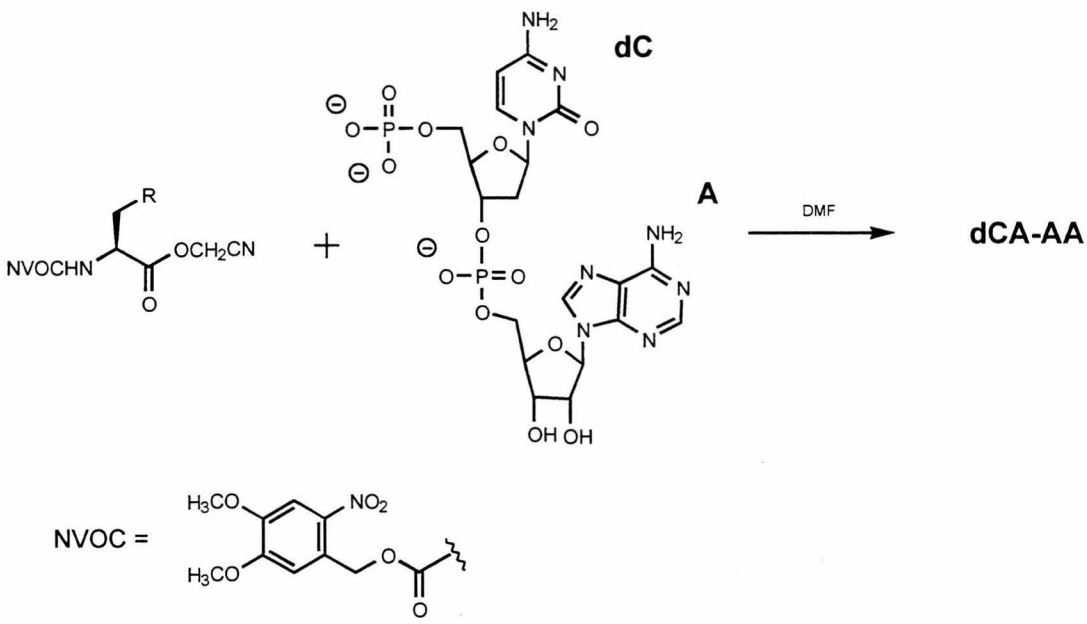

Figure 5.1. The general strategy for dCA-amino acid synthesis.

General strategy for dCA-amino acid synthesis is shown in Figure 5.1. The synthesis of dCA-Phe is described below as a general procedure. To a solution of 18.0 mg dCA (tetrabutylammonium salt, ~15 mmol) in 400 μL anhydrous DMF under argon was added 51 mg NVOC-4-(nitroveratrylcarboxy)-phenylalanine cyanomethyl ester (75 mmol, 5 equiv; see below). The clear pale yellow solution was stirred for 3 hr, then quenched with 200 μL 25 mM NH_4OAc (pH 4.5). In many cases, shorter reaction times and only two-three fold excess cyanomethyl ester are sufficient. In some cases, however, reaction may be incomplete, as monitored by analytical HPLC; a spatula tip of tetrabutylammonium acetate forces the reaction to completion. The crude product was purified by reverse-phase semi-preparative HPLC (Whatman Partisil 10 ODS-3 column, 9.4 mm × 50 cm), using a gradient from 25 mM NH_4OAc (pH 4.5) to CH_3CN. The appropriate fractions were combined, frozen, and lyophilized. To remove ammonium ions, which inhibit T4 RNA ligase in the ligation of the product to the tRNA, the white solid was redissolved in 10 mM acetic acid/CH_3CN, frozen, and lyophilized, providing 14 mg (75%) of the desired product as a fluffy white solid. Small amounts of material were quantified by their UV-vis spectra, assuming ε_{350} ~6350 per nitroveratryl group. To avoid promoting deaminoacylation, solutions of the product were always kept acidic (pH 4.5).

5.5 Preparation of Amino Acids

A large number of natural and unnatural amino acids have been prepared during the course of our studies on the nicotinic receptor. In these studies, we use nitroveratryloxy-carbonyl (NVOC) as the photocleavable amino protecting group. And all the amino acids are converted to the cyanomethyl active ester for coupling to

dinucleotide dCA (Figure 5.1). In Figure 5.2, we have shown a list of amino acids that can be readily protected and activated. The syntheses of a number of novel amino acids are reported in the following sections.

5.5.1 Syntheses of L-Homo-Tyrosine and 4-Methylphenylalanine

We used the recently developed (-)-pseudoephedrine methodology by the Myers (12) group to synthesize 4-methylphenylalanine **3** and homo-tyrosine **9**. The pseudoephedrine glycinamide **1** was prepared according to the literature procedure. It was recrystalized from toluene and dried under vacuum (0.1 mmHg) at 55°C for 24 hours. The dryness of this reagent is critical; therefore, before use, it was weighed out carefully into flamed flasks and azotroped at least once with dry toluene followed by further drying under high vacuum for 5-10 minutes. The probably more important factor for this chemistry to work is to use adequate amount of base. It was noted in literature that the optimal amount of base LDA (generated from n-BuLi and diisopropylamine) should be ca. 1.95 eq (a little less than 2 eq), one equivalent of which is used up by the hydroxyl group and the rest is used to deprotonate the amino group which subsequently isomerizes to generate the carbanion for alkylation at the α-carbon of glycine moiety. Therefore, the n-BuLi used (~1.6 M in hexane, Aldrich) needs to be titrated carefully. We found the method developed by Ireland using menthol as the standard and 2,2'-bipyridyl as the indicator is a reliable one for this purpose. The concentration of n-BuLi thus determined was 1.695 M in these studies.

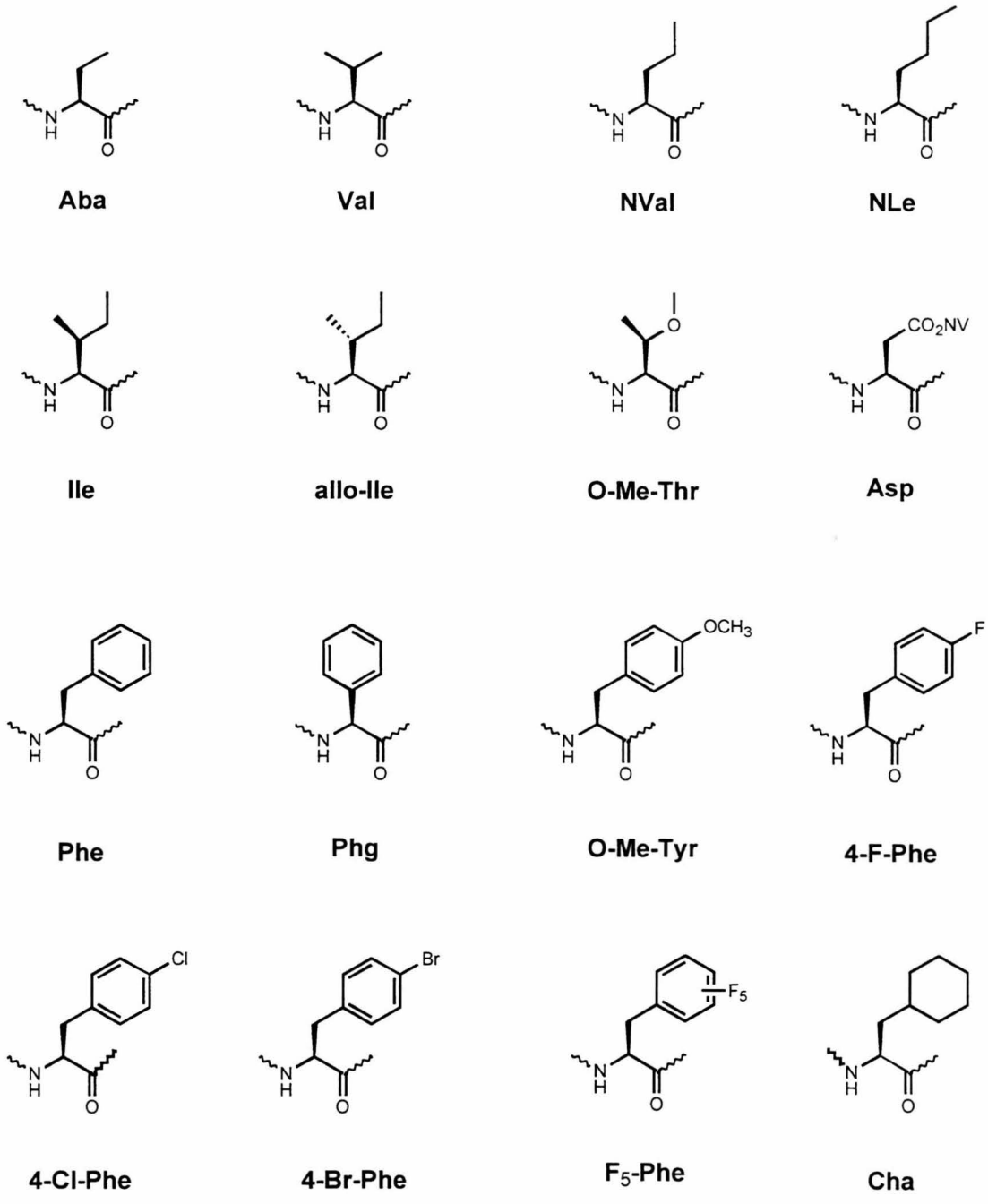

Figure 5.2. Chemical structures of readily available amino acids. Abbreviation codes for non-common residues: NVal, nor-valine; Nle, nor-leucine; Phg, phenylglycine; F_5-Phe, pentafluorophenylalanine; Cha, cyclohexylalanine.

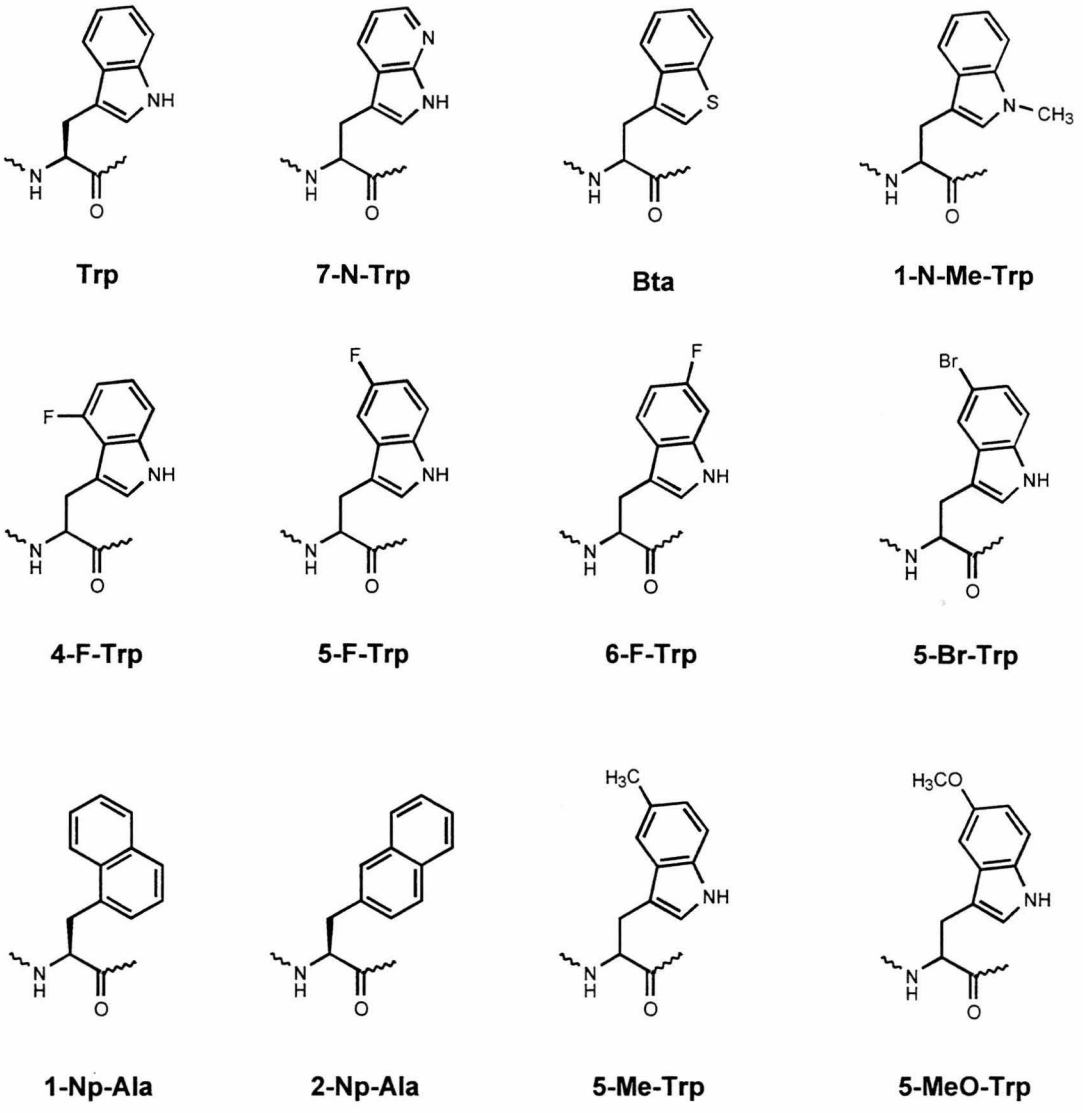

Figure 5.2. (continued) Chemical structures for readily available amino acids. Abbreviation codes for non-common residues: Bta, 3-benzothienylalanine; 1-Np-Ala, 1-naphthylalanine; 2-Np-Ala, 2-naphthylalanine; 5-MeO-Trp, 5-methoxytryptophan.

The synthesis of 4-methylphenylalanine **3** is quite straightforward, as shown in Scheme 5.5.1. In four steps, we obtained the properly protected/activated derivative with an overall yield of 28% (see experimental for details).

Scheme 5.5.1

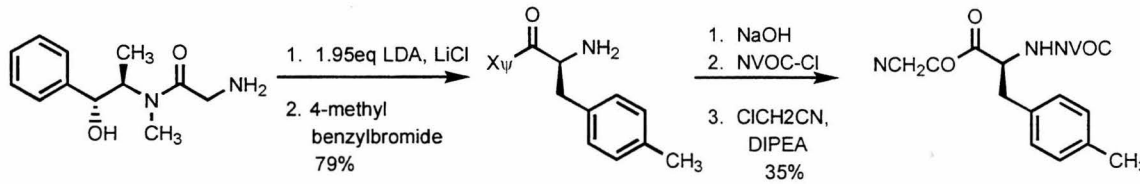

1 **2** **3**

The synthesis of homo-tyrosine **9** was a little more complicated due to the requirement for protection of the phenyl hydroxyl group. We found that the *tert*-butyldimethylsilyl (TBDMS or TBS) is compatible with the strongly basic alkylation conditions. The syntheses of the alkylating compound **6** and homo-tyrosine are illustrated in Scheme 5.5.2 and 5.5.3.

Scheme 5.5.2

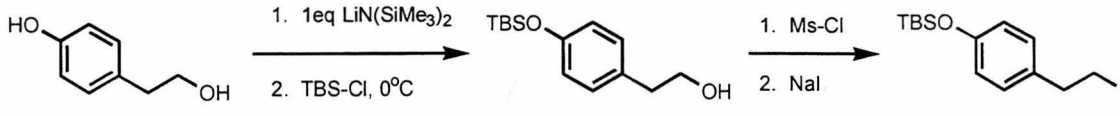

4 **5** **6**

Scheme 5.5.3

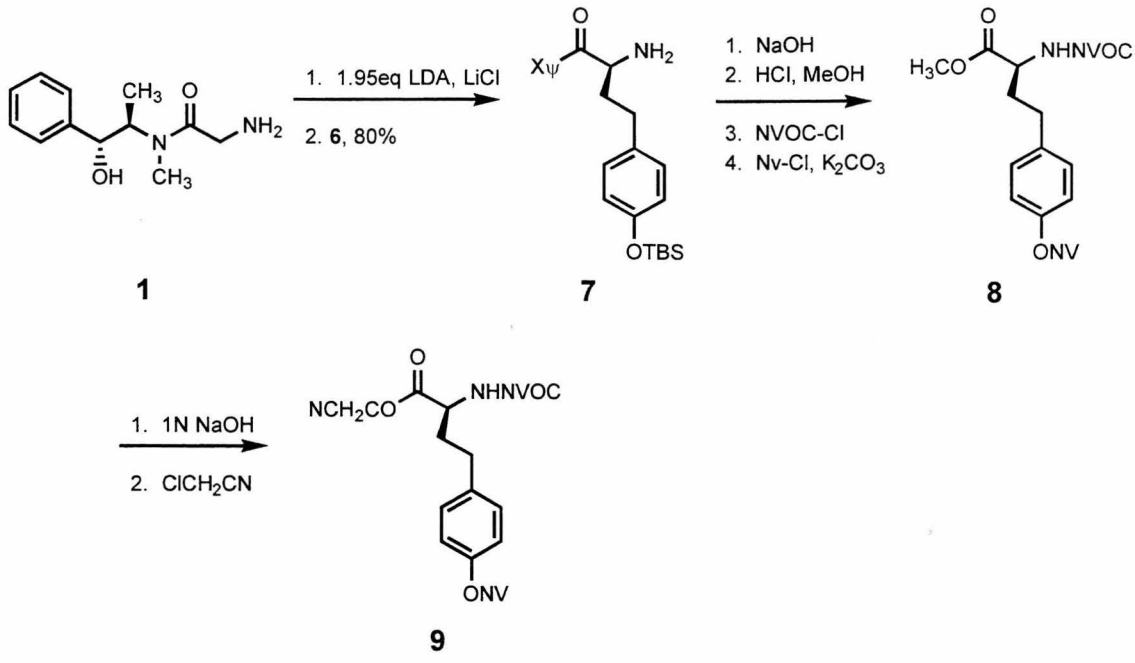

5.5.2 Syntheses of Amino Acids Containing a Quaternary Ammonium Group

In Chapter 3, we discussed the potentially broad applications of the tethered agonist approach in studying neuroproteins. Here we present the syntheses of a few amino acids containing a positively charged quaternary ammonium side chain group.

We started our effort with ε-trimethyl lysine (Figure 5.3). This residue is commercially available from Sigma and former group member Patrick C. Kearney prepared the corresponding NVOC protected cyanomethyl ester. The coupling to dCA was done under standard conditions. However, in an attempt to repeat the synthesis, we experienced difficulties to make the cyanomethyl ester. Similarly, residues such as **11**, **12**, **13**, and **14** also failed to form the active ester, presumably due to inner salt formation

under these conditions. After numerous futile attempts to form the cyanomethyl ester, we finally devised a general method which incorporates the active ester prior to the introduction of the charged side chain group. We present the syntheses of two amino acids, Tyr-O3Q and Lys-Carbamylcholine, in Schemes 5.5.4 and 5.5.5.

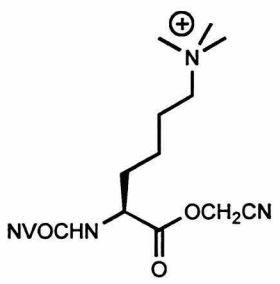

ε-TM-Lys 10

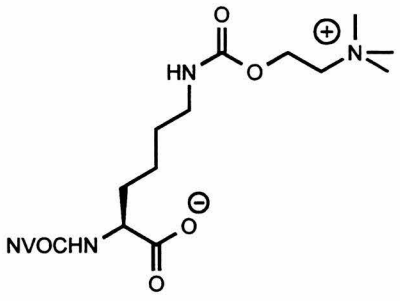

11

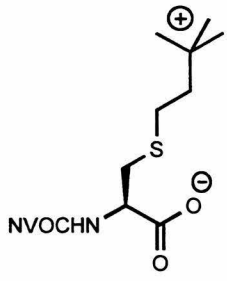

12

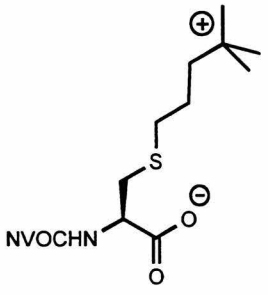

13

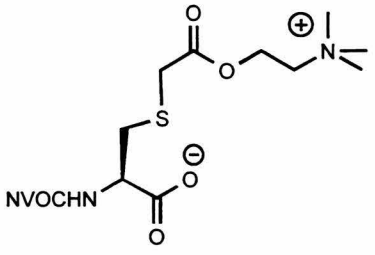

14

Figure 5.3. The amino acid residues containing side chain quaternary ammonium group which were not amenable for direct cyanomethyl ester formation.

Scheme 5.5.4

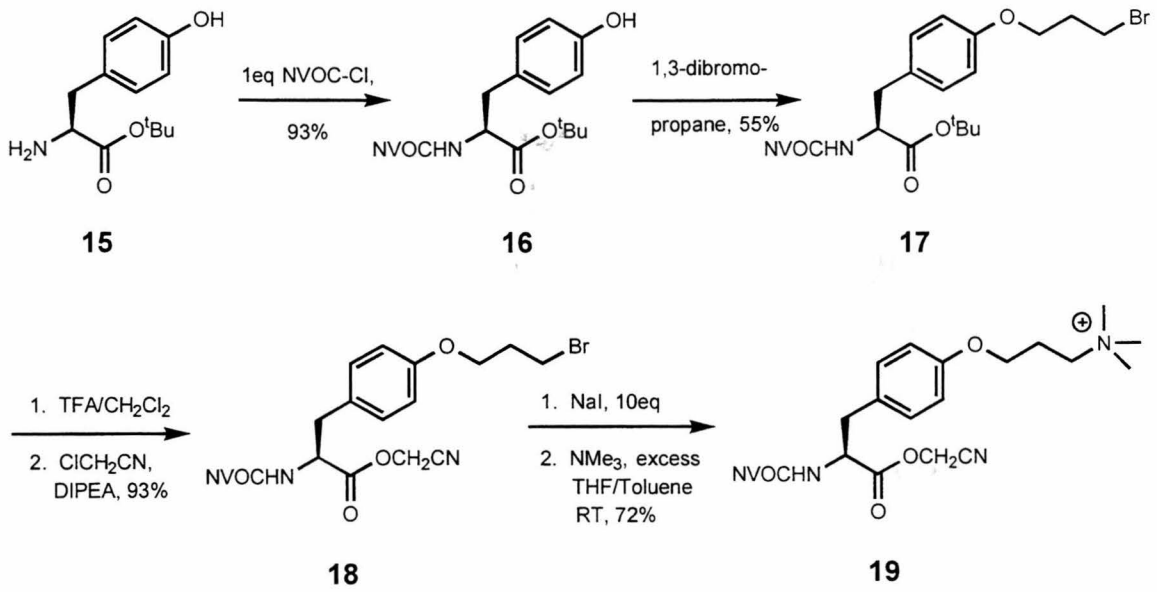

Scheme 5.5.5

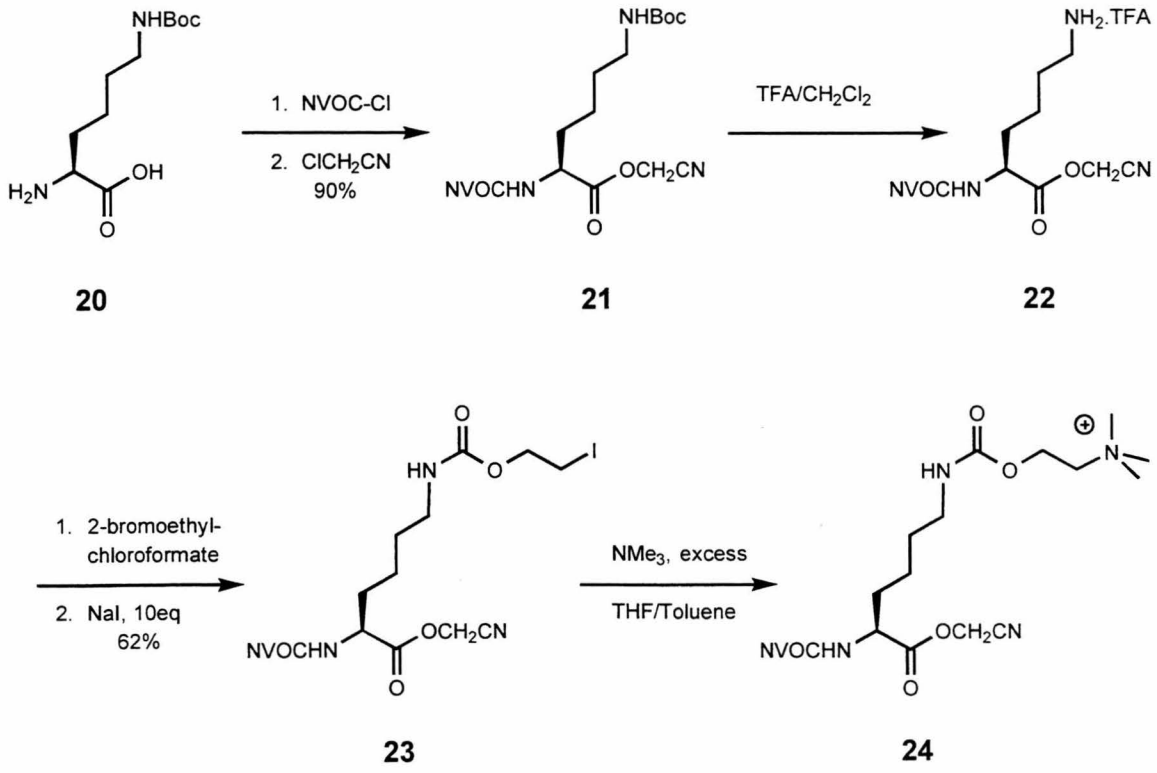

5.5.3 Syntheses of Tryptophan Analogs

In Chapter 2, we described mutagenesis studies at the four different Trp sites that are thought to contribute to ACh binding in the nAChR. Many Trp analogs involved are commercially available and they can be readily converted to the NVOC protected cyanomethyl ester derivatives (see Figure 5.2 for structures). In the following, we document the syntheses of a few Trp analogs that are worth special attention.

The synthetic strategy was based on the method developed by Roberts and coworkers (13), in which indole derivatives react with reagent ethyl-3-bromo-2-hydroxyimino-propanoate **26** to produce intermediates that can be reduced conveniently to the corresponding amino acid esters (in Scheme 5.5.6, we use 5-CN-indole as an exemplary indole derivative).

Scheme 5.5.6

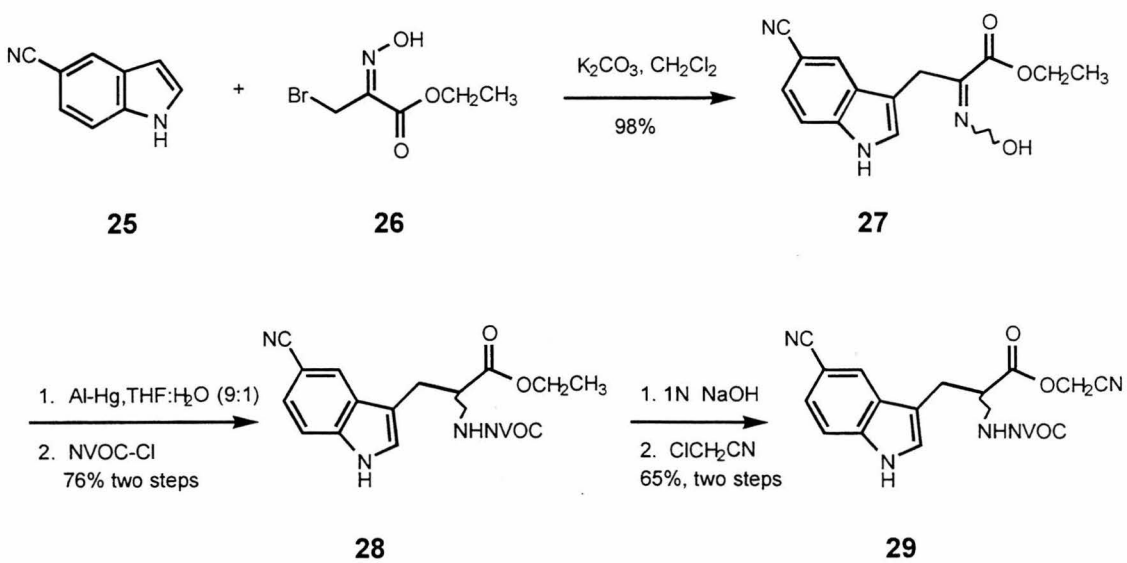

The mechanism of the reaction is not clearly understood. Generally speaking, this reaction works really well with electron-rich indole derivatives. The reaction did not work when 7-aza-indole was used. Although 7-aza-indole is not very electron-deficient compared to others such as tetrafluoroindole, it may form pyridinium type of salts, which are much worse substrates for this reaction. The reduction with Al-amalgam deserves a mentioning. Sufficient amount of water in the reaction mixture is needed for the reaction to complete. We found that mixed solvent of THF:H_2O in the ratio of 9:1 was ideal and reaction was in general done in a few hours.

Using this method, the syntheses of Trp analogs were then simplified to the syntheses of the corresponding indole derivatives. In the following, we describe the synthetic schemes for 5,7-difluoro-, 5,6,7-trifluoro- (14), and 4,5,6,7-tetrafluoroindoles (15) (Schemes 5.5.7, 5.5.8, and 5.5.9). In an attempt to synthesize 5,6-difluoroindole using the same methodology for 5,7-difluoroindole, the Pd-catalyzed Stephens-Castro reaction failed to provide any desired product. We suspect that an ortho-fluorine substitution facilitates the reaction as in the case of 5,7-difluoro- or 5,6,7-trifluoroindole, although the yield was still very low.

Scheme 5.5.7

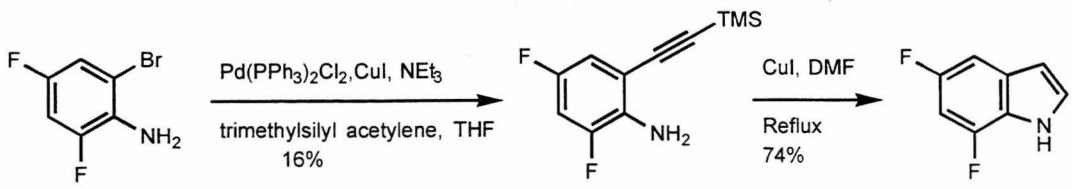

30 **31** **32**

Scheme 5.5.8

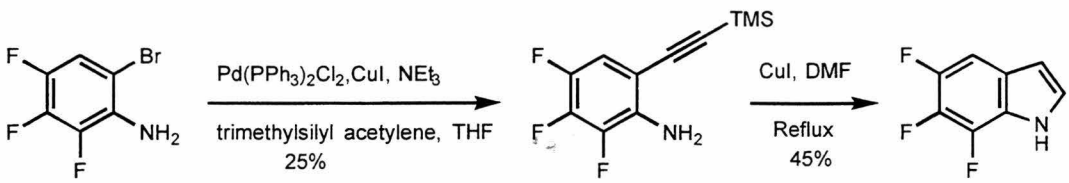

33 **34** **35**

Scheme 5.5.9

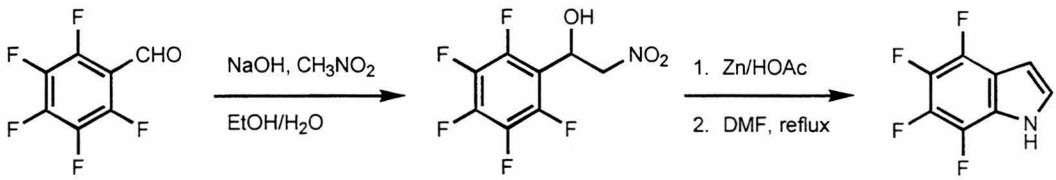

36 **37** **38**

5.5.4 Syntheses of Residues Containing Side Chain Carbonyl Groups

Amino acid residues containing a side chain carbonyl group have been incorporated in soluble proteins in vitro and further biochemical modification on this reactive functional group in intact protein can be realized with hydrazide-bearing biophysical molecular probes (16). In the following, the syntheses of two such residues, 4-acetyl-phenylalanine **42** and 4-acetonyl-tyrosine **46**, are described in Schemes 5.5.10 and 5.5.11. These residues are currently under investigation by Justin P. Gallivan on the nAChR expressed in *Xenopus* oocytes.

Scheme 5.5.10

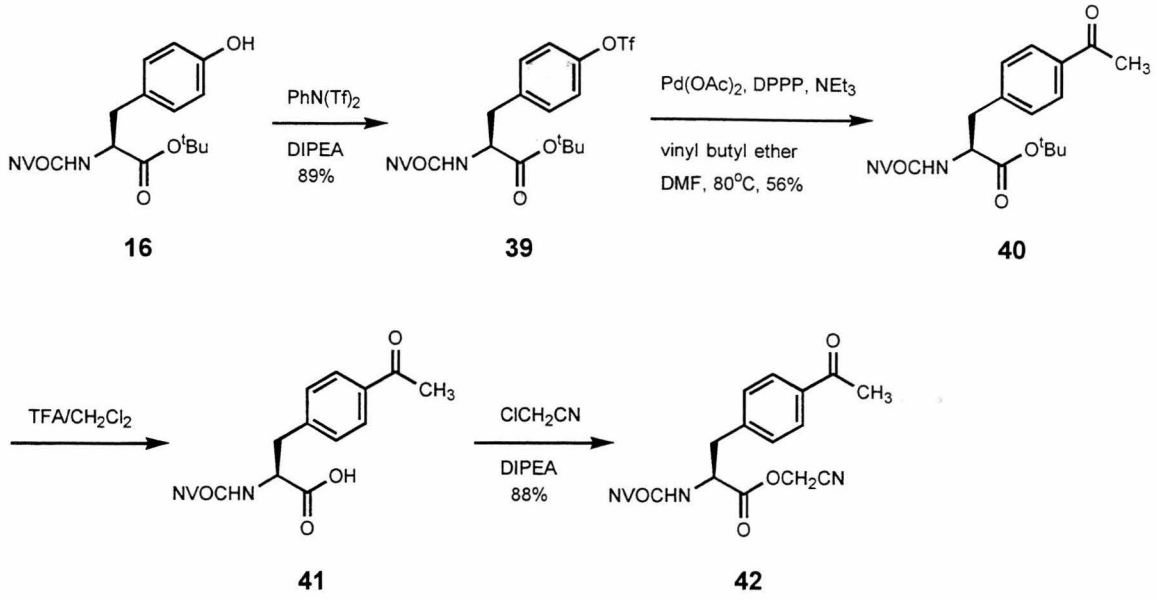

16 **39** **40** **41** **42**

Scheme 5.5.11

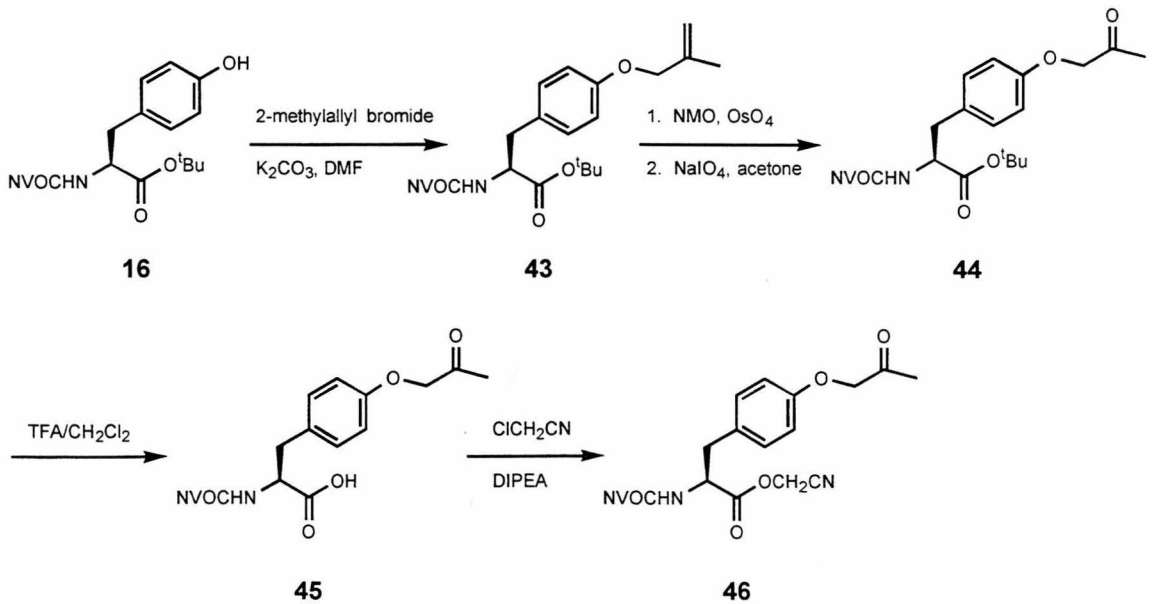

16 **43** **44** **45** **46**

5.5.5 Syntheses of L-*allo*-O-Me-Thr and dCA-Thr

During the course of these studies, we also synthesized dCA-Thr and related compounds. Shown in Schemes 5.5.12 and 5.5.13 are the syntheses of L-*allo*-O-Me-Thr (17) and dCA-Thr.

Scheme 5.5.12

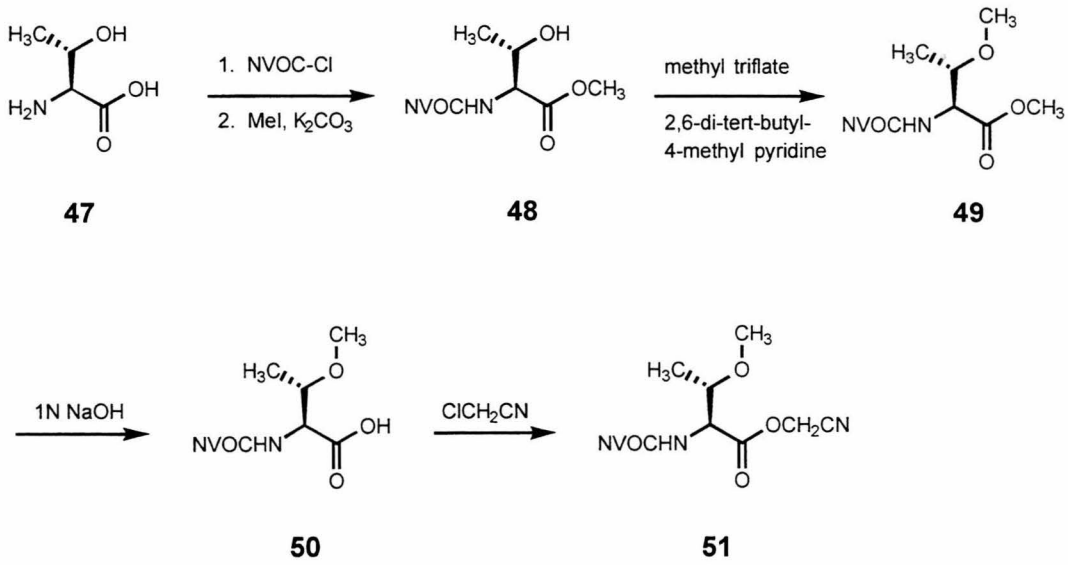

Scheme 5.5.13

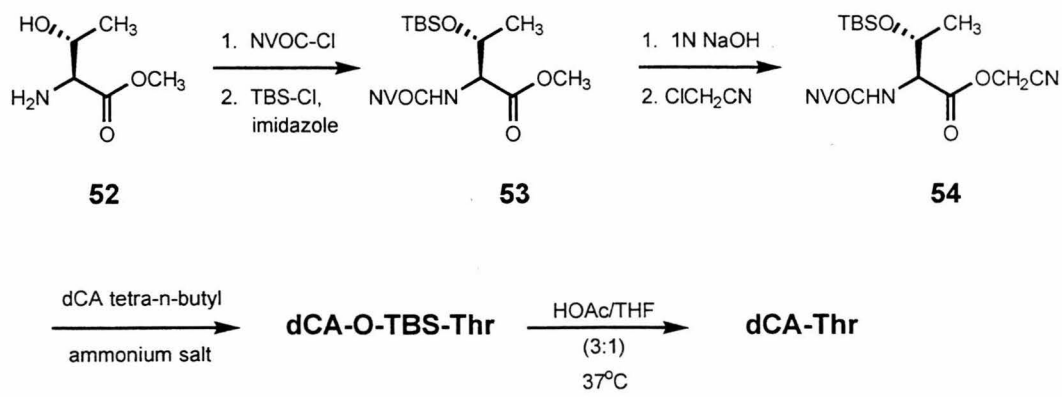

5.6 Experimental Section

General Methods. Tetrahydrofuran was distilled from sodium benzophenone ketyl. Methylene chloride and acetonitrile were distilled from CaH_2. Reported synthetic yields refer to material dried to constant weight under vacuum, typically 50 mTorr. Flash chromatography was on 230-400 mesh silica gel with the solvent indicated. All NMR shifts are reported as δ ppm downfield from TMS. ^1H NMR spectra were recorded at 300 MHz in $CDCl_3$ and ^{13}C NMR spectra at 75 MHz in $CDCl_3$ using a GE QE-300 spectrometer, except where noted. FAB, ESI, and HRMS determinations were performed at the University of California, Riverside, University of Nebraska-Lincoln, and California Institute of Technology. All reagents were obtained from Aldrich, Sigma, or other commercial sources where not explicitly noted.

Nitroveratryl chloride. To a solution of 4.26 g nitroveratryl alcohol (Lancaster, 20.0 mmol) in 150 mL dry CH_2Cl_2 under argon (a small amount of material remained undissolved) was added 1.9 mL thionyl chloride (26.0 mmol, 1.3 equiv). The solution was stirred in the dark for 3 hr, after which time it turned dark brown and was rotoevaporated to a solid which was filtered through silica with CH_2Cl_2. The filtrate was rotoevaporated, providing 4.07 g (88%) of a light yellow solid. ^1H NMR ($CDCl_3$) δ 7.69 (s, 1H), 7.11 (s, 1H), 5.01 (s, 2H), 4.02 (s, 3H), 3.97 (s, 3H).

Nitroveratryloxycarbonyl chloride (NVOC-Cl). To a mixture of 4.00 g nitroveratryl alcohol (18.76 mmol) in 200 mL dry CH_2Cl_2 under argon, cooled in an ice-water bath, was added 1.6 mL pyridine (19.78 mmol, 1.05eq). To the resulting pale

yellow solution was added in one portion 2.78 g triphosgene (9.37 mmol, 1.5eq). After 10 min, the solution was rotoevaporated to a pale brown solid and partially redissolved in 50 mL CH_2Cl_2. The mixture was filtered through silica, using more CH_2Cl_2 to dissolve the remaining material. The filtrate was rotoevaporated and dried to provide 4.77 g of crude material. This was recrystallized from toluene (55°C to -20°C), providing 3.8 g (74%) of NVOC-Cl as light orange crystals. ^{1}H NMR ($CDCl_3$) δ 7.76 (s, 1H), 7.02 (s, 1H), 5.73 (s, 2H), 4.03 (s, 3H), 3.99 (s, 3H).

A general procedure for protection and activation of amino acids listed in Figure 5.2 - 4-MeO-Phe as an example. To a 10 ml solution in dioxane containing 128 mg (0.33 mmol) of NVOC-Cl was added in one portion an aqueous solution containing 98 mg (0.33 mmol) of the amino acid and 49 mg of sodium carbonate. One hour later, the bright yellow reaction mixture was diluted with methylene chloride and washed with 1M KH_2PO_4 (pH 4). The organic layer was dried over sodium sulfate and concentrated under vacuum. The crude product, usually contaminated with a little bit of nitroveratryl alcohol, was used directly in next step without purification. To the flask containing the crude product was added 0.2 ml of chloroacetonitrile, 0.2 ml of diisopropylethylamine and 3-5 ml of DMF. The reaction was kept in the dark overnight, and then diluted with 25 ml CH_2Cl_2, washed with 2×25 ml KH_2PO_4 (1M), and dried over Na_2SO_4. Flash column chromatography using ethyl acetate:petroleum ether (50:50) provided 170 mg (74%) of off-white solid. ^{1}H NMR ($CDCl_3$) δ 7.71 (s, 1H), 7.08 (d, J=8.4 Hz, 2H), 6.92 (s, 1H), 6.86 (d, J=8.4 Hz, 2H), 5.56 (AB, 2H), 5.56 (d, J=8.3 Hz, 1H), 5.24 (d, 2H), 4.76 (m, 3H), 3.95 (s, 3H), 3.79 (s, 3H), 3.11 (d, 2H).

dCA-NVOC-4-MeO-Phe. Prepared by the ligation procedure described in section 5.4. FAB-MS: calcd for $C_{39}H_{46}N_{10}O_{21}P_2$: 1052.7; found $[M-H]^-$: 1051.0.

dCA-NVOC-1-Np-Ala. Prepared by the ligation procedure described in section 5.4. FAB-MS: calcd for $C_{42}H_{48}N_{10}O_{20}P_2$: 1074; found $[M+H]^+$: 1035.2.

dCA-NVOC-Aba. Prepared by the ligation procedure described in section 5.4. HR FAB-MS: calcd for $C_{33}H_{42}N_{10}O_{20}P_2$: 960.6674; found $[M-H]^-$: 959.1937.

dCA-NVOC-NVal. Prepared by the ligation procedure described in section 5.4. HR FAB-MS: calcd for $C_{34}H_{464}N_{10}O_{20}P_2$: 974.2208; found $[M-H]^-$: 973.2158.

dCA-NVOC-Ile. Prepared by the ligation procedure described in section 5.4. FAB-MS: calcd for $C_{35}H_{46}N_{10}O_{20}P_2$: 988.7; found $[M+H]^+$: 989.3

dCA-NVOC-*allo*-Ile. Prepared by the ligation procedure described in section 5.4. FAB-MS: calcd for $C_{35}H_{46}N_{10}O_{20}P_2$: 988.7; found $[M+H]^+$: 989.2.

dCA-NVOC-O-Me-Thr. Prepared by the ligation procedure described in section 5.4. HR FAB-MS: calcd for $C_{34}H_{44}N_{10}O_{21}P_2$: 990.2157; found $[M-H]^-$: 989.2157.

dCA-NVOC-Asp. Prepared by the ligation procedure described in section 5.4. FAB-MS: calcd for $C_{42}H_{49}N_{11}O_{26}P_2$: 1185.8; found $[M-H]^-$: 1184.0.

dCA-NVOC-Phg. Prepared by the ligation procedure described in section 5.4. FAB-MS: calcd for $C_{37}H_{42}N_{10}O_{20}P_2$: 1008.2052; found $[M-H]^-$: 1007.1981.

dCA-NVOC-4-Cl-Phe. Prepared by the ligation procedure described in section 5.4. FAB-MS: calcd for $C_{38}H_{43}ClN_{10}O_{20}P_2$: 1056.2; found $[M-H]^-$: 1052.2.

dCA-NVOC-4-Br-Phe. Prepared by the ligation procedure described in section 5.4. FAB-MS: calcd for $C_{38}H_{43}ClN_{10}O_{20}P_2$: 1100.1; found $[M-H]^-$: 1098.5.

dCA-NVOC-F_5-Phe. Prepared by the ligation procedure described in section 5.4. HR FAB-MS: calcd for $C_{38}H_{39}N_{10}O_{20}P_2F_5$: 1112.1737; found $[M-H]^-$: 1111.2648.

dCA-NVOC-Cha. Prepared by the ligation procedure described in section 5.4. HR FAB-MS: calcd for $C_{38}H_{50}N_{10}O_{20}P_2$: 1028.2678; found $[M-H]^-$: 1027.2580.

dCA-NVOC-Trp. Prepared by the ligation procedure described in section 5.4. FAB-MS: calcd for $C_{40}H_{45}N_{11}O_{20}P_2$: 1061.8; found $[M]^+$: 1061.2.

dCA-NVOC-7-N-Trp. Prepared by the ligation procedure described in section 5.4. FAB-MS: calcd for $C_{37}H_{44}N_{12}O_{20}P_2$: 1062.7; found $[M-H]^-$: 1061.0.

dCA-NVOC-Bta. Prepared by the ligation procedure described in section 5.4. HR FAB-MS: calcd for $C_{40}H_{44}N_{10}O_{20}P_2S$: 1078.1929; found $[M-H]^-$: 1077.1899.

dCA-NVOC-1-N-Me-Trp. Prepared by the ligation procedure described in section 5.4. FAB-MS: calcd for $C_{41}H_{47}N_{11}O_{20}P_2$: 1075.2; found $[M-H]^-$: 1074.0.

dCA-NVOC-4-F-Trp. Prepared by the ligation procedure described in section 5.4. HR FAB-MS: calcd for $C_{40}H_{44}N_{11}O_{20}P_2F$: 1079.2223; found $[M-H]^-$: 1078.2188.

dCA-NVOC-5-F-Trp. Prepared by the ligation procedure described in section 5.4. HR FAB-MS: calcd for $C_{40}H_{44}N_{11}O_{20}P_2F$: 1079.2223; found $[M-H]^-$: 1078.2176.

dCA-NVOC-6-F-Trp. Prepared by the ligation procedure described in section 5.4. HR FAB-MS: calcd for $C_{40}H_{44}N_{11}O_{20}P_2F$: 1079.2223; found $[M-H]^-$: 1078.2130.

dCA-NVOC-5-Br-Trp. Prepared by the ligation procedure described in section 5.4. HR FAB-MS: calcd for $C_{40}H_{44}N_{11}O_{20}P_2Br$: 1139.1412; found $[M-H]^-$: 1138.1350.

dCA-NVOC-2-Np-Ala. Prepared by the ligation procedure described in section 5.4. FAB-MS: calcd for $C_{42}H_{48}N_{10}O_{20}P_2$: 1074; found $[M+H]^+$: 1035.2.

dCA-NVOC-5-MeO-Trp. Prepared by the ligation procedure described in section 5.4. HR FAB-MS: calcd for $C_{41}H_{47}N_{11}O_{21}P_2$: 1091.2423; found $[M-H]^-$: 1090.2343.

(-)-Pseudoephedrine-4-methylphenylalaninamide 2. To a flame-dried Schlenck flask was added 560 mg LiCl (13.1 mmol, 6eq). The setup was flame-dried again. 6 ml THF was added, followed by addition of 0.62 ml diisopropylamine (4.38 mmol, 2eq). At -80°C, 2.51 ml n-BuLi (1.695 M in hexane, 5.65 mmol, 1.95eq) was added slowly along the inner surface of the flask. The mixture was stirred for 20 minutes, then a solution of 486 mg (-)-pseudoephedrine glycinamide **1** (2.19 mmol) in 3 ml THF was added slowly. A yellow opaque mixture resulted, which was further stirred at -80°C for 20 minutes, then at 0°C for 20 minutes, which produced a bright yellow slurry. At 0°C, a solution of 450 mg 4-methylbenzylbromide in 2 ml THF was added, and the yellow color disappeared quickly. The reaction was quenched 2hr later with 35 ml HCl (1N) and washed with 35 ml ethyl acetate. The aqueous layer was basicified with ca. 3†ml 50% NaOH to pH 13-14, extracted with 4×40 ml CH_2Cl_2, and the organic layer was dried over K_2CO_3. Flash chromatography using NEt_3:MeOH:CH_2Cl_2 (2.5:2.5:95) provided 565 mg (79%) white solid. ^{1}HNMR ($CDCl_3$) δ 7.50-7.10 (m, 9H), 4.88 (m, 1H), 4.56 (d, J=9.4Hz, 1H), 3.99 (t, 1H), 3.44 (m, 3H), 2.88 (m, 2H), 2.72 (s,3H), 2.43 (s, 3H), 0.90 (d, J=6.7Hz, 3H). There are also minor rotomer peaks at 3.06 (s), 2.46 (s), 1.09 (d).

NVOC-4-Methylphenylalanine cyanomethyl ester 3. To a flask containing 550 mg **2** (1.69 mmol) were added 5 ml H_2O and 1.7 ml 1N NaOH (1.7 mmol, 1eq). The

mixture was refluxed for 3 hours and extracted with 2×15 ml CH_2Cl_2 after cooling to room temperature. The aqueous layer was added in one portion to a stirring solution of 476 mg NVOC-Cl (1.7 mmol, 1eq) in 10 ml dioxane. Gas was generated and the mixture was stirred for 25 minutes, acidified with 1M KH_2PO_4 and extracted with 2×20 ml CH_2Cl_2. The organic layers were combined and dried over Na_2SO_4. Solvent was then rotoevaporated and the resulting residue was used directly in the next step. The residue was redissolved in 1 ml DMF, 0.4 ml chloroacetonitrile (6.32 mmol, 3.6eq) and 0.4 ml diisopropylethylamine (2.3 mmol, 1.36eq) were added. The reaction was kept in the dark overnight, diluted with 40 ml ethyl acetate, washed with 2×40ml KH_2PO_4 (1 M), and the organic layer was dried over Na_2SO_4. Flash chromatography using ethyl acetate:petroleum ether (40:60) provided 430 mg (57% for three steps) solid. ^{1}HNMR ($CDCl_3$) δ 7.71 (s, 1H), 7.27 (d, J=9.8Hz, 2H), 7.04 (d, J=9.8Hz, 2H), 6.93 (s,1H), 5.50 (m, 3H), 4.80 (m, 3H), 3.92 (s, 3H), 3.91 (s, 3H), 3.13 (m, 2H), 2.34 (s, 3H).

dCA-NVOC-4-Methylphenylalanine. Prepared by the ligation procedure described in section 5.4. FAB-MS calcd for $C_{39}H_{46}N_{10}O_{20}P_2$: 1036; found for $[M+H^+]$: 1037.

4-tert-Butyldimethylsilyloxyphenethyliodide 6. To a solution of 3.14g 4-Hydroxy-phenethyl alcohol **4** (30 mmol) in 300 ml dry THF was slowly added 17.75 ml n-buLi (1.695 M in hexane) (30 mmol, 1eq) at -78°C. Precipitates formed. The mixture was stirred at -78°C for 30 minutes then at room temperature for 30 minutes. The mixture was cooled to -78°C, and 4.6 g t-butyldimethylsilyl chloride (30 mmol, 1eq) was added as a solid in one portion. The reaction was slowly warmed to room

temperature and kept for 3 hours. A clear solution resulted. The volatiles were rotoevaporated off, and the residue was purified by flash chromatography using ethyl acetate:petroleum ether (10:90), providing 3.62 g (98% after recovered starting material) 4-t-butyldimethylsiloxyphenethyl alcohol **5**. This product was then converted to the corresponding mesylate by mixing with 5.4 ml diisopropylethylamine (88 mmol, 6.1eq) and 1.3 ml mesyl chloride (16.2 mmol, 1.13eq) in 50ml CH_2Cl_2 at 0°C. After 40 minutes, the reaction mixture was washed once with 50 ml water. CH_2Cl_2 was rotoevaporated off, providing a clear oil as the desired mesylate. The mesylate was then dissolved in 75 ml acetone, and 23 g NaI (153 mmol, 10.7eq) was added. The mixture was stirred in the dark overnight. Acetone was rotoevaporated. The solid was redissolved in water and CH_2Cl_2 (50 ml each). (Note that the top layer is the CH_2Cl_2 in this case). The organic layer was dried over Na_2SO_4. Flash chromatography using petroleum ether provided 4.87 g (91% for three steps) product as a colorless oil. ^{1}HNMR($CDCl_3$) δ 7.08 (d, 2H), 6.82 (d, 2H), 3.78 (t, 2H), 3.13 9t, 2H), 1.03 (s, 9H), 0.24 (s, 6H); ^{13}CNMR($CDCl_3$) δ 154.64, 133.62, 129.50, 120.31, 39.87, 25.92, 18.37, 6.63, -4.13.

(-)-Pseudoephedrine-4-t-butyldimethylsilyl-homo-tyrosinamide 7. To a flame-dried Schlenck flask was added 560 mg LiCl (13.1mmol, 6eq). The setup was flame-dried again. 6 ml THF was added, followed by addition of 0.62ml diisopropylamine (4.38mmol, 2eq). At -80°C, 2.51 ml n-buLi (1.695 M in hexane) (5.65 mmol, 1.95eq) was added slowly along the inner surface of the flask. The mixture was stirred for 20 minutes, then a solution of 486 mg (-)-pseudoephedrine glycinamide (2.19 mmol) in 3 ml THF was added slowly. A yellow opaque mixture resulted which was further stirred at -

80°C for 20 minutes, then at 0°C for 20 minutes, which produced a bright yellow slurry. At 0°C, a solution of 870 mg 4-t-butyldimethylsiloxyphenethyliodide **6** in 3 ml THF was added. The reaction was kept at 4°C overnight. 40 ml H_2O was added to the reaction, the mixture was extracted with 4×40ml CH_2Cl_2, and the organic layer was dried over K_2CO_3. Flash chromatography using NEt_3:MeOH:CH_2Cl_2 (2:2:96) provided 800 mg (80%) white solid. ^{1}HNMR ($CDCl_3$) δ 7.30 (m, 5H), 7.08(d, 2H), 6.81 (d, 2H), 4.75 (m, 1H), 4.58 (d, 1H), 3.80 (m, 3H), 2.75 (s, 3H), 2.70 (m, 2H), 2.43 (s, 1H), 1.80 (m, 2H), 1.07 (s, 9H), 1.00 (d, 3H), 0.26 (s, 6H); There are also some minor rotomer peaks: 2.99(s), 0.93(d), 0.22 (s).

Homo-Tyrosine. To a solution of 2.45g **7** (5.37 mmol) in 10 ml MeOH were added 25 ml H_2O and 16.5 ml 1N NaOH (16.5 mmol, 3eq). The mixture was refluxed for 4 hours and TLC showed complete hydrolysis. Extraction with 2×25 ml CH_2Cl_2 provided an aqueous solution of homo-tyrosine. The aqueous phase was then lyophylized to give 2.7 g white solid. Due to the excess NaOH used and water trapped in the solid, the yield is higher than the theoretical yield.1.28g. The product is used directly for the next step. ^{1}HNMR (D_2O) δ 6.97 (d, J=8.6Hz, 2H), 6.53 (d, J=8.6Hz, 2H), 3.22 (t, 1H), 2.44 (t, 2H), 1.78 (m, 2H).

NVOC-Homo-Tyrosine methyl ester. Into a solution of 600mg homo-tyrosine salt (1.19 mmol) in 50 ml MeOH gaseous HCl was bubbled for ten minutes, which resulted a light yellow solution. The mixture was then refluxed for 5 hours. The volatiles were rotoevaporated off. The solid was used directly in the next step by dissolving in 10 ml H_2O with 252 mg Na_2CO_3 (2.38 mmol, 2eq). The resulting solution was then

added in one portion to a solution of 328 mg NVOC-Cl (1.19 mmol, 1eq) in 10 ml dioxane. The reaction was kept for 30 minutes, acidified with 20 ml 1M KH_2PO_4, and extracted with 3×30 ml CH_2Cl_2. The combined organic layer was dried over Na_2SO_4. Flash chromatography using ethyl acetate:petroleum ether (50:50) provided 330 mg (62% for two steps) solid. ^{1}HNMR($CDCl_3$) δ 7.68 (s, 1H), 6.99 (d, J=8.0Hz, 2H), 6.95 (s, 1H), 6.75 (d, J=8.0Hz, 2H), 5.65 (d, J=8.7Hz, 1H), 5.57 (d, J=15.1Hz, 1H), 5.45 (d, J=15.1Hz, 1H), 4.37 (m, 1H), 3.97 (s, 3H), 3.92 (s, 3H), 3.68 (s, 3H), 2.60 (t, 2H), 2.10 (m, 1H), 1.94 (m,1H).

NVOC-4-NV-Homo-Tyrosine methyl ester 8. To a solution of 290 mg NVOC-homo-tyrosine methyl ester (0.647 mmol) in 40 ml dry acetonitrile, were added 98 mg K_2CO_3 (0.712 mmol, 1.1eq) and 165 mg NV-Cl (0.712 mmol, 1.1eq). The mixture was refluxed overnight. The volatiles were then rotoevaporated off. Flash chromatography using ethyl acetate: petroleum ether (60:40) provided 350mg (84%) solid. ^{1}HNMR($CDCl_3$) δ 7.80 (s, 1H), 7.74 (s, 1H), 7.37 (s, 1H), 7.13 (d, J=9.0Hz, 2H), 7.03 (s, 1H), 6.94 (d, J=9.0Hz, 2H), 5.50 (m, 5H), 4.44 (m, 1H), 4.03 (s,3H), 4.01 (s, 3H), 3.99 (s, 3H), 3.98 (s, 3H), 3.74 (s, 3H), 2.69 (t, 2H), 2.20 (m, 1H), 2.00 (m, 1H).

NVOC-4-NV-Homo-Tyrosine cyanomethyl ester 9. To a solution of 330 mg NVOC-4-NV-homo-tyrosine methyl ester (0.513 mmol) in 10ml CH_2Cl_2 were added 10 ml 1N NaOH and 10 drops of Aliquat 336. The reaction was stirred vigorously at room temperature for 7 hours. The reaction was stopped and the two layers were separated. The aqueous layer was extracted once with 15 ml CH_2Cl_2. The combined organic layer was dried over Na_2SO_4. Flash chromatography using ethyl

acetate:petroleum ether:acetic acid (50:50:2) provided the acid which was used directly in the next step. The acid was dissolved in 1 ml DMF, 0.2 mL chloroacetonitrile (3.16 mmol, 6eq) and 0.2 ml diisopropylethylamine (1.15 mmol, 2.24eq) were added. The reaction was kept in the dark overnight, then diluted with 40 ml ethyl acetate, and washed with 2×40ml KH_2PO_4 (1 M). The organic layer was dried over Na_2SO_4. Flash chromatography using ethyl acetate:petroleum ether (50:50) provided 300 mg (87% for two steps) oily material. ^{1}HNMR ($CDCl_3$) δ 7.78 (s, 1H), 7.73 (s, 1H), 7.35 (s, 1H), 7.13 (d, J=8.2Hz, 2H), 7.01 (s, 1H), 6.95 (d, J=8.2Hz, 2H), 5.56 (m, 5H), 4.79 (d, J=16.4Hz, 1H), 4.67 (d, J=16.4Hz, 1H), 4.45 (m, 1H), 4.02 (s, 3H), 3.99 (s, 3H), 3.98 (s, 3H), 3.95 (s, 3H), 2.69 (t, 2H), 2.20 (m,1H), 2.08 (m,1H).

dCA-NVOC-4-NV-Homo-Tyrosine. Prepared by the ligation procedure described in section 5.4. FAB-MS: calcd for $C_{48}H_{55}N_{11}O_{25}P_2$: 1247; found for [$M^+$]: 1247.

NVOC-Tyrosine t-butyl ester 16. To a mixture of 1.18 g L-tyrosine t-butyl ester **15** (5 mmol), 0.54 mg Na_2CO_3 (5 mmol, 1eq) in 20 mL each water and THF (two clear layers) was added a solution of 1.40 g NVOC-Cl (5 mmol, 1eq) in 25 mL THF. After 15 min the cloudy yellow mixture was rotoevaporated and partitioned between 10 mL water and 30 mL CH_2Cl_2. The layers were separated and the aqueous layer extracted with 3×10 mL more CH_2Cl_2. The organic layers were combined, dried (Na_2SO_4), and filtered. The crude material was chromatographed (CH_2Cl_2 to 5:1 CH_2Cl_2:ethyl acetate), affording 2.22 g (93%) of a pale yellow foamy solid. ^{1}H NMR ($CDCl_3$) δ 7.68 (s, 1H), 6.99 (d, J=8.4 Hz, 1H), 6.97 (s, 1H), 6.70 (d, J=8.4 Hz, 1H), 6.65 (s, 1H), 5.56 (d, J=8.3 Hz, 1H), 5.54

and 5.45 (AB, J=15.2 Hz, 1H), 4.50 (d, J=8.3, 6.1 Hz, 1H), 3.92 (s, 3H), 3.91 (s, 3H), 3.05 (dd, J=14.2, 5.9 Hz, 1H), 2.97 (dd, J=14.2, 6.5 Hz, 1H), 1.44 (s, 9H).

NVOC-4-O-3-Bromopropyl tyrosine t-butyl ester 17. To a flame-dried 100 mL flask was added 330 mg (1.0 mmol, 2eq) of cesium carbonate, followed by 0.8 g (4.0 mmol, 8eq) of 1, 3-dibromopropane and 15 mL anhydrous DMF. A solution of 238 mg (0.5 mmol) **16** in 10 mL DMF was then injected slowly into the mixture via a syringe pump during seven hours. Reaction was kept in the dark overnight and was stopped after disappearance of starting material. Added 30 mL of water to the reaction mixture, extracted with 3×30 mL ethyl acetate. The combined organic layers were washed with water once and dried over sodium sulfate. Flash chromatography using ethyl acetate:petrolium ether (from 10% to 30%) provided 170 mg (57%) product. ^{1}HNMR ($CDCl_3$) δ 7.68 (s, 1H), 7.07 (d, J=8.4 Hz, 2H), 6.96 (s, 1H), 6.84 (d, J=8.4 Hz, 2H), 5.56 (d, J=8.3 Hz, 1H), 5.54 and 5.45 (AB, J=15.2 Hz, 1H), 5.33 (d, 1H), 4.50 (m, 1H), 4.07 (m, 2H), 3.95 (s, 6H), 3.60 (t, 2H), 3.05 (m, 2H), 2.31 (m, 2H), 1.42 (s, 9H).

NVOC-4-O-3-Bromopropyl tyrosine cyanomethyl ester 18. To the azotropically dried (with toluene) **17** (170 mg) in 1 mL of methylene chloride was added slowly 1.7 mL of TFA. The mixture was stirred at room temperature for one hour. TFA was removed by passing argon through the reaction solution. The residue was rotoevaporated with toluene twice (2×10 mL) and used directly in the next step by dissolving in 3 mL of DMF, 0.4 mL of chloroacetonitrile and 57 μL of diisopropylethylamine. Reaction was kept at room temperature for 14 hours. Stopped the reaction by adding 20 mL of 1M KH_2PO_4. Extracted with 2×50 mL ethyl acetate.

153 mg (93%) product was obtained after flash chromatography. ^{1}HNMR ($CDCl_3$) δ 7.66 (s, 1H), 7.04 (d, J=8.4 Hz, 2H), 6.90 (s, 1H), 6.83 (d, J=8.4 Hz, 2H), 5.54 and 5.45 (AB, J=15.2 Hz, 1H), 5.46 (b, 1H), 4.74 (m, 3H), 4.06 (m, 2H), 3.93 (s, 6H), 3.57 (t, 2H), 3.08 (m, 2H), 2.28(m, 2H).

NVOC-Tyr-O3Q 19. Compound **18** (153 mg) was mixed with 10eq of sodium iodide in 10 mL acetone at room temperature. All the sodium iodide was dissolved in about five minutes. About one hour later, precipitates started to form. Reaction was kept stirring in the dark overnight. Acetone was then rotoevaporated off and the solid was partitioned between water and methylene chloride (25 mL each). The organic layer was dried over sodium sulfate and concentrated to give 160 mg pure yellowish solid, yield 97%. This product was carried on to make **19**. To a 25 mL flask containing the iodide was added 7 ml of dry toluene and 12 mL of dry THF. To this resulting solution at 0 °C was quickly added about 1.2 mL of trimethylamine (pre-cooled at -5°C to -10°C for one hour). The reaction was kept in the dark for six days at room temperature. Precipitates formed on the inner wall of the flask. Argon was purged through the mixture to get rid of the amine, which was trapped by a 6N HCl solution. When most of the amine were removed (indicated as neutral by wet pH paper), the solvent was then decanted off and the solid was rinsed with ethyl acetate three times and dried under high vacuum. Yield, 130 mg (74%). ^{1}HNMR ($CDCl_3$) δ 7.72 (s, 1H), 7.22 (d, J=8.4 Hz, 2H), 6.96 (s, 1H), 7.09 (s, 1H), 6.88 (d, J=8.4 Hz, 2H), 6.36 (b, 1H), 5.54 and 5.45 (AB, J=15.2 Hz, 1H), 4.82 (s, 2H), 4.50 (m, 1H), 4.07 (m, 2H), 3.95 (s, 3H), 3,90 (s, 3H), 3.47 (t, 2H), 3.08 (m, 9H), 2.98 (m, 2H), 2.00-2.10 (shoulder, 2H).

dCA-NVOC-Tyr-O3Q. Prepared by the ligation procedure described in section 5.4. FAB-MS calcd for $C_{44}H_{57}N_{11}O_{21}P_2$: 1137.5; found for $[M^+]$: 1137.

α-NVOC-ε-Boc-Lysine cyanomethyl ester 21. To a 10 ml solution in dioxane containing 1.0 g (4.06 mmol) of NVOC-Cl was added in one portion an aqueous solution containing 1.12 g (4.06 mmol) of the amino acid and 0.86 g (2eq) of sodium carbonate. One hour later, the bright yellow reaction mixture was diluted with methylene chloride and washed with 1M KH_2PO_4 (pH 4). The organic layer was dried over sodium sulfate and concentrated under vacuum. The crude product was used directly in next step by dissolving in 1.0 ml of chloroacetonitrile, 1.0 ml of diisopropylethylamine and 10 ml of DMF. The reaction was kept in the dark overnight, and then diluted with 25 ml CH_2Cl_2, washed with 2×25 ml KH_2PO_4 (1M), and dried over Na_2SO_4. Flash column chromatography using ethyl acetate:petroleum ether (50:50) provided 1.94 g (90%) of yellowish solid. ^{1}H NMR ^{1}HNMR ($CDCl_3$) δ 7.76 (s, 1H), 7.04 (s, 1H), 5.88 (b, 1H), 5.66 and 5.45 (AB, J=15.2 Hz, 1H), 4.80 (s, 3H), 4.43 (m, 1H), 4.04 (s, 3H), 4.00 (s, 3H), 3.18 (b, 2H), 1.94 (m, 2H), 1.50 (s & b, 13H).

α-NVOC-Lysine cyanomethyl ester 22. 566 mg (1.06 mmol) of **21** was dissolved in 5 mL of CH_2Cl_2 and 5 mL of trifluoroacetic acid (TFA). The mixture was kept stirring at room temperature for about 40 minutes. Argon was purged through the mixture to get rid of TFA. Residual solvents were rotoevaporated off and the resulting oil was dried on vacuum line over night. 5 mL of toluene was then added and rotoevaporated off. After drying again on the high vacuum line for about 10 minutes, this product was dissolved in 15 mL of dry THF. At 0°C, the solution was slowly

injected over 20 minutes into a solution containing 0.88 g (4.24 mmol, 4eq, 90% purity) of 2-bromoethylchloroformate, 0.41 g (3.18 mmol, 3eq) of diisopropylamine, and 10 mL of THF. The reaction was allowed to complete two hours after the addition. THF was rotoevaporated off and the residue was redissolved in CH_2Cl_2, and washed with KH_2PO_4 (1M) and water, dried over sodium sulfate. Flash column chromatography with ethylacetate:petroleum ether (from 50:50 to 60:40) provided 400 mg (65%) of desired product. ^{1}HNMR ($CDCl_3$) δ 7.66 (s,1H), 6.97 (s, 1H), 5.89 (d, 1H), 5.49 (m, 2H), 5.14 (b, 1H), 4.77 (m, 2H), 4.33 (b, 3H), 3.96 (s, 3H), 3.91 (s, 3H), 3.44 (m, 2H), 3.14 (b, 3H), 1.80 (b, 2H), 1.48 (b, 4H).

α-NVOC-ε-2-Iodoethyloxycarbonyl lysine cyanomethyl ester 23. 270 mg (0.463 mmol) of the product obtained above was dissolved in 12 mL of acetone, followed by addition of 0.89 g (4.63 mmol, 10eq) of sodium iodide. All the sodium iodide was dissolved in about five minutes. About one hour later, precipitates started to form. Reaction was kept stirring in the dark overnight. Acetone was then rotoevaporated off and the solid was partitioned between water and methylene chloride (25 mL each). The organic layer was dried over sodium sulfate and concentrated to give 280 mg pure yellowish solid, yield 96%. ^{1}HNMR ($CDCl_3$) δ 7.63 (s, 1H), 6.97 (s, 1H), 5.94 (b, 1H), 5.44 and 5.38 (AB, 1H), 5.13 (b, 1H), 4.84 and 4.70 (AB, 2H), 4.35 (m, 1H), 4.24 (t, 2H), 3.97 (s, 3H), 3.89 (s, 3H), 3.24 (t, 2H), 3.16 (m, 2H), 1.80 (b, 2H), 1.48 (m, 4H).

NVOC-Lys-carbamylcholine 24. To a 25 mL flask containing 30 mg of the iodide **23** was added 7 ml of dry toluene and 12 mL of dry THF. To this resulting solution at 0° C was quickly added about 1.2 mL of trimethylamine (pre-cooled at -5°C -

-10°C for one hour). The reaction was kept in the dark for six days at room temperature. Precipitates formed on the inner wall of the flask. Argon was purged through the mixture to get rid of the amine, which was trapped by a 6N HCl solution. When most of the amine were removed (indicated as neutral by pH paper), the solvent was then decanted off and the solid was rinsed with ethyl acetate three times and dried under high vacuum. This material was used in dCA coupling without further purification. ^{1}HNMR ($CDCl_3$) δ 7.72 (s, 1H), 7.20 (s, 1H), 6.68 (d, 1H), 6.14 (b, 1H), 5.44 and 5.38 (AB, 1H), 4.85 (s, 2H), 4.43 (b, 2H), 4.2 (m, 1H), 4.01 (s, 3H), 3.91 (s, 3H), 3.62 (m, 2H), 3.20 (s, 9H), 3.12 (m, 2H), 1.84 (b, 2H), 1.50 (m, 4H).

dCA-NVOC-Lys-Carbamylcholine. Prepared by the ligation procedure described in section 5.4. FAB-MS calcd for $C_{41}H_{59}N_{12}O_{22}P_2$: 1133.9; found for $[M^+]$: 1139.

Ethyl 3-bromo-2-hydroxyimino-propanoate 26. To a three-necked 250 mL flask was added 24 g of ethyl pyruvate. At 65°C and under a steady stream of nitrogen was added dropwise 12.5 mL of bromine over 1.2 hours. (Caution: safety shield would be used. Also, nitrogen takes away the by-product HBr, which was passed through a 3N NaOH solution). Two hours later, a golden liquid resulted and it was carried on to the next step without purification. The liquid was dissolved in 150 mL of CH_2Cl_2 and was mixed with a 200 mL aqueous solution containing 34 g of hydroxyamine sulfate. The reaction was kept stirring vigorously overnight. Separated the two layers. The aqueous layer was extracted with 100 mL of CH_2Cl_2. The organic layers were combined and dried over sodium sulfate. CH_2Cl_2 was rotoevaporated off and the resulting oil was redissolved

in minimal amount of ethyl acetate. Petroleum ether was added until solution turned cloudy. Stored in the refrigerator. Obtained 18.2 g (42%) of pure product. (There was still a lot of product in the mother liquid). ^{1}HNMR ($CDCl_3$) δ 10.64 (b, 1H), 4.38 (q, 2H), 4.26 (s, 2H), 1.40 (t, 3H).

5-CN-Tryptophan precursor 27. In a 100 mL flask, 0.42 g (2 mmol) of **26** and 0.98 g (6.89 mmol, 3.45eq) of 5-cyano-indole were dissolved in 20 mL of dry CH_2Cl_2. To the solution, 0.32 g (3 mmol, 1.5eq) of sodium carbonate was added. The reaction was kept stirring vigorously for 24 hours. Added 50 mL each of CH_2Cl_2 and water. Collected the precipitates by filtration (360 mg). Organic layer from mother liquid was dried and flash chromatography gave additional 170 mg of product. Total yield, 530 mg (98%). ^{1}HNMR (CD_3CN) δ 9.96 (b, 1H), 9.58 (b, 1H), 8.09 (s, 1H), 7.52 (d, 1H), 7.38 (d, 1H), 7.25 (d, 1H), 4.20 (q, 2H), 3.99 (b, 2H), 1.23 (t, 3H).

NVOC-5-CN-Tryptophan ethyl ester 28. 1) The reduction of **27** was carried out as follows: in a small Erlenmeyer flask, 0.66 g Al shots was treated for three minutes with 8% NaOH. The shots were then rinsed with water, treated for 5 minutes with 2% $HgCl_2$ solution. The formed Al-Hg was dropped into a 10 ml THF:H_2O (9:1) solution containing 80 mg of **28**. The mixture was stirred at room temperature for 20 hours. The resulting mixture with gray precipitates was then filtered through a short silica gel pad using first EtOAc and then EtOAc:MeOH as the eluents. The solvent was rotoevaporated off to provide an oily material which was used directly in the next step. ^{1}HNMR ($CDCl_3$) δ 9.48 (b, 1H), 7.95 (s, 1H), 7.34 (m, 1H), 7.15 (d, 1H), 6.99 (s, 1H), 4.20 (m, 2H), 3.84 (m, 1H), 3.29 (dd, 1H), 3.09 (dd, 1H), 1.91 (b, 2H), 1.27 (t, 3H). 2) The product

obtained above was then reacted with 92 mg of NVOC-Cl using standard methods. A total of 112 mg of **28** was obtained, yield, 76%. ^{1}HNMR (DMSO) δ 8.49 (s, 1H), 7.91 (s, 1H), 7.71 (s, 1H), 7.42 (d, 1H), 7.18 (d, 1H), 6.96 (s, 1H), 5.47 (m, 3H), 4.71 (m, 1H), 4.16 (m, 2H), 3.96 (s, 3H), 3.93 (s, 3H), 3.37 (m, 2H), 1.25 (t, 3H).

NVOC-5-CN-Tryptophan cyanomethyl ester 29. 110 mg of 28 was dissolved in 10 mL of dioxane and 2 mL of water at slightly elevated temperature (**28** is not soluble in MeOH or CH_3CN). After cooled down to room temperature, 0.3 mL of 1N NaOH was added and the mixture was stirred for one hour. TLC indicated that there was still some starting material left. Warmed up the reaction to 37°C for 5 minutes and added another 0.3 mL of 1N NaOH. 15 minutes later, the reaction went completion. Added 35 mL of CH_2Cl_2 , 10 mL of 1M KH2PO4, and 20 mL of water. The phases were separated and the aqueous layer was extracted again with 20 mL of CH_2Cl_2. The organic layers were combined and dried over sodium sulfate. The solvent was rotoevaporated off to afford product which was used directly in the next step for cyanomethylation, which was done using standard methods. 65 mg of **29** (58% for two steps) was obtained. ^{1}HNMR (DMSO) δ 11.52 (b, 1H), 8.24 (d, 1H), 8.15 (s, 1H), 7.69 (s, 1H), 7.49 (d, 1H), 7.39 (m, 2H), 7.08 (s, 1H), 5.30 (m, 2H), 4.97 (s, 2H), 4.45 (m, 1H), 3.85 (s, 3H), 3.82 (s, 3H), 3.34 (d, 2H), 3.10 (m, 2H).

dCA-NVOC-5-CN-Trp. Prepared by the ligation procedure described in section 5.4. FAB-MS: calcd for $C_{39}H_{46}N_{10}O_{20}P_2$: 1036; found $[M+H]^+$:1037.

3, 5-Difluorophenylacetylene derivative 31. To a flamed-dried flask was added 1.54 g (5.0 mmol) of **30**, 12 mL of triethylamine and 3 mL of THF. Argon was purged through the solution for 5 minutes. 285 mg (8% eq) of catalyst bis(triphenylphosphine) palladium dichloride and 77 mg of CuI (8% eq) were then added, followed by of 1.06 mL (0.74 g, 7.44 mmol) of trimethylsilylacetylene. The reaction was kept stirring at room temperature for 15 hours. TLC showed that there was still at least 50% starting material left. Stopped the reaction by distilling off the solvent. The residue was purified via flash chromatography using silica gel pre-treated with 3% NEt_3 in hexanes. Yield, 180 mg (16%). ^{1}H NMR ($CDCl_3$) δ 6.80 (m, 2H), 4.09 (b, 2H), 0.29 (s, 9H).

5,7-Difluoroindole 32. 180 mg of **31** was dissolved in 7 mL of DMF. After purging the solution with argon for two minutes, 10 mg (6% eq) of CuI was added. The mixture was then heated up to reflux for 5 hours. Diluted with EtOAc and washed with water. 90 mg (74%) of **32** was obtained after chromatography (petroleum ether). ^{1}H NMR ($CDCl_3$) δ 8.31 (b, 1H), 7.27 (m, 1H), 7.11 (m, 1H), 6.74 (m, 1H), 6.55 (m, 1H).

dCA-NVOC-5,7-F_2-Trp. Prepared by the ligation procedure described in section 5.4. HR FAB-MS: calcd for $C_{40}H_{43}N_{11}O_{20}P_2F_2$: 1097.2129; found $[M-H]^-$: 1096.2011.

3,4,5-Trifluorophenylacetylene derivative 34. To a flame-dried flask were added 0.94 g (4.16 mmol) of **33** and 12 mL of triethylamine. Argon was purged through the solution for 5 minutes. 29 mg (1% eq) of catalyst bis (triphenylphosphine) palladium dichloride and 8 mg of CuI (1% eq) were then added, followed by 0.88 mL (0.613 g,

6.24 mmol) of trimethylsilylacetylene. The reaction was kept stirring at room temperature for 15 hours. TLC showed that there was still at least 50% starting material left. Added another 29 mg of catalysts and 0.4 mL of trimethylsilylacetylene. 20 hours later, the reaction was still incomplete. Stopped the reaction by distilling off the solvent. The residue was purified via flash chromatography using silica gel pre-treated with 3% NEt_3 in hexanes. Yield, 250 mg (25%) (68% based on recovered starting material). ^1H NMR ($CDCl_3$) δ 6.92 (m, 1H), 4.19 (b, 2H), 0.26 (s, 9H).

5,6,7-Trifluoroindole 35. 250 mg of **34** was dissolved in 7 mL of DMF. After purging the solution with argon for two minutes, 10 mg (5% eq) of CuI was added. The mixture was then heated up to reflux for 5 hours. Diluted with EtOAc and washed with water. 80 mg (45%) of **35** was obtained after chromatography (petroleum ether). ^1H NMR ($CDCl_3$) δ 8.35 (b, 1H), 7.28 (m, 1H), 7.16 (m, 1H), 6.53 (m, 1H).

dCA-NVOC-5,6,7-F_3-Trp. Prepared by the ligation procedure described in section 5.4. HR FAB-MS: calcd for $C_{40}H_{42}N_{11}O_{20}P_2F_3$: 1115.2034; found $[M-H]^-$: 1114.1959.

1-Pentafluorophenyl-2-nitro-ethanol 37. To a solution of 10 g (0.05 mol) of pentafluorobenzylaldehyde and 3.17g (0.052 mol) of nitromethane in 50 mL of MeOH, was added dropwise a solution of 2.5 g (0.055 mol) NaOH in 5 mL of water at 0°C. After stirring in an ice-water bath for one and one half hours at 0°C to room temperature, 50 mL of water was added, followed by addition of 1N HCl to adjust to pH 4. Mixture changed color from orange to greenish during the course. Extracted the mixture with

EtOAc 2×75 mL and the combined organic layer was washed once with water and dried over sodium sulfate. The solvent was rotoevaporated off to give 14.2 g of light orange oil (still contains about 20% EtOAc). ^{1}H NMR ($CDCl_3$) δ 5.86 (d, 1H), 5.01 (m, 1H), 4.64 (dd, 1H), 4.45 (b, 1H).

4,5,6,7-Tetrafluoroindole 38. To a mixture of acetic acid, water, and ethanol (35 mL:50 mL:18 mL) at 60°C was added a solution of **37** in the same solvent mix (cold) with stirring over 15 minutes. Meanwhile 10 g of zinc powder was added in small portions. After addition, the resulting mixture was heated to reflux for one hour. The reaction was cooled down and the solvent was rotoevaporated off. Ethanol was added to extract the product. However, emulsion occurred. Filtered off insolubles and filtrate was concentrated. Flash chromatography yielded some pure reduced product (low yield), which was used in the next reaction. 160 mg of the product obtained above was dissolved in 10 mL dry DMF, and the solution was purged with argon for three minutes. The solution was then heated up to reflux for 8 hours. Diluted with EtOAc and washed with water. 100 mg (yield for this step, 75%) of **38** was obtained as needle crystals after chromatography. ^{1}H NMR ($CDCl_3$) δ 8.62 (b, 1H), 7.25 (m, 1H), 6.66 (m, 1H).

dCA-NVOC-4,5,6,7-F_4-Trp. Prepared by the ligation procedure described in section 5.4. HR FAB-MS: calcd for $C_{40}H_{41}N_{11}O_{20}P_2F_4$: 1133.1940; found $[M-H]^-$: 1132.1831.

NVOC-4-(Trifluoromethanesulfonyl)phenylalanine t-butyl ester 39. A solution of 0.825 g (1.73 mmol) NVOC-tyrosine t-butyl ester and 0.41 mL

diisopropylethylamine (1.2 eq) in 25 mL dry CH_2Cl_2 was cooled to 0†°C under argon. N-phenyltrifluoromethanesulfonimide (0.94 g, 2.65 mmol, 1.34 eq) was then added in one portion. 12 hours later the reaction was quenched by adding 25 mL of water. The layers were gently shaken and separated and the aqueous layer extracted with 2×10 mL more CH_2Cl_2. The organic layers were combined, dried (Na_2SO_4), and filtered. The crude product was chromatographed (3:7 EtOAc:petroleum ether), providing 0.94 g (89%) of a pale yellow foamy solid. ^{1}H NMR ($CDCl_3$) δ 7.70 (s, 1H), 7.30 (d, J=8.7 Hz, 2H), 7.21 (d, J=8.7 Hz, 2H), 6.99 (s, 1H), 5.55 (d, J=8.3 Hz, 1H), 5.51 (m, 2H), 4.55 (m, 1H), 3.97 (s, 3H), 3.95 (s, 3H), 3.14 (d, J=6.3 Hz, 2H), 1.39 (s, 9H).

NVOC-4-Acetylphenylalanine t-butyl ester 40. To an oven-dried three-necked flask were added 280 mg (0.46mmol) of **39**, 2.6 mg $Pd(OAc)_2$ (0.025eq), 5.3 mg 1,3-bis(diphenylphosphino)propane (DPPP) (0.0275eq) and 5ml anhydrous DMF. To the stirring mixture were added 0.1 ml diisopropylethylamine (DIPEA) (0.57 mmol, 1.25eq) and 0.3 ml vinyl butyl ether (2.32 mmol, 5eq). The reaction was kept in an 80°C sand bath. More reagents were added 6 hours later: 5 mg $Pd(OAc)_2$, 10 mg DPPP, 0.1 ml DIPEA, and 0.3 ml vinyl butyl ether. After stirring overnight another addition of the above reagents was made. The reaction was then cooled and quenched by the addition of 10 ml 3N HCl. 30 minutes later, the mixture was extracted with 2×20ml ethyl acetate, the organic layer was dried over Na_2SO_4. Column chromatography using ethyl acetate: petroleum ether (30:70) provided 130 mg (56%) product. ^{1}HNMR ($CDCl_3$) δ 7.88 (d, J=8.5Hz, 2H), 7.68 (s, 1H), 7.28 (d, J=8.5Hz, 2H), 6.95 (s, 1H), 5.62 (d, J=7.7Hz, 1H), 5.48 (dd, 2H), 4.58 (m, 1H), 3.95(s,3H), 3.93 (s, 3H), 2.58 (s, 3H), 1.42 (s, 9H) ^{13}CNMR($CDCl_3$) δ 198.09, 170.84, 155.76, 154.15, 148.63, 142.40, 136.49, 130.16,

128.98, 128.51, 110.47, 108.70, 83.27, 64.26, 60.85, 56.89, 55.56, 38.70, 28.47, 27.03, 14.70.

NVOC-4-Acetylphenylalanine cyanomethyl ester 42. To a solution of 130 mg (0.258 mmol) **40** in 2.5 ml CH_2Cl_2 was added 2.5 ml trifluoroacetic acid (TFA). The mixture was stirred at room temperature for 2 hours. TFA was removed by passing argon through the solution and the resulting residue was redissloved in 25 ml CH_2Cl_2, washed with 2×25 ml KH_2PO_4 (1M), and dried over Na_2SO_4. The solvent was rotoevaporated. The crude product **41** was dissloved in 0.5 ml DMF, 0.1 ml chloroacetonitrile (1.58 mmol, 6eq) and 0.1 ml DIPEA (0.575 mmol, 2.9eq) were then added. The reaction was kept in the dark overnight, and then diluted with 25 ml CH_2Cl_2, washed with 2×25 ml KH_2PO_4 (1M), and dried over Na_2SO_4. Flash column chromatography using ethyl acetate:petroleum ether (50:50) provided 110 mg (88%) of off-white solid. ^{1}HNMR($CDCl_3$) δ 7.86 (d, J=7.5Hz,2H), 7.63 (s,1H), 7.26 (d, J=7.5Hz, 2H), 6.90 (s,1H), 5.98 (d, J=9.0, 1H), 5.42 (dd,2H), 4.76 (m 3H), 3.88 (s,3H), 3.84 (s, 3H), 3.20 (m, 2H), 2.55 (s. 3H).

dCA-NVOC-4-Acetylphenylalanine. Prepared by the ligation procedure described in section 5.4. FAB-MS calcd for $C_{40}H_{46}N_{10}O_{21}P_2$: 1064; $[M-H]^-$: 1063.

Allylation of NVOC-Tyrosine t-butyl ester - 43. To a solution of 1.05 g (2.21 mmol) **16** in 12 ml anhydrous DMF were added 1.02 g potassium carbonate powder and 0.532 g (4.42 mmol, 2eq) of 2-methyl allylbromide. The reaction was kept stirring in the dark for 12 hours. Diluted with 50 ml EtOAc, washed with water, brine, and dried

over Na_2SO_4. Flash column chromatography using ethyl acetate:petroleum ether (10:40) provided 0.8 g (68%) of off-white solid. ^{1}HNMR($CDCl_3$) δ 7.66 (d, 1H), 7.06 (d, 2H), 6.94 (s, 1H), 6.80 (d, 2H), 5.50 (m, 3H), 5.05 (s, 1H), 4.94 (s, 1H), 4.46 (m, 1H), 4.36 (s, 2H), 3.90 (s, 6H), 3.01 (m, 2H), 1.79 (s, 3H), 1.40 (s, 9H). ^{13}CNMR($CDCl_3$) δ 170.92, 157.83, 155.34, 153.71, 147.90, 140.85, 139.35, 130.39, 128.57, 128.13, 114.72, 112.70, 109.41, 108.02, 82.37, 71.63, 63.66, 56.45, 56.37, 55.42, 37.29, 28.00, 19.47.

NVOC-4-Acetonyl tyrosine t-butyl ester 44. To a solution of 0.8 g (1.51 mmol) of **43** in 15 ml acetone was added 1 mL of OsO_4 in water (4% by weight), followed by 0.43 g (0.356 mmol, 2.36eq) N-methyl morpholine oxide (NMO). Reaction was quenched 26 hours later by addition of 2 g of $NaHSO_3$ and 10 mL of water. The mixture was stirred for 20 minutes. Diluted with 50 mL of EtOAc and the layers were separated. The crude diol product was dissolved in 20 mL of acetone and reacted with three-fold excess of sodium periodate. Three hours later, solvent was rotoevaporated off and the residue was partitioned between EtOAc and water (35 mL each). Organic layer was dried over Na_2SO_4. The residue was purified by flash column chromatography (ethyl acetate:petroleum ether (10:40)), providing 0.68 g (85%) of off-white solid. ^{1}HNMR($CDCl_3$) δ 7.54 (s, 1H), 7.00 (d, 2H), 6.85 (s, 1H), 6.70 (d, 2H), 5.66 (d, 1H), 5.33 (m, 2H), 4.41 (s, 2H), 4.36 (m, 1H), 3.79 (s, 6H), 2.90 (m, 2H), 2.13 (s, 3H), 1.30 (s, 9H).

NVOC-4-Acetonyl tyrosine cyanomethyl ester 46. To a solution of 266 mg (0.5 mmol) **44** in 2.5 ml CH_2Cl_2 was added 2.5 ml trifluoroacetic acid (TFA). The mixture was stirred at room temperature for 2 hours. TFA was purged by passing argon

through the solution and the resulting residue was redissloved in 25 ml CH_2Cl_2, washed with 2×25 ml KH_2PO_4 (1M), and dried over Na_2SO_4. The solvent was rotoevaporated off and the crude product **45** was dissloved in 0.5 ml DMF, 0.1 ml chloroacetonitrile (1.58 mmol, 3.2eq) and 0.1 ml DIPEA (0.575 mmol, 1.15eq). The reaction was kept in the dark overnight, and then diluted with 25 ml CH_2Cl_2, washed with 2×25 ml KH_2PO_4 (1M), and dried over Na_2SO_4. The residue was purified by flash column chromatography (ethyl acetate:petroleum ether (50:50)), providing 230 mg (87%) of yellowish solid. ^{1}HNMR ($CDCl_3$) δ 7.71 (s, 1H), 7.09 (d, 2H), 6.93 (s, 1H), 6.85 (d, 2H), 5.57 and 5.46 (AB, 1H), 5.25 (d, 1H), 4.75 (m, 3H), 4.54 (s, 2H), 3.96 (s, 3H), 3.95 (s, 3H), 3.11 (d, 2H), 2.28 (s, 3H).

dCA-NVOC-4-Acetonyltyrosine. Prepared by the ligation procedure described in section 5.4. HR FAB-MS: calcd for $C_{41}H_{48}N_{10}O_{22}P_2$: 1094.2419; found $[M-H]^-$: 1093.2383.

NVOC-L-*allo*-Threonine methyl ester 48. To a solution of 231.3 mg (0.84 mmol) of NVOC-Cl in 10 ml dioxane was added in one portion an aqueous solution containing 100 mg (0.84 mmol) of L-*allo*-Threonine **47** and 89 mg (0.84 mmol) of sodium carbonate. One hour later, the bright yellow reaction mixture was diluted with methylene chloride and washed with 1M KH_2PO_4 (pH 4). The organic layer was dried over sodium sulfate and concentrated under vacuum. The crude product was used directly in the next step without further purification. To the flask containing the crude product were added 5 ml of DMF and 2 mL of MeI, followed by 135 mg of sodium carbonate. The reaction was kept stirring in the dark overnight, and then diluted with

25 ml CH_2Cl_2, washed with 2×25 ml KH_2PO_4 (1M), and dried over Na_2SO_4. Flash column chromatography using ethyl acetate:petroleum ether (50:50) provided 253 mg (81% for two steps) **48** as a solid. ^{1}HNMR ($CDCl_3$) δ 7.72 (s, 1H), 7.00 (s, 1H), 5.84 (d, 1H), 5.54 (s, 2H), 4.46 (m, 1H), 4.19 (m, 1H), 4.00 (s, 3H), 3.95 (s, 3H), 3.79 (s, 3H), 2.59 (d, 1H), 1.23 (d, 3H).

NVOC-L-*allo*-O-Methyl-Threonine methyl ester 49. To a solution of 50 mg (0.134 mmol) of **48** in 5 mL of dry CH_2Cl_2 was added 1.38 g (6. mmol, 50eq) 2,6-di-t-butyl-4-methyl pyridine, followed by 0.38 ml (551 mg, 3.3 mmol, 25eq) methyl triflate (CAUTION: extremely toxic). The reaction was kept stirring at room temperature for two days. It was then quenched carefully with 8% sodium bicarbonate. Diluted with 25 ml CH_2Cl_2, washed with 2×25 ml KH_2PO_4 (1M), and dried over Na_2SO_4. Flash column chromatography using ethyl acetate:petroleum ether (50:50) provided 30 mg (58%) **49** as a solid. ^{1}H NMR ($CDCl_3$) δ 7.72 (s, 1H), 7.03 (s, 1H), 5.58 (m, 3H), 4.56 (m, 1H), 4.03 (s, 3H), 3.86 (s, 3H), 3.76 (s, 3H), 3.71 (m, 1H), 3.37 (s, 3H), 1.20 (s, 3H).

NVOC-L-*allo*-O-Methyl-Threonine cyanomethyl ester 51. To a solution of 30 mg (0.078 mmol) of **49** in 3 mL of MeOH and 0.5 mL of water was added 80 μL of 1N NaOH. The mixture was stirred for a few hours. Diluted with 10 mL of CH_2Cl_2, 3 mL of 1M KH_2PO_4, and 10 mL of water. The phases were separated and the aqueous layer was extracted again with another 10 mL of CH_2Cl_2. The organic layers were combined and dried over sodium sulfate. The solvent was then rotoevaporated off to afford **50** which was used directly in the next step. Cyanomethylation was done using standard methods. 23 mg of **51** (74% for two steps) was obtained. ^{1}HNMR ($CDCl_3$) δ

7.72 (s, 1H), 6.99 (s, 1H), 5.69 (d, 1H), 5.60 and 5.48 (AB, 2H), 4.87 and 4.73 (AB, 2H), 4.55 (m, 1H), 4.01 (s, 3H), 3.95 (s, 3H), 3.72 (m, 1H), 3.36 (s, 3H), 1.27 (d, 3H).

dCA-NVOC-L-*allo*-O-Me-Thr. Prepared by the ligation procedure described in section 5.4. HR FAB-MS: calcd for $C_{34}H_{44}N_{10}O_{21}P_2$: 990.2157; found $[M-H]^-$: 989.2112.

NVOC-O-t-Butyldimethylsilyl threonine methyl ester 53. To a solution of 276 mg (1.0 mmol) of NVOC-Cl in 10 ml dioxane was added in one portion an aqueous solution containing 170 mg (1.0 mmol) of threonine methyl ester **52** and 106 mg (1.0 mmol) of sodium carbonate. One hour later, the bright yellow reaction mixture was diluted with methylene chloride and washed with 1M KH_2PO_4 (pH 4). The organic layer was dried over sodium sulfate and concentrated under vacuum. The crude product was used directly in next step without further purification. To the flask containing the crude product were added 5 ml of DMF and 300 mg (2.0 mmol) of TBS-Cl, followed by 99 mg (1.5 mmol) of imidazole. The reaction was kept in the dark overnight, and then diluted with 25 ml CH_2Cl_2, washed with 2×25 ml KH_2PO_4 (1M), and dried over Na_2SO_4. Flash column chromatography using ethyl acetate:petroleum ether (from 10:90 to 20:80) provided 474 mg (98% for two steps) **53** as a solid. ^{1}H NMR ($CDCl_3$) δ 7.73 (s, 1H), 7.08 (s, 1H), 5.60 (m, 3H), 4.46 (m, 2H), 4.26 (d, 1H), 4.04 (d, 1H), 3.96 (s, 3H), 3.75 (s, 3H), 1.23 (m, 3H), 0.84 (s, 9H), 0.04 (s, 3H), 0.01 (s, 3H).

NVOC-O-t-Butyldimethylsilyl threonine cyanomethyl ester 54. To a solution of 474 mg (0.975 mmol) of **53** in 15 mL of MeOH and 3 mL of water was added 1.5 mL

of 1N NaOH. The mixture was stirred for 29 hours. There was still some starting material left. Quenched the reaction by adding 30 mL of CH_2Cl_2, 10 mL of 1M KH_2PO_4, and 20 mL of water. The phases were separated and the aqueous layer was extracted again with another 20 mL of CH_2Cl_2. The organic layers were combined and dried over sodium sulfate. The solvent was rotoevaporated off to afford 350 mg of the free acid after column chromatography, which was used directly in the next step. Cyanomethyl ester formation was done using standard methods. 330 mg of **54** (72% for two steps) was obtained. ^{1}HNMR ($CDCl_3$) δ 7.76 (s, 1H), 7.05 (s, 1H), 5.60 (m, 3H), 4.78 (m, 2H), 4.50 (m, 1H), 4.36 (m, 1H), 4.04 (s, 3H), 3.96 (s, 3H), 1.28 (d, 3H), 0.85 (s, 9H), 0.07 (s, 3H), 0.02 (s, 3H).

dCA-NVOC-Thr. dCA-NVOC-L-O-TBS-Thr was prepared by the ligation procedure described in section 5.4. The HPLC purified product dCA-NVOC-L-O-TBS-Thr was treated with acetic acid:THF (3:1) at 37°C for 24 hours. Analytical HPLC indicated 60% deprotection of the TBS group. The product was purified without further reaction. FAB-MS: calcd for $C_{33}H_{42}N_{10}O_{21}P_2$: 976.7; found $[M-H]^-$: 975.2.

5.7 References

1. Y. Zhang, A. Auerbach, *Soc. Neurosci. Abst.* **21**, 1582 (1995).

2. D. Colquhoun, B. Sakmann, *J. Physiol.* **369**, 501-557 (1985).

3. D. Colquhoun, A. G. Hawkes, in *Single Channel Recording* B. Sakmann, E. Neher, Eds. (Plenum Press, New York, 1995) pp. 397-479.

4. W. Sigurdson, J. Chen, M. Akabas, A. Karlin, A. Auerbach, *Biophys. J.* **66**, A212-A212 (1994).

5. C. Labarca, et al., *Nature* **376**, 514-516 (1995).

6. M. W. Nowak, et al., *Science* **268**, 439-442 (1995).

7. M. E. Saks, et al., *J. Biol. Chem* **271**, 23169-75 (1996).

8. M. W. Nowak, et al., *Methods Enzymol.* (in press).

9. P. Kearney, et al., *Mol. Pharmacol.* **50**, 1401-1412 (1996).

10. M. W. Quick, J. Naeve, N. Davidson, H. A. Lester, *BioTechniques* **13**, 357-361 (1992).

11. J. D. Ellman, P. G. Schultz, et al., *Methods Enzymol.* **202**, 301-336 (1991).

12. A. G. Myers, J. L. Gleason, T. Y. Yoon, *J. Am. Chem. Soc.* **117**, 8488-8489 (1995).

13. T. L. Gilchrist, D. A. Lingham, T. G. Roberts, *J. Chem. Soc., C. C.* , 1089 (1979).

14. V. Kumar, et al., *J. Org. Chem.* **57**, 6995-6998 (1992).

15. H. M. Rajh, et al., *int. J. Peptide & Protein Res.* **14**, 68-79 (1979).

16. V. W. Cornish, K. M. Hahn, P. G. Schultz, *J. Am. Chem. Soc.* **118**, 8150-8151 (1996).

17. D. A. Evans, A. M. Ratz, B. E. Huff, G. S. Sheppard, *Tetrahedron Lett.* **35**, 7171-7172 (1994).

Chapter 6

Exploring the Cation-π Interaction in Molecular Recognition:

Design and Synthesis of A Potential Alkali Metal Ion Host

6.1 Introduction

Cyclophanes are a very important class of bridged aromatic molecules which play a broad and prominent role in superamolecular chemistry - an interdisciplinary science which lies at the interfaces between chemistry and biology, physics, and materials science (1-4). During the last fifteen years or so, the Dougherty group has been active in this field, in particular, we are interested in molecular recognition studies in water due to its direct relevance to biological systems (5). Using cyclophane-based hosts, among other tools, we have been especially concerned with the cation-π interaction - the stabilizing force between a positively charged species and the electron-rich face of an aromatic ring (6, 7). We have extensively documented that host P, and a series of related hosts, can bind positively charged quaternary ammonium guests, alkylated imminium guests, and sulfonium guests with high affinity in water (Figure 6.1). We have also shown

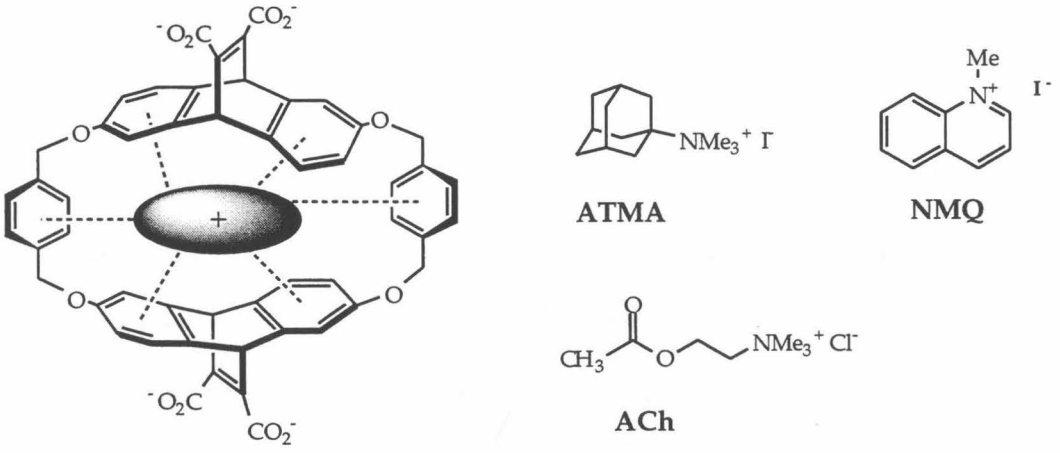

Figure 6.1. Host P and representative guests N-methylquinolinium (NMQ), adamantyltrimethylammonium (ATMA), and acetylcholine (ACh).

that cation-π binding of transition states can lead to novel forms of catalysis (8). After our initial report on the cation-π interaction, other groups, most noticeably those of Collet and Schneider, described observations of similar type of interactions in their host-guest systems (9, 10).

In biological systems, a large body of evidence indicates a prominent role for cation-π interactions in structural biology in general (7, 11). It has also been shown that in enzymatic methyltransfer reactions, the S^+-CH_3 unit of S-adenosylmethionine (SAM) can align favorably with aromatic side chains from the enzyme to assist catalysis by cation-π interactions (12). Mutagenesis studies in voltage-gated K^+ channels suggested a role for such interactions in channel blockade by the organic cation tetraethylammonium (TEA) (13, 14). Perhaps most interesting to us, cation-π interactions have been shown to be critical in the binding of the prototypical neurotransmitter acetylcholine (ACh) by acetylcholinesterase (15, 16). In Chapter 2, we provided convincing mutagenesis data supporting a role for cation-π interactions in binding ACh by the nicotinic acetylcholine receptor (nAChR).

The fundamental nature of the cation-π interaction is substantially elucidated in gas phase studies of ion-molecule complexes. In as early as 1981, Kebarle showed that in the gas phase, K^+ binds to a benzene molecule with $\Delta H = 19.2$ kcal/mol, which is about 1 kcal/mol stronger than the interaction energy between K^+ and water. In fact, in complexes like K^+S_n (S stands for benzene or H_2O), when n = 1, 2, 3, or 4 , K^+- benzene complexes are formed more favorably over K^+- H_2O complexes (17). Subsequent studies with other alkali metals binding to benzene clearly established the prominent importance of electrostatics in cation-π interactions (18, 19). A systematic computational

study performed by Sandro Mecozzi and Anthony P. West Jr. in our group confirmed the prominent role of electrostatics in cation-π interactions, in which essentially 100% of the variation in cation-π binding energy is attributable to variation in the electrostatic component in binding (20, 21).

Given all these results, it is then conceivable that cyclophane hosts with complementary size and shape to that of alkali metal ions such as K^+ may bind them significantly via cation-π interactions under proper conditions. Indeed, Shinkai has shown that in the crystal structure of a calixarene-metal complex, the cation Na^+ is in close contact with two benzene rings in addition to two ether oxygens (22). In a gas phase study using positive secondary ion mass spectroscopy (SIMS) and electrospray ionization mass spectroscopy (ESI-MS), Shinkai has observed complexes formed between alkali metal ions and an all-hydrocarbon cyclophane host (designed to retain the cation-π binding ability while removing the metal-oxygen interactions). Signals for Rb^+ and Cs^+ complexes were very intense compared to signals for Li^+, Na^+, and K^+ complexes, consistent with the fact that the cavity size of the cyclophane host matches the ionic radius of Cs^+ most closely (23).

Our interest in designing cyclophane receptors for hydrophilic cations such as K^+, RNH_3^+, and guanidinium ions dates back several years ago. Richard E. Barrans, Jr., and Alison McCurdy in our group had devoted substantial effort in trying to obtain a host to complex K^+ ion (24, 25). In addition to the fundamental interest in developing metal ion binding hosts, these studies were also aimed to gain insights into the remarkable ion selectivity associated with potassium channels. Extensive mutagenesis studies with these proteins have pinpointed a highly conserved peptide triplet - **GYG** - in the pore region to

be crucial in ion selectivity (26, 27). Recall that these channels are often tetramers, and modeling studies suggested that four tyrosines (one each from the triplet **GYG**) could form the narrowest constriction in the channel pore to confer the ion selection filter (28). Computational studies by Robert A. Kumpf in our group indicated that it is plausible to create a K^+-Êselective channel using cation-π interactions (29). However, a recent crystal structure of the potassium channel from *Streptomyces lividans* disqualifies such a model, suggesting that the main chain carbonyl groups line the selectivity filter (30). Nevertheless, we set out about five years ago to design new cyclophane hosts which may bind K^+ selectively.

The design of new hosts takes advantage of our well-studied ethenoanthracene system (31, 32). Connecting two such units produces a ring of four benzenes. CPK modeling suggested a two-atom linker would provide a rigid cavity of proper size for a Na^+ or K^+ ion. We envisioned hosts with benzo-, etheno-, ethano-, and ether- linkers (shown in Figure 6.2). All these hosts contain cavities of similar size which are smaller than the previously studied ones (24, 25). In the following sections, we describe the synthesis of one of the hosts, host IV.

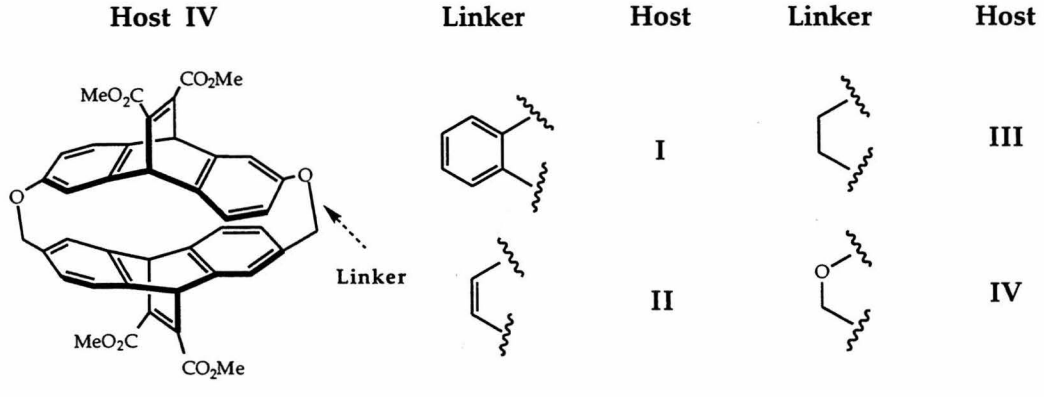

Figure 6.2. Designed hosts for alkali metal binding.

6.2 Synthesis of Host IV

The retrosynthetic analysis of all the hosts leads to a common precursor, 2,6-bis(trifloxy)-11,12-dicarbomethoxyethenoanthracene (bistriflate half molecule), **4** (Figure 6.3, retrosynthesis of host IV). Aryl triflates are widely used compounds in palladium-catalyzed carbon-carbon bond forming cross-coupling reactions (33). For the synthesis of host I, II, and III, sequential palladium-catalyzed coupling reactions may be used. However, we pursued most vigorously the synthesis of host IV and in the following, we report its synthesis (Figure 6.4).

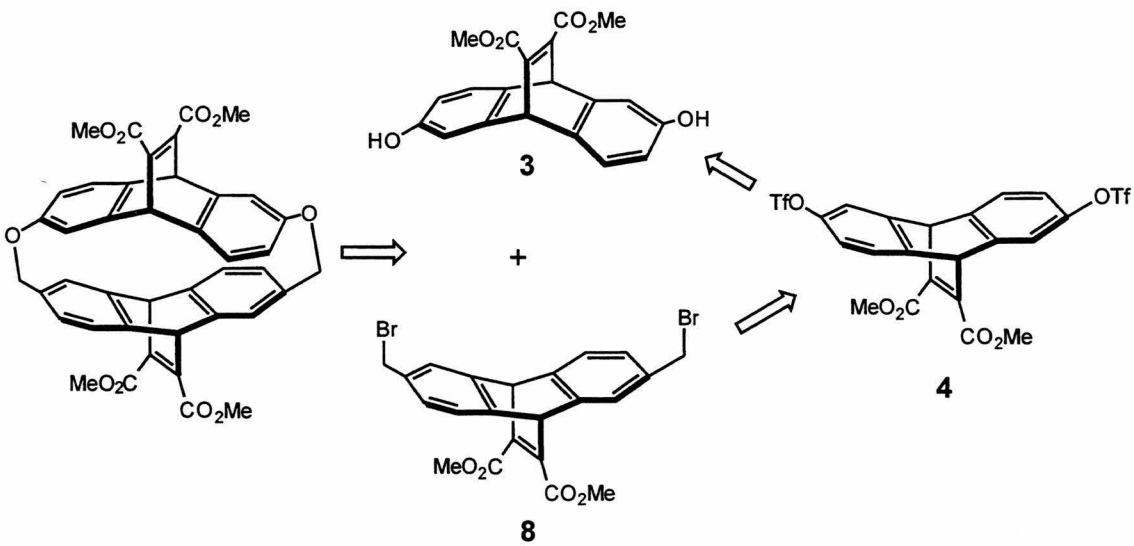

Figure 6.3. Retrosynthetic analysis of host IV.

The key intermediate, bistriflate **4**, is readily available from the corresponding 2,6-bishydroxy half molecule **3**. Compound **3** was synthesized in four steps according to the previously published procedure (5, 31); we only mention here that deprotection of the *tert*-butyldimethylsilyl (TBS) group of Diels-Alder product of **2** was done in about three

hours instead of six and half hours as in the described procedure, which we found prolonged reaction time promoted side-reactions. It should also be noted that we attempted to synthesize bistriflate **4** directly via the Diels-Alder reaction between 2,6-bistrifloxy-anthracene and dimethyl acetylene dicarboxylate(DMAD). However, after 5 days refluxing in toluene, there were still significant amounts of starting materials left as indicated by TLC.

With the bistriflate **4** in hand, we immediately converted it into the bisvinyl compound **5** using the Stille coupling reaction (34). In general, this is a good reaction and yields as high as 90% could be obtained reliably if 8 or more molar equivalents of vinyltributyltin were used (substantial amount of mono-vinylated intermediate could be isolated if less tin reagent was used).

The synthesis of host III was attempted at this point. We tried the cross-coupling reaction between bistriflate **4** and alkylborane derivative of **5** under standard Suzuki conditions (35). Palladium-catalyzed reactions are multi-component reactions and aryl triflates and halides can be reduced *in situ* under these conditions. Therefore, due to the necessary dilute and reducing conditions used in our system, we were not able to isolate any desired products.

Realizing the greater reliability and feasibility of the phenyl ether bond formation in cyclophane synthesis (1), we moved on quickly to the synthesis of host IV. The bisvinyl compound **5** was converted to the corresponding bisaryl aldehyde **6** in two steps using OsO_4/NMO and $NaIO_4$. The resulting aldehyde was then reduced using $NaBH_4$ at

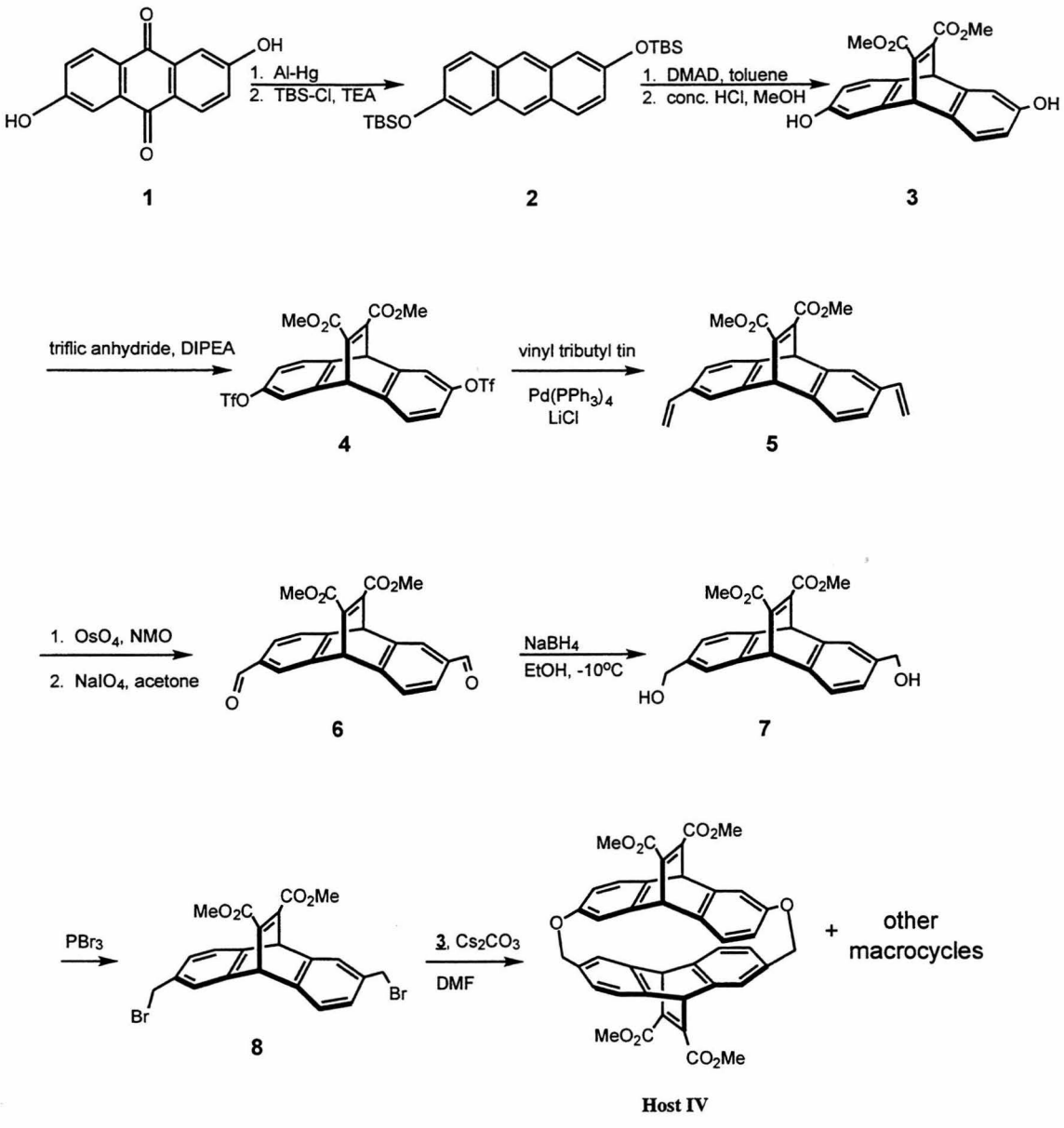

Scheme 6.1. The synthetic scheme for host IV.

low temperature to furnish the bisaryl methyl alcohol **7**, which was then converted to the corresponding bromide **8** using PBr_3 in CH_2Cl_2. As described previously (5), the macrocyclization was carried out by condensing **8** and **3** in a suspension of cesium carbonate in anhydrous DMF. The desired host IV (dimer) was isolated in ca. 6% yield, along with tetramer in 20% yield.

We performed preliminary alkali metal binding studies using fast-atom bombardment mass spectroscopy (FAB) and positive electrospray ionization mass spectroscopy (ESI-MS). The control molecules **9** we used was the methyl ether derivative of compound **3** which is shown in Figure 6.4. Although peaks corresponding to host/Na^+, host/K^+, and host/Cs^+ were seen, they were not much stronger than complexes formed with the control molecule when all of them were normalized to background matrix peaks. We realize at the foremost that this study demands more than trivial and ordinary efforts from a mass spectroscopy scientist, and we tried to collaborate with some of them. However, the lack of interest from them eventually called for a stop to further studies.

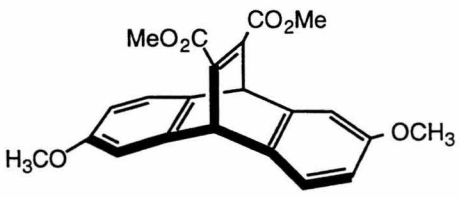

9

Figure 6.4. The structure of the control molecule for MS studies.

In summary, we have successfully synthesized host IV in ten steps with an overall yield of 0.34%. One novel feature in the synthesis is the use of aryl triflate chemistry. A very interesting future direction for this project is to incorporate this host into membrane structures. Parker and Rosser have demonstrated that a neutral cyclophane host, although it does not bind acetylcholine appreciably in solution, can transport acetylcholine across artificial membranes (36). We could perform similar experiments and determine if metal ion transport, even selective ion transport, across membranes can be achieved.

6.3 Synthesis of a 3/4 Molecule Towards a Tetraamide Host

Although our prototypical host P (with four external carboxylates removed from the binding cavity) is soluble enough in water to allow many binding studies performed, we constantly looked for new ways to improve its water solubility. Laura S. Mizoue in our group initiated a study about six years ago to exploit the potential of amide linkers as solubilizing groups (37). The introduction of amide linkers also brings new features into the host. Hydrogen bonds between host and bound guests may now be available and further modification on amide nitrogens is possible, leading to novel host derivatives.

In conjunction with her approach, we focused on hosts based on 2,6-biscarboxy half molecule **10** rather than 2,6-bisaminoethenoanthracene unit which was being studied by Laura S. Mizoue. The initial target was a tetraamide host with p-xylenyldiamine as the linker (Figure 6.5). CPK model study suggested that this host contains a cavity that is slightly larger than that of host P. We report here the synthesis of the **3/4** molecule **12**, a precursor to the designed tetraamide host. Unfortunately, this project was abandoned immediately after we found that some of the tetraamide hosts made by Laura S. Mizoue

were less soluble in water than host P due to aggregation. And at about the same time, I started working on the unnatural amino acid project.

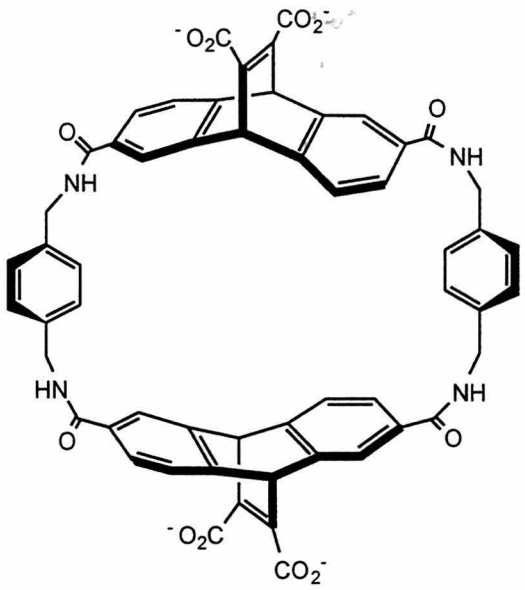

Figure 6.5. The tetraamide host. Note that the amide bonds are not specified in either cis- or trans- conformation.

The synthesis of **10** was achieved using a palladium-catalyzed hydrocarboxylation reaction with bistriflate compound **4** (38). The reaction was carried out smoothly in a sand bath of ca. 85°C under 1 atm CO. The choice of DMSO as the solvent was noted in the literature as critical to the success of the reaction. The **3/4** molecule **12** was easily assembled by coupling **10** with mono-protected *p*-xylenyldiamine **11** using standard carbodiimide chemistry, followed by trifluoroacetic acid treatment to remove the t-Boc group. The resulting **3/4** molecule was purified and later it was used in molecular self-assembly studies by Jonathan E. Forman and Eric Co in our group (39).

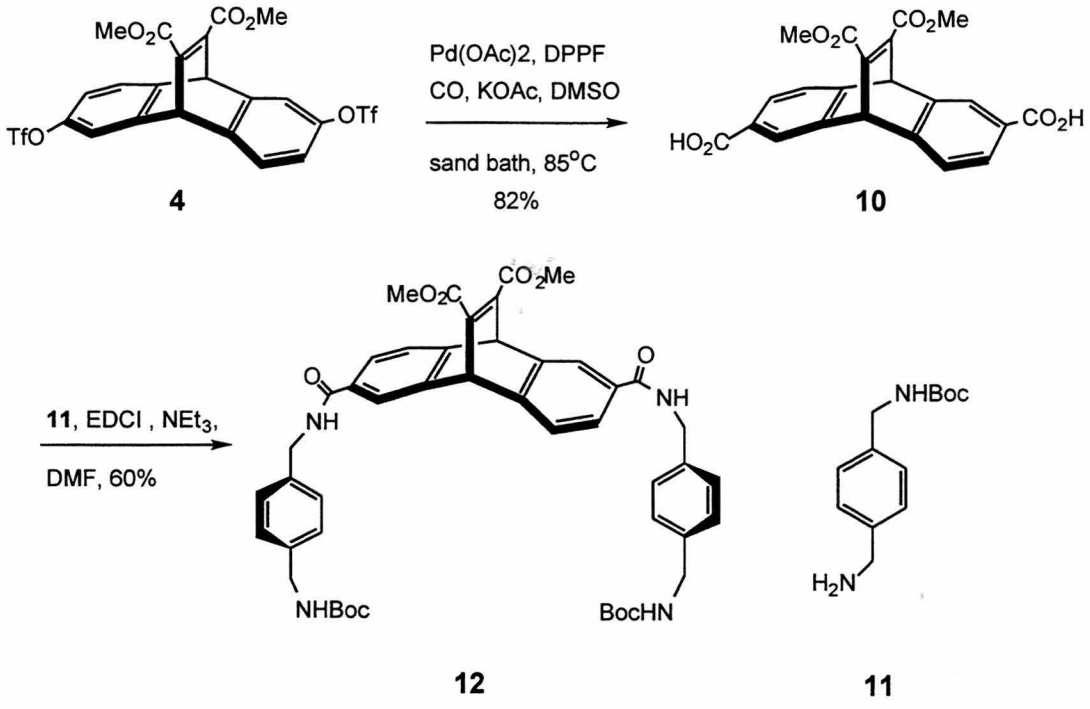

Figure 6.6. Synthesis of **3/4** molecule for tetraamide host. DPPF, 1,1'-bis(diphenylphosphino)ferrocene.

6.4 Purification of the Tetraphosphate Host P4P

One salient feature in our host P design is that the four carboxylate groups are removed away from the binding cavity and therefore serve mainly as solubilizing groups. However, they could have long-range electrostatic impacts on binding of positively charged guests. Theory indicated this is plausible and molecular recognition studies with a water-soluble neutral host suggested that each carboxylate in host P could contribute some 0.3 kcal/mol to binding cationic guests (40).

To further evaluate the effects of these long-range electrostatic interactions, it is desirable to study hosts bearing more negative charges than host P. Former group

members Alison McCurdy attempted but Sandro Mecozzi successfully synthesized a tetraphosphate host (Figure 6.7), in which four phosphate groups subsitute for the four carboxylates in host P, providing a molecule with a total of eight negative charges (25, 40). My contribution to the project was the purification of host P4P by semi-preparative reverse phase HPLC. We used pH 4.5 ammonium acetate (25 mM) buffer as the aqueous phase. The purified host was found to be comparably soluble as host P; in pD = 9 borate buffer, saturation can be reached at about 1 mM. Some initial binding studies were attempted and this work is now being carried out by our group member Sarah M. Ngola.

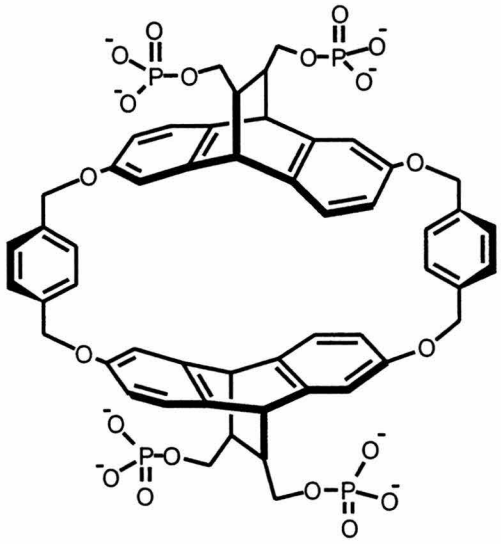

Figure 6.7. The tetraphosphate host P4P which bears eight external negative charges.

6.5 Experimental Section

General Methods. Tetrahydrofuran was distilled from sodium benzophenone ketyl. Methylene chloride and acetonitrile were distilled from CaH_2. Reported synthetic yields refer to material dried to constant weight under vacuum, typically 50 mTorr. Flash chromatography was on 230-400 mesh silica gel with the solvent indicated. All NMR shifts are reported as δ ppm downfield from TMS. ^1H NMR spectra were recorded at 300 MHz in $CDCl_3$ and ^{13}C NMR spectra at 75 MHz in $CDCl_3$ using a GE QE-300 spectrometer, except where noted. FAB, ESI, and HRMS determinations were performed at the University of California, Riverside, University of Nebraska-Lincoln, and California Institute of Technology. All reagents were obtained from Aldrich, Sigma, or other commercial sources where not explicitly noted.

2, 6-dihydroxyanthracene. To a 2L 3-necked round-bottom flask equiped with a mechanical stirrer was added anthraflavic acid **1** (30g, 0.125mol), ethanol (95%, 240ml), water (540ml), and saturated ammonium hydroxide (120ml). Aluminum amalgam, made from granular Al (65.4g, 20eq), was added in small portions. The mixture was then heated up slowly, while stirring, to a water bath temperature of 60-65°C. After 2.5 hrs, a light brown solution was obtained. The reaction mixture was cooled down to room temperature and then poured, while stirring, into 1L of ice containing 120ml conc. HCl, yellow precipitates formed. Sodium bicarbonate was used to bring pH to about 5. Mixture was kept refrigerated overnight. Solids formed at bottom and the solution was then cannulated out. The rest was lyophilized overnight. 2.5L of acetone was used to extract product from the solid, and insolubles were filtered off through a celite pad. The filtrate was concentrated and the resulting solid was crystalized from

Ethanol:Acetone:Water = 160ml:40ml:25ml. Yield, 18g, 60%. Color, yellowish. ^{1}HNMR (acetone-d_6) δ 7.28 (dd, 2H), 7.38 (d, 2H), 7.98 (d, 2H), 8.28 (s, 2H), 8.68 (s, 2H).

2, 6-bis (t-butyldimethylsiloxy) anthracene 2. 3.67g (17.5mmol) of crude product of **2,** after drying under vacuum overnight, was dissolved in 45ml of anhydrous DMF. Under argon, 53 ml of *tert*-butyldimethylsilyl chloride (TBDMS-Cl) in THF (1.0 M) was added in one portion, followed by slow addition of 6 ml (3eq) of triethylamine (NEt_3). The reaction was kept at room temperature for 3 hrs. TLC showed complete disappearance of starting material. THF was removed under vacuum and the residual DMF solution was cooled in an ice-bath. Yellow crystals formed. Filtration and recrystalization from isooctane yielded 5.55g product (72%). ^{1}HNMR ($CDCl_3$) δ 8.17 (s.2H), 7.82 (d,2H), 7.25 (d, 2H), 7.07 (dd,2H), 1.02 (s, 18H), 0.26 (s, 12H).

2, 6-bis (t-butyldimethylsiloxy)-9, 10-dihydro-11, 12-dicarbomethoxy-ethenoanthracene. To a 25ml round-bottom flask were added 5ml of freshly distilled toluene, 1.35g (~3 mmol) of **2** and 1.9ml (15.4 mmol) of dimethyl acetylenedicarboxylate (DMAD). The mixture was refluxed for 48 hrs and then concentrated. The residue was crystalized from methanol. White solid, yield 1.325g (~70%). ^{1}HNMR ($CDCl_3$) δ 7.05 (d,2H), 6.75 (d, 2H), 6.3 (dd, 2H), 5.15 (s, 2H), 3.8 (s, 6H), 0.9 (s, 18H), 0.13 (s, 12H).

2, 6-dihydroxy-9, 10-dihydro-11, 12-dicarbomethoxyethenoanthracene (**±3**). To a 250ml round bottom flask, were added 5.84g (10 mmol) of Diels-Alder product from above, 140ml of methanol and 7ml of methylene chloride. While stirring, 7 ml of conc. HCl was added slowly. The mixture was kept stirring at room temperature for ca.

3 hrs, followed by removal of solvent under vacuum. The residue was dissolved in 180 ml of ethyl acetate and washed with 50 ml of water. The aqueous layer was extracted with 25 ml of ethyl acetate. The combined organic layer was then concentrated and the resulting oil was purified via flash chromatography with ether:hexane from 50:50 up to 100% ether. A clear oil was obtained, which solidified after drying on the vacuum line. Yield, 3.6g (~98%). ^{1}HNMR (acetone-d_6) δ 7.25 (d, 2H), 7.00 (d, 2H), 6.50 (dd, 2H), 5.50 (s, 2H), 3.80 (s, 6H).

2, 6-bistrifloxy-9, 10-dihydro-11, 12-dicarbomethoxyethenoanthracene (±**4**). Compound **3** (4.1g , 11.65 mmol) was dried on a vacuum line for 10 hrs. To the flask, under argon, were added 125 ml of methylene chloride and 7.3g (25.6 mmol, 2.2eq) of triflic anhydride. At 0°C, 5 ml (28.5 mmol, 2.5eq) of diisopropylethylamine was added dropwise. A brown solution was obtained. The reaction was kept stirring for additional 1.2 hours in an ice-water bath. The reaction mixture was then washed with 50 ml of water, dried over sodium sulfate, and concentrated under vacuum. Purification using flash chromatography with mix eluent methylene chloride:hexane (30:50) yielded 6.0g (84%) colorless oil. ^{1}HNMR ($CDCl_3$) δ 7.46 (d, 2H), 7.36 (d, 2H), 7.04 (dd, 2H), 5.56 (s, 2H), 3.84 (s, 6H).

2, 6-bisvinyl- 9, 10-dihydro-11, 12- dicarbomethoxyethenoanthracene (±**5**). An oven-dried 100 ml flask, under argon, weas charged with 1.66g (2.70 mmol) of **4**, 0.482g (9.2 mmol) of LiCl, 138mg (0,12 mmol,5% moleq) of $Pd(PPh_3)_4$, 2.7g (8.52 mmol) of vinyltributyltin, and a few crystals of 4-*tert*-butylcatechol (polymerization inhibitor), followed by addition of 25 ml of dry dioxane. The mixture was kept refluxing for 6.5 hours and a dark solution resulted. The reaction was stopped, reaction mixture

was cooled down to room temperature and diluted with 150 ml of ethyl acetate. It was then washed with 4x50 ml of 5% KF solution. The precipitates were filtered off. The organic layer was dried over sodium sulfate and concentrated under vacuum. The residue was purified via column chromatography using hexane:methylene chloride (55:45) as the eluent. Yield, 0.9g (90%), clear oil. ^{1}HNMR ($CDCl_3$) δ 7.50 (d, 2H), 7.38 (d, 2H), 7.04 (dd, 2H), 6.62 (dd, 2H), 5.68 (d, 2H), 5.45 (s, 2H), 5.20 (d, 2H), 3.8 (s, 6H).

Macrocyclization - Suzuki Coupling. (a) A 10 ml oven-dried flask was charged with 130 mg of the bisvinylated compound **5** (0.35mmol) and 1.40 ml of 9-BBN solution (0.5N in THF, Aldrich). The mixture was kept at 0°C for 2 hrs and then at room temperature for 4 hrs. (b) To another 500ml oven-dried flask were added 22 mg (0.025mmol, 7.5% mol eq) of $Pd(dppf)_2Cl_2$, 111mg (0.5 mmol) of K_3PO_4, 215 mg (0.35 mmol) of **4**, and then 260 ml of dry THF. To this solution, the hydroboration reaction mixture prepared in (a) (diluted to ca. 30ml) was transfered. The resulting mixture was then heated up to reflux under argon for 3 days. A dark solution was observed. Reaction was stopped and solvent was taken off under vacuum. The residue was extracted with ethyl acetate and washed with water. Organic phase was dried over sodium sulfate and concentrated under vacuum. However, no desired products could be identified from the column fractions. (Similar reaction conditions were applied to the monovinylated half molecule and did not work either).

2, 6- bisformal-9, 10-dihydro-11, 12-dicarbomethoxyethenoanthracene (±6). To a 250ml round bottom flask were added squentially 1.633g (4.39 mmol) of bisvinyl compound **5**, 50 ml acetone, and 1.8 ml of 4% (wt) OsO_4 in water. A black solution rapidly formed. To the stirring solution, 1.13g (9.65 mmol, 2.2 eq) of N-

methylmorphiorature overnight. The color of the reaction changed from black to dark green, then to green and finally to yellow. TLC indicated disappearance of the starting material. The catalyst OsO_4 was reduced by stirring with 2.5g of sodium bisulfite in 18 ml of water. The mixture was then acidified using 1N HCl. Extraction with 5×75 ml of ethyl acetate. Combined organic layers and dried over sodium sulfate. The crude product thus obtained after removing solvents was directly used in next step (it showed satisfactory ^{1}HNMR patterns). The crude product was re-dissolved in 15 ml acetone, and was mixed with 8g of sodium periodate (6 eq) in 35 ml of water. After 45 minutes, the reaction was stopped and reaction mixture was extracted with 3×75 ml of ethyl acetate. The combined organic layers were washed with brine once and dried over sodium sulfate and concentrated. Yield, 1.438g (88%). ^{1}HNMR ($CDCl_3$) δ 9.94 (s, 2H), 7.95 (d, 2H), 7.60 (m, 4H), 5.64 (s, 2H), 3.80 (s, 6H).

2,6-bishydroxymethyl-9,10-dihydro-11,12-dicarbomethoxyethenoanthracene (±**7**). To a flask containing 1.438g of **6** in 10 ml of methanol at -15°C to -20°C, was added ca. 200 mg (6eq) of sodium borohydride. The reaction was kept stirring under argon for an hour and all starting materials disappeared. Quenched the reaction with 5 ml 1N HCl. The mixture was diluted with 100 ml of ethyl acetate and 100 ml of brine. The aqueous phase was extracted twice with 50 ml of ethyl acetate. Organic layers were combined, washed once with brine, and dried over sodium sulfate. 0.95g (65%) of product (white solid) was obtained by flash chromatography using ethyl acetate/hexane (from 50:50 to 70:30). ^{1}HNMR ($CDCl_3$) δ 7.4-7.3 (b, 4H), 7.0 (dd, 2H), 5.44 (s, 2H), 4.8 (b, 2H), 4.6 (s, 2H), 3.8 (s, 6H).

2, 6-bisbromomethyl-9, 10- dihydro-11, 12-dicarbomethoxyethenoanthracene (±**8**). To the solution of **7** (0.81 g, 2.13 mmol) in 20 ml of methylene chloride, was added 2.19 ml of phosphorous tribromide (1.0 M). The reaction was kept stirring at room temperature for half an hour and TLC showed complete disappearance of starting material. The reaction was quenched by addition of 10 ml of water and neutralized with saturated sodium bicarbonate solution. Caution: emulsion may result. The two layers were separated and the aqueous layer was extracted twice with 50 ml of ethyl ether. All the organic layers were combined and dried over sodium sulfate. Purification with flash chromatography produced 1g white solid (93%). ^{1}HNMR ($CDCl_3$) δ 7.42 (d, 2H), 7.38 (d, 2H), 7.06 (dd, 2H), 5.43 (s,2H), 4.42 (s, 4H), 3.8 (s, 6H). ^{13}CNMR: δ 166.2, 147.1, 144.7, 144.2, 135.8, 127.0, 125.3, 125.1, 124.75, 124.7, 52.6, 52.4, 33.8.

Macrocyclization—Synthesis of host IV. To a suspension of 882 mg (5eq) of cesium carbonate in 25 ml anhydrous DMF in an oven-dried 250 ml round bottom flask, was added slowly via a syringe pump a 25 ml solution containing 253 mg (0.5 mmol) of **8** and 176 mg (0.5 mmol) of **3** during a course of 48 hours. (Note that **8** was recrystalized from ethyl acetate/petroleum ether before macrocyclization). The reaction was kept stirring for an additional 48 hours after injection was complete. TLC showed that there was no more **8** left. The salts were filtered off and the filtrate was concentrated under vacuum. The residue was extracted with chloroform with sonication and solids were filtered off again. The chloroform solution was concentrated and the products were isolated by flash chromatography. Column size: 3cm×22cm. Solvents used: 50 ml methylene chloride; 500 ml 5% ethyl acetate in methylene chloride; 250 ml 10% ethyl acetate in methylene chloride; and 250 ml 20% ethyl acetate in methylene chloride. Obtained host IV (dimer): 23 mg (6.6%); tetramer: 78 mg (22.4%). ^{1}HNMR ($CDCl_3$) δ

6.99 (m, 4H), 6.83 (m, 4H), 6.43 (m, 4H), 5.11 (m, 6H), 4.92 (s, 2H), 3.72 (m, 12H) HR FAB-MS: calcd for $C_{42}H_{33}O_{10}$: 696.1995; found $[M+H]^+$: 697.2082. For the tetramaer, HR FAB-MS: calcd for $C_{84}H_{66}O_{20}$: 1392.3990; found $[M+H]^+$: 1393.4043.

2, 6-Dicarboxy-9, 10-dihydro-11, 12-dicarbomethoxyethenoanthracene (±10). To a 25ml oven-dried round bottom flask were added 604mg (1 mmol) of **4**, 24mg (0.1eq) of catalyst $Pd(OAc)_2$, 222mg (40%) of DPPF, and 784mg (8 mol eq) of KOAc, followed by addition of 8 ml of dry DMSO. The mixture was then purged by CO for seven minutes and maintained under a balloon of CO and heated up in a sand bath: 85-90°C. The mixture turned black after about 3 hours. The reaction was cooled down to room temperature four hours later and was diluted with 120 ml of ethyl acetate. After adjusting the pH to 2~4 using 3N HCl, the mixture was washed with 3×50 ml of water. Organic phases were combined and dried over sodium sulfate and concentrated. The product was isolated by flash chromatography through a short column using EtOAc:Hex:HOAc (40:60:5). Yield, 329 mg (82%), pale yellow solid. ^{1}HNMR (DMSO-d_6) δ 12.3 (b, 2H), 8.05 (d, 2H), 7.6 (dd, 2H), 7.5 (d, 2H), 5.8 (s, 2H), 3.7 (s, 6H). ^{13}CNMR: 169.0, 166.5, 148, 146.5, 144.6, 122.9, 129.2, 128.8, 127.8, 123.2, 53.0, 51.3.

N-Boc-xylenyldiamine 11. To a 250ml flask was added 10.8g (8eq) of xylenyldiamine and 100 ml of dioxane (caution: highly toxic). While stirring, a solution of Boc_2O (2.18g, 10mmol) in 50 ml of dioxane was added dropwise within 2 hours. A milky solution appeared 5 minutes later after initial addition and maintained to the end. The mixture was kept overnight. The solvent was then taken off under vacuum. The residue was dissolved in 100 ml of water and the precipitates were filtered off. The

aqueous solution was extracted with 3×70ml of methylene chloride. The combined organic layers were dried over sodium sulfate and concentrated under vacuum. After flash chromatography using EtOAc:Hex:NEt_3 = 50:50:7, 1.78g of **11** was obtained, yield 75%. ^{1}HNMR ($CDCl_3$) δ 7.20 (s, 4H), 4.8 (b, 1H), 4.24 (d, 2H), 3.75 (s, 2H), 1.52 (s, 2H), 1.44 (s, 9H).

3/4 Molecule 12. A 100ml flask was charged with 320 mg (0.78 mmol) of compound **10**, 555 mg (2.35 mmol, 3eq) of N-Boc-xylenyldiamine **11**, 320 mg (2.35 mmol) of 1-N-hydroxyl-benzotriazole (HOBt), 450mg (2.35 mmol) of dimethylaminopropylethylcarbodiimide hydrogen chloride (EDCI), and 16ml of DMF, followed by addition of 0.5ml of triethylamine. The mixture was kept stirring for two days. Reaction mixture was diluted with 150 ml of ethyl acetate and washed with 3×50ml of water, and 2×50ml of 5% sodium bicarbonate. Combined organic layers were dried over sodium sulfate and concentrated under vacuum. Purification by Column chromatography using EtOAc:Hex = 50:50 produced 400 mg pure **12** (60%). ^{1}HNMR ($CDCl_3$) δ 8.00 (s, 2H), 7.60 (m, 4H), 7.42 (s, 8H), 6.47 (b. 2H), 5.72 (s, 2H), 5.00 (b, 2H), 4.76 (d, 4H), 4.42 (d, 4H), 3.94 (s, 6H), 1.6 (s, 18H).

Tetraamide Host - Macrocyclization (a) The active ester. An oven-dried flask was charged with 220 mg (0.539mmol) of diacid compound **12**, 0.922g (5.39 mmol) of pentafluorophenol, 0.62 g (3.23 mmol) of EDCI, 0,326 g (3.23 mmol) of triethylamine, and 5 ml of DMF. The mixture was stirred for 5 days under argon. Diluted with 50 ml of ethyl acetate and then washed with 5% sodium bicarbonate 3×30ml, water 2×30ml. Dried over sodium sulfate and concentrated. The residue was then put on vacuum line for 2 days. This was then made into a bulk solution in 10 ml of DMF. (b) To a 50ml

flask, was added 121.4 mg (0.143 mmol) of **12**, followed by 0.5 ml of trifluoroacetic acid in 0.5 ml of THF. The deprotection was monitored by TLC. 2.65 ml of the solution made in (a) (~.143mmol based on **12**) was then added in and it was diluted to 30 ml. This mixture was then added slowly within 2 hours into a 70 ml DMF solution containing 3 ml of NEt_3. The reaction was kept for 5 days. DMF was removed under vacuum and the residue was stored for further separation.

Purification of tetraphosphate host P4P. The tetraphosphate host P4P was purified using semi-preparative reverse phase HPLC. It elutes at t = ~12 min with a linear solvent gradient from 0%-50% of CH_3CN in a pH 4.5 ammoniumm acetate buffer (25 mM). A total of about 4 mg of P4P was isolated. ^{1}HNMR (500 MHz) (pD = 9 borate buffer) δ 7.23 (s, 8H), 7.12 (d, 4H), 7.00 (s, 4H), 6.64 (d, 4H), 5.10 (m, 8H), 4.27 (s, 4H), 3.53 (m, 4H), 3.06 (m, 4H), 1.57 (m, 4H). FAB-MS: calcd for $C_{52}H_{52}O_{20}P_4$: 1120.2; found $[M-H]^-$: 1119.6.

6.6 References

1. F. Diederich, *Cyclophanes*. J. F. Stoddart, Eds., Monographs in Supramolecular Chemistry (The Royal Society of Chemistry, Cambridge, UK, 1991).
2. J.-M. Lehn, *Angew. Chem. Int. Ed. Engl.* **27**, 89-112 (1988).
3. E. Weber, Eds., *Supramolecular Chemistry I - Directed Synthesis and Molecular Recognition* , vol. 165 (Springer-Verlag, Germany, 1993).
4. E. Weber, Eds., *Supramolecular Chemistry II - Host Design and Molecular Recognition* , vol. 175 (Springer-Verlag, Germany, 1995).
5. P. C. Kearney, et al., *J. Am. Chem. Soc.* **115**, 9907-9919 (1993).
6. D. A. Dougherty, in *Comprehensive Supramolecular Chemistry* F. Vögtle, Eds. (Pergamon Press, New York, 1996), vol. 2, pp. 195-209.
7. D. A. Dougherty, *Science* **271**, 163-168 (1996).
8. A. McCurdy, L. Jimenez, D. A. Stauffer, D. A. Dougherty, *J. Am. Chem. Soc.* **114**, 10314-10321 (1992).
9. A. Collet, J.-P. Dutasta, B. Lozach, J. Canceill, *Top. Curr. Chem.* **165**, 104-129 (1993).
10. H.-J. Schneider, D. Güttes, U. Schneider, *J. Am. Chem. Soc.* **110**, 6449-6454 (1988).
11. J. C. Ma, D. A. Dougherty, *Chem. Rev.* **97**, 1303-1324 (1997).
12. X. Cheng, S. Kumar, J. Posfai, J. W. Pflugrath, R. J. Roberts, *Cell* **74**, 299-307 (1993).
13. R. MacKinnon, G. Yellen, *Science* **250**, 276-279 (1990).
14. L. Heginbotham, R. MacKinnon, *Neuron* **8**, 483-491 (1992).
15. J. L. Sussman, et al., *Science* **253**, 872-879 (1991).

16. M. Harel, et al., *Proc. Natl. Acad. Sci. USA* **90**, 9031-9035 (1993).

17. J. Sunner, K. Nishizawa, P. Kebarle, *J. Phys. Chem.* **85**, 1814-1820 (1981).

18. B. C. Guo, J. W. Purnell, A. W. Castleman Jr., *Chem. Phys. Lett.* **168**, 155-160 (1990).

19. R. W. Taft, et al., *Pure Appl. Chem.* **62**, 17-23 (1990).

20. S. Mecozzi, A. P. West Jr., D. A. Dougherty, *Proc. Natl. Acad. Sci. USA* **93**, 10566-10571 (1996).

21. S. Mecozzi, A. P. West Jr., D. A. Dougherty, *J. Am. Chem. Soc.* **118**, 2307-2308 (1996).

22. A. Ikeda, H. Tsuzuki, S. Shinkai, *Tetrahedron Lett.* **35**, 8417-8420 (1994).

23. F. Inokuchi, Y. Miyahara, T. Inazu, S. Shinkai, *Angew. Chem. Int. Ed. Engl.* **34**, 1364-1366 (1995).

24. R. E. J. Barrans, Jr., *Ph. D. Thesis* (California Institute of Technology, 1993).

25. A. McCurdy, *Ph. D. Thesis* (California Institute of Technology, 1995).

26. L. Heginbotham, Z. Lu, T. Abramson, R. MacKinnon, *Biophys. J.* **66**, 1061-1067 (1994).

27. S. K. Silverman, H. A. Lester, D. A. Dougherty, *Biophys. J.* (submitted).

28. H. R. Guy, S. R. Durell, in *Ion Channels and Genetic Diseases* D. C. Dawson, R. A. Frizzell, Eds. (Rockefeller University Press, New York, 1995) pp. 1-16.

29. R. A. Kumpf, D. A. Dougherty, *Science* **261**, 1708-1710 (1993).

30. D. A. Doyle, R. Mackinnon, et al., *Science* **280**, 69-77 (1998).

31. M. A. Petti, T. J. Shepodd, D. A. Dougherty, *Tetrahedron Lett.* **27**, 807-810 (1986).

32. M. A. Petti, T. J. Shepodd, J. Barrans, R. E., D. A. Dougherty, *J. Am. Chem. Soc.* ***110***, 6825-6840 (1988).

33. K. Ritter, *Synthesis* , 735-762 (1993).

34. A. M. Echavarren, J. K. Stille, *J. Am. Chem. Soc.* **109**, 5478-5486 (1987).

35. O. Takayuki, N. Miyaura, A. Suzuki, *J. Org. Chem.* **58**, 2201-2206 (1993).

36. D. Parker, M. Rosser, *J. Chem. Soc. Perkin Trans. 2* , 85-89 (1995).

37. L. S. Mizoue, *Ph. D. Thesis* (California Institute of Technology, 1995).

38. S. Cacchi, A. Lupi, *Tetra. Lett.* **33**, 3939-3942 (1992).

39. J. F. Forman, *Ph. D. Thesis* (California Institute of Technology, 1996).

40. S. Mecozzi, *Ph.D. Thesis* (California Institute of Technology, 1996).